Harnessing Ubiquitin Variants to Combat Viral Infection *in planta*

by

Anuradha De Silva

A Thesis submitted to the Faculty of Graduate Studies of The University of Manitoba in partial fulfilment of the requirements of the degree of

DOCTOR OF PHILOSOPHY

Department of Microbiology
University of Manitoba
Winnipeg, Manitoba, Canada

Copyright © 2024 Anuradha De Silva

ABSTRACT

Many notable viruses encode a protease with deubiquitinating (DUB) activity, which is essential for viral replication and evasion of ubiquitin (Ub)-mediated host antiviral responses. The activity of viral DUBs thus promotes viral replication by protecting viral proteins from the Ub-dependent antiviral system in the host. Therefore, viral proteases with DUB activity are potential therapeutic targets for small-molecule antiviral inhibitor compounds.

The recent development of protein-based inhibitors based on variants of Ub (UbVs) as an antiviral strategy is promising due to the remarkable target specificity and potency of UbVs for their target DUB. Several cell culture-based studies demonstrate that cellular expression of UbVs suppresses animal virus replication in animal cells. However, delivering UbVs to the cytosol of human cells remains a significant challenge. Interestingly, several economically important crops are susceptible to plant viruses that depend on DUB proteases, whose replication could potentially be blocked by transgenic expression of UbVs. As a preliminary study to explore this strategy, I tested UbVs against the Turnip Yellow Mosaic Virus (TYMV) in collaboration with researchers from Dr. Sachdev Sidhu's lab (University of Waterloo). Next, I demonstrated the binding specificity of the UbVs for TYMV PRO by testing their affinity against a panel of recombinant plant DUBs that I generated from the model plant *Arabidopsis thaliana*. Strikingly, none of the UbVs were found to have significant affinity for any of the plant DUBs, whereas one of the UbVs was found to have a low nanomolar affinity for TMYV PRO. Additionally, small angle X-ray scattering and X-ray crystallography analyses illustrated how the tightest binding UbV interacts with TYMV PRO. Further insight into the utility of this UbV as an antiviral agent in plants was gained through transgenic expression of the UbV in *A. thaliana* in collaboration with the Dr. Stasolla laboratory and testing the resiliency of the

transgenic plants to infection by TYMV in collaboration with USDA. Together, the research demonstrates that a UbV can block the proteolytic activity of TYMV PRO and reduce viral replication of TYMV in transgenic *A. thaliana* plants, and a similar approach could be used against additional plant viruses of economic importance.

ACKNOWLEDGEMENTS

First and foremost, I would like to express my sincere gratitude to my supervisor, Dr. Brian Mark, for his invaluable guidance, encouragement, and support throughout my graduate studies. Your insight, knowledge, and unwavering belief have been instrumental in my development as a researcher. I am also grateful to my committee members, Dr. Ivan Oresnik and Dr. Olivia Wilkins, for their thoughtful feedback and stimulating discussions during committee meetings. Their expertise and willingness to challenge me have significantly improved the quality of my research.

I would like to acknowledge the following funding sources for their financial support: the Natural Sciences and Engineering Research Council, Research Manitoba, and the University of Manitoba. Many thanks to the wonderful collaborators who have enriched my research experience: Dr. Sachdev Sidhu and Dr. Jacky Chung (University of Waterloo), Dr. John Weiland and Dr. Melvin Bolton (United States Department of Agriculture), Dr. Claudio Stasolla and Dr. Mohommed Mira (University of Manitoba), Dr. Trushar Patel (University of Lethbridge), Dr. Mazdak Khajehpour (University of Manitoba) and Dr. Marjolein Kikkert, (Leiden University Medical Centre). I am grateful to the entire faculty in the Department of Microbiology for their unwavering support and guidance.

My journey would not have been possible without the unwavering support of my lab members, both past and present. I would like to express my heartfelt thanks to Ankoor, Michael, Jenny, Cole, Veronica, Grace, Kristen, Mehraferin, and Rakesh for everything. I would also like to extend a deep and respectful thank you to Dr. Judith Winogrodzki. Her immense talent as a scientist is deeply missed by all who know her.

Finally, I want to express my deepest gratitude to my family and friends for their unwavering love and support throughout my journey. You have always been there for me, and I am incredibly grateful for your presence in my life.

TABLE OF CONTENTS

ABSTRACT ii

ACKNOWLEDGEMENTS iv

TABLE OF CONTENTS v

PERMISSIONS viii

AUTHOR CONTRIBUTIONS ix

LIST OF TABLES x

LIST OF FIGURES xi

LIST OF ABBREVIATIONS xiii

CHAPTER 1: Literature Review 1

1.1 Introduction to deubiquitinases 1

1.1.1 Ub-specific protease (USP/UBP) 2

1.1.2 Ubiquitin C-terminal hydrolases (UCH) 6

1.1.3 Ovarian tumor protease (OTU) 8

1.1.4 Machado-Joseph Domain containing deubiquitinase (MJD) 10

1.1.5 Zinc finger with UFM1-specific peptidase domain protein (ZUFSP) 12

1.1.6 Motif interacting with Ub-containing novel DUB family (MINDY) 15

1.1.7 JAB1/MOV34/MPR1 PAD1 N-terminal (MPN)(JAMM) domain proteins (JAMM) 15

1.2 Role of virally encoded deubiquitinases 18

1.2.1 Family Tymoviridae and Role of TYMV PRO 25

1.3 Inhibitors targeting the DUB domain of viruses 29

1.4 Protein-based alternatives to small molecular inhibitors 30

1.5 Thesis Objectives 33

CHAPTER 2: Biochemical Analysis of TYMV PRO and UbV3 34

2.1 Introduction 36

2.2 Materials and Methods 39

2.2.1 Construction of protein expression plasmids 39

2.2.2 Selection of Ubiquitin Variants 39

2.2.3 Construction of mutants of UbV3 using site-directed mutagenesis 40

2.2.4 Protein expression and purification of TYMV PRO, plant DUBs and UbVs 40

2.2.5 EC_{50} and IC_{50} Assays 41

2.2.6 ELISA assays to evaluate the binding and specificity of UbVs and deubiquitinases 42
2.2.7 Ub-AMC deubiquitinase assay 43
2.2.8 Michaelis-Menten Kinetic of TYMV PRO 43
2.2.9 Inhibition Assays 44
2.2.10 K48- and K63-linked polyUb chain cleavage assay with the presence of UbV3 44
2.2.11Cleavage of the Pro↓Hel site from the TYMV polyprotein by PRO and its inhibition by UbV3 45
2.2.12 Gel filtration protein coupling of TYMV PRO and UbV3 45
2.2.13 Covalent linkage of UbV3 and TYMV PRO 46
2.2.14 Crystallization and Structure Determination 47
2.2.15 Small-angle X-ray Scattering Analysis 48

2.3 Results **48**

2.3.1 Screening of UbVs that bind with TYMV PRO 48
2.3.2 UbV3 inhibits the DUB and polyprotein cleavage activity of TYMV PRO 50
2.3.4 Evaluating off-target inhibition of cellular plant DUBs by UbVs. 54
2.3.6 UbV3 dimerization drives TYMV PRO inhibition 61

2.4 Discussion **69**

Chapter 3: Development of transgenic *A. thaliana* that is resistant to TYMV infection **73**

3.1 Introduction **75**

3.2 Material and Methods **77**

3.2.1 Molecular cloning and construction of UbV3 expressing transgenic plant lines 77
3.2.2 Phenotype analysis 78
3.2.3 Quantification and detection of FLAG-tagged UbV3 78
3.2.4 Subcellular fractionation of FLAG-tagged UbV3 79
3.2.5 Subcellular Localization 80
3.2.6 Inhibition of TYMV PRO with cytosolic extracts from transgenic *A. thaliana* 80
3.2.7 Protoplast infection study 80
3.2.8 Inoculation of TYMV and infection study 81

3.3 Results **82**

3.3.1 Transgenic expression of UbV3 does not adversely affect *A. thaliana* physiology 82
3.3.2 UbV3 protein is present in the cytosol and organelle fractions of transgenic *A. thaliana* .. 84
3.3.3 UbV3 suppresses TMYV replication *in planta* 87

3.4 Discussion **90**

Chapter 4: Biochemical Analysis of Machado-Joseph domain containing deubiquitinases in *A. thaliana* **92**

4.1 Introduction **94**

4.2 Materials and Methods **95**

4.2.1 DNA constructs 95

4.2.2 Protein expression and purification of AtAT3G 95

4.2.3 DUB Assays 96

4.3 Results **97**

4.3.1 Construction of MJD family DUBs of *A. thaliana* 97

4.3.3 Exploring the DUB activity of AtAT3G 100

4.4 Discussion **101**

Chapter 5: Biochemical Analysis of Porcine Reproductive Respiratory Syndrome Virus (PRRSV) Papain-like Protease 2 **103**

Contribution Statement **104**

5.1 Introduction **105**

5.2 Materials and Methodology **107**

5.2.1 Site-directed mutagenesis of PRRSV DV385-578 for in vitro activity assays 107

5.2.2 Expression and purification 107

5.2.3 Kinetic characterization of wild-type and mutant PRRSV DV PLP $_{385-578}$ 108

5.3 Results **109**

5.4 Discussion **113**

Chapter 6: Conclusion **115**

6.1 Summary of Findings **115**

6.2 Future Directions **116**

Appendix **120**

References **135**

PERMISSIONS

Figures, tables and passages within this thesis have been adapted from published works in academic journals that I have authored.

Chapter 1:

van Vliet, J. E. V., **De Silva, A**., Mark, B.L., Kikkert, M. Viral deubiquitinating proteases and the promising strategies of their inhibitors. Virus Research. 2024. doi.org/10.1016/j.virusres.2024.199368.

This is an open-access article under the terms of the Creative Commons CC-BY license and does not require permission to be obtained to reuse this article's content.

Chapter 2 and 3:

De Silva A, Kim K, Weiland J, Hwang J, Chung J, Pereira HS, Patel TR, Teyra J, Patel A, Mira MM, Khajehpour M, Bolton M, Stasolla C, Sidhu SS, Mark BL (2024). Suppressing Tymovirus replication in plants using a variant of ubiquitin (*Under review at PLoS Pathogens*).

Chapter 5:

Bailey-Elkin BA, Knaap RC, **De Silva A**, Boekhoud IM, Mous S, van Vught N, Khajehpour M, van den Born E, Kikkert M, Mark BL. Demonstrating the importance of porcine reproductive and respiratory syndrome virus papain-like protease 2 deubiquitinating activity in viral replication by structure-guided mutagenesis. PLoS Pathogens. 2023. doi.org/10.1371/journal.ppat.1011872.

This is an open-access article under the terms of the Creative Commons CC-BY license 4.0 international (CC BY) license and does not require permission to be obtained to reuse this article's content.

AUTHOR CONTRIBUTIONS

Section 1.4 in Chapter 1, the literature review was shared with Vera J. van Vliet. Multiple authors contributed to the work described in Chapter 2. Dr. Jihyun Hwang performed the TYMV PRO polyprotein cleavage activity with the presence of UbV3, the X-ray structure determination of the complex of TYMV PRO and UbV3 was performed by Dr. Kihun Kim, and the Small-angle X-ray Scattering data analysis was completed by Dr. Higor Pereira.

With guidance from Dr. Mohommed Mira (a Postdoctoral fellow in Dr. Stasolla's lab), I generated transgenic *A. thaliana* that expressed the UbV3 protein as described in Chapter 3. Dr. John Weiland performed the TYMV infection of wild-type and transgenic *A. thaliana*, and I completed the biochemical analysis of the infected plant tissues.

I performed all the work presented in Chapter 4 with advice from Dr. Kihun Kim (Postdoctoral fellow in Dr. Mark's lab). The conceptualization of the project in Chapter 5 was completed before I arrived in the Mark lab, and the first draft of the manuscript was also submitted to the Plos Pathogens journal for review. After revision, reviewers requested detailed kinetic characterization of PRRSV PLpro wt and its mutant enzymes be included in the manuscript, and I was able to carry out these critical experiments, which led to the publication of the manuscript. The research work presented here was done by myself following discussions with Dr. Mark and Dr. Khajehpour.

LIST OF TABLES

Table 2.1 DNA Constructs 39

Table 2. 2 Non-liner regression analysis of fitting the kinetic profiles of Ub-AMC hydrolysis by TYMV PRO and *A. thaliana* DUBs in the presence of different concentrations of UbV3 to equation $y=Y_0+ae^{bx}$ 58

Table 2. 3 The data collection and refinement data for UbV3 and TYMV PRO-UbV3 complex..... 67

Table 3. 1 Primer used to construct binary vector pK2GW7 77

Table 4. 1 DNA Constructs of MJD family DUBs 95

Table 5. 1 Linear regression analysis results of the fluorescence time traces of Ub-AMC hydrolysis by PRRSV $DV_{385-578}$ and mutants over time. The data was fitted to the equation: $y=y_0+(V_0)*x$, to obtain initial rates (V_0). 111

Table 5. 2 Michaelis-Menten kinetics parameters of PRRSV $DV_{385-578}$ and mutants of PRRSV $DV_{385-578}$ for Ub-AMC substrate 112

LIST OF FIGURES

Figure 1. 1 Structure of UBP14 and superposition of Alphafold structure of UBP14 4

Figure 1. 2 Alphafold structures of UCH family proteins in *A. thaliana* and human UCHL1 deubiquitinase structure 7

Figure 1. 3 Alphafold predicted structures of OTLD1 of *A. thaliana* 10

Figure 1. 4 Phylogenetic relationship of MJD family DUBs of human and predicted plant DUBs 11

Figure 1. 5 Crystal structure of HsZUFSP bound to Ub (PDB: 6FGE) and compared with Alphafold predicted At3g48380 14

Figure 1. 6 Phylogenetic relationship of MINDY family DUBs of human and *A. thaliana* 15

Figure 1. 7 Crystal structure of HsAMSH-LP bound to Ub (PDB: 2ZNY) and compared with Alphafold predicted AtG16144 17

Figure 1. 8 The phylogenetic tree of viral proteases with deubiquitinating activity 21

Figure 1. 9 Alphafold structures of BNYVV and RSV proteases and superposition with TYMV PRO 23

Figure 1. 10 Superposition of the MRFV PRO-Ub and TYMV PRO-Ub 27

Figure 1. 11 Predicted structures of APLV and OMV and superposition with TYMV PRO 28

Figure 1. 12 X-ray crystal structures of ubiquitin variants in complex with CCHFV OUT, MERS-CoV PLpro and SARS-CoV-2 PLpro 31

Figure 2. 1 Binding of UbVs to TYMV PRO 49

Figure 2. 2 UbV3 interacts with TYMV PRO 50

Figure 2. 3 UbV3 inhibits the K48- and K63-linked poly Ub chain cleavage 51

Figure 2. 4 Inhibition of TYMV PRO mediated cleavage of PRO↓Hel by UbV3 53

Figure 2. 5 Western blot analysis of UbV3 inhibition of Pro↓Hel cleavage 54

Figure 2. 6 The binding potency of UbVs against TYMV PRO and *A. thaliana* DUBs 55

Figure 2. 7 The DUB activity of TYMV PRO and *A. thaliana* DUBs in the presence of UbV3 57

Figure 2. 8 Crystal structure of UbV3 dimer 61

Figure 2. 9 Complex crystal structure of TYMV PRO and UbV3 dimer 64

Figure 2. 10 Interaction between TYMV PRO and UbV3 other than its C-terminal tail 66

Figure 3. 1 Characterization of UbV3 expression in *A. thaliana* lines 83

Figure 3. 2 Subcellular fractionation and quantification of transgene expression in leaf and inflorescence in wild-type and transgenic *A. thaliana* 85

Figure 3. 3 Hydrolysis of 1µM Ub-AMC by 500nM TYMV PRO in the presence of varying concentrations of protoplast cytoplasmic fractions 86

Figure 3. 4 UbV3-mediated suppression of TYMV replication *in planta* 89

Figure 4. 1 Construction of MJD family DUBs of *A. thaliana* 98

Figure 4. 2 Superposition of X-ray structure of HsATAXIN and predicted MJD DUBs of *A. thaliana* 99

Figure 4. 3 DUB activity of AtAT3G and AtAT3G C20S 100

Figure 5. 1 Deubiquitinase activity of $PRRSV_{385-578}$ enzyme and Michaelis- Menton plot for PRRSV $DV_{385-578}$ mutants 110

LIST OF ABBREVIATIONS

+ssRNA	Positive single-stranded RNA virus
AdV	Adenovirus
AMSH	Associated molecule with the SH3-domain of STAM
APLV	Andean potato latent virus
APMMV	Andean potato mild mosaic virus
BLVS	Blackberry virus S
BNYVV	Beet necrotic yellow vein virus
CCHFV	Crimean-Congo hemorrhagic fever virus
CP	Coat protein
Col-0	Colombia 0
CSDaV	Citrus sudden death associated virus
DAS-ELISA	Double antibody sandwich enzyme-linked immunosorbent assay
DTT	Dithiothreitol
DUB	Deubiquitinase
DUGV	Dugbe virus
EAV	Equine arteritis virus
EDTA	Ethylenediaminetetraacetic acid
EMV	Eggplant mosaic virus
ERVEV	Erve virus
FMDV	Foot- and -mouth disease virus
FPLC	Fast protein liquid chromatography
GST	Glutathione S-transferase
GSyV1	Grapevine Syrah virus 1
h	Hour
HAZV	Hazara virus
HCoV	Human Coronavirus
HEK	Human embryonic kidney
Hel	Helicase
HEPES	4-(2-hydroxyethyl)-1-piperazineethanesulfonic acid
IBV	Avian infectious bronchitis virus
IFN	Interferon

IPTG	Isopropyl β-D-1-thiogalactopyranoside
ISG-15	Interferon-stimulated gene 15
JAMM	JAB1/MPN/Mov34 metalloenzymes
Kan	Kanamycin
kDa	Kilodaltons
KUPEV	Kupe virus
L	Liter
LB	Lysogeny broth medium
M	Molar
MCMV	Murine cytomegalovirus
MERS	Middle East respiratory syndrome coronavirus
MET	Methyltransferase
MHV	Murine hepatitis virus
MJD	Machado Josephin domain protease
mg	Milligram
mL	Milliliter
mM	Millimolar
MRFV	Maize rayado fino virus
mRNA	Messenger RNA
Ni-NTA	Nickel-nitrilotriacetic acid
nM	Nanomolar
Nsp	Non structural protein
OBDV	Oat blue dwarf virus
OD600	Optical density measured at 600 nm
OLV3	Olive latent virus 3
OMV	Okra mosaic virus
ORF	Open reading frame
OTU	Ovarian tumor
PAGE	Polyacrylamide gel electrophoresis
PCR	Polymerase chain reaction
PEDV	Porcine epidemic diarrhea virus
PEG	Polyethylene glycol
PLpro	Papain-like protease

PRO	Protease
RdRp	RNA-dependent RNA polymerase
Rpm	Revolutions per minute
PRRSV	Porcine reproductive respiratory syndrome
RSV	Rice stripe tenuivirus
SADS-CoV	Swine acute diarrhea syndrome coronavirus
SARS-CoV	Severe acute respiratory syndrome coronavirus
SAXS	Small angle X-ray scattering
SDS	Sodium dodecyl sulfate
SUMO	Small Ub-like modifiers
TBMV	Tomato blistering mosaic virus
TGEV	Transmissible gastroenteritis virus
TRIS	Tris(Hydroxymethyl)aminomethane
TYMV	Turnip yellow mosaic virus
Ub	Ubiquitin
Ub-AMC	Ub-7-amido-4-methylcoumarin
Ubl	Ub-like modifiers
UBP	Ubiquitin binding domain
UbV	Ubiquitin variant
UCH	Ubiquitin C-terminal hydrolase
UPS	Ubiquitin proteasome system
USP	Ubiquitin-specific protease
WT	Wild-type

Contributions statement:

I wrote sections 1.1, 1.2 and 1.3 in this literature review, and 1.4 was a shared work with Vera J. E. van Vliet (1). All the figures were made by me, and all the listed authors took part in editing the final manuscript.

CHAPTER 1: LITERATURE REVIEW

1.1 Introduction to deubiquitinases

Post-translational modifications of proteins by ubiquitin (Ub) and Ub-like modifiers (Ubl) have emerged as major regulatory mechanisms in various cellular activities, including signal transduction, transcription, membrane protein trafficking, autophagy, nuclear transport, and immune responses (2–4). Major modifiers include Nedd8, interferon-stimulated gene 15 (ISG15), and a small Ub-like modifier (SUMO)(5). The attachment of Ub and Ubl to target proteins involves three enzymatic actions: activating enzyme (E1), conjugating enzymes (E2), and ligases (E3), which determine target specificity (2,6). These enzymatic cascades promote protein degradation by the Ub-proteasome system (UPS), the critical machinery for degrading cytoplasmic and nuclear proteins (4,7), as well as several other signalling systems, such as activating innate immunity (8,9).

Deubiquitination, a vital counteracting process to ubiquitination, is catalyzed by deubiquitinating enzymes (DUBs). These enzymes remove ubiquitin (Ub) from proteins by cleaving the peptide or isopeptide bond between Ub and its substrate proteins and between Ub molecules in a chain. This reversal alters the fate of ubiquitinated proteins, impacting the molecular and cellular functions associated with them (10–14).

The human genome encodes nearly 100 DUBs, which are classified into two main groups: cysteine proteases and metalloproteases. Cysteine protease DUBs encompass six major subfamily groups: the Ub-specific protease (USP/UBP) superfamily, the ovarian tumor (OTU) superfamily, the Machado–Josephin domain (MJD) superfamily, the Ub C-terminal hydrolase (UCH) superfamily, motif interacting with Ub-containing novel DUB (MINDY), and zinc finger with UFM1-specific peptidase domain (ZUFSP) (15–19). On the other hand, metalloproteases include the Jab1/Mov34/Mpr1 Pad1 N-terminal (MPN+) domain

superfamily, known as JAMM domain proteins, which exhibit zinc-binding and function as metalloproteases (17). JAMM DUBs typically contain a catalytic domain surrounded by additional domains such as the Ub-specific protease domain, the Ubl domain, the meprin and tumour necrosis factor (TNF) receptor-associated factors (TRAF) homology (MATH) domain, and the zinc-finger Ub-specific protease (ZnF-UBP), among others (16,20). These enzymes possess conserved amino acid sequence motifs surrounding catalytically active residues, and their protein structures are thoroughly reviewed in terms of mechanisms and interactive specificity.

In plants, the model *Arabidopsis thaliana* genome encodes confirmed and predicted DUBs that can be classified into all seven subfamilies (21). However, the molecular mechanism and physiological functions are still elusive, even for the confirmed plant DUB. The following sections mainly focus on the function and structure of plant deubiquitinases of *A. thaliana* since I used this model plant as a host system to demonstrate how the transgenic can be used to suppress viral DUB activity *in planta*.

1.1.1 Ub-specific protease (USP/UBP)

Arabidopsis UBPs are a protein family with 27 members crucial for plant development (22). Similar to human USPs, they share a UBP domain and are classified into 14 subfamilies based on additional domains that likely regulate protein interactions (23–25).

Subfamily Domains and Function:

- UBP10/9/11/5/8: DUSP domains - protein-protein interaction or substrate recognition (26).
- UBP15/16/17/18/19: ZnF-MYND (Myeloid-type zinc finger domain, Nervy and DEAF-1 domains)-potential protein-protein interaction (27).

- UBP12/13: MATH (Meprin and TRAF homology domains) -folding and receptor interaction (28,29).
- UBP1/2/14: ZnF-UBP domains – contain ubiquitin-associated (UBA) domains related to poly-Ub binding (23).
- UBP6/7/26: UBL domains -present in ubiquitin pathway and other proteins (30).

UBP1 and UBP2 share high sequence similarity and can cleave ubiquitin chains *in vitro* (22). While single mutant plants (*ubp1* and *ubp2*) show no phenotypic changes, however, they display stunted growth and chlorotic leaves when exposed to canavanine (an anti-herbivory compound), indicating a role for UBPs in this metabolism (22). UBP3 and UBP4 are important for pollen development and transmission (31). They are redundant, meaning single mutants plants (*ubp3* and *ubp4*) show no phenotypic deficits, but a double mutant (*ubp3 ubp4*) where the activity of UBP3 and UBP4 were removed fails to mature pollen and thus appear to be required for pollen germination (32). UBP6 responds to external stimuli since Arabidopsis UBP6 complements a yeast mutant lacking its UBP6 counterpart and restores canavanine resistance, indicating a role in response to external stimuli (33). UBP6 also has a calmodulin-binding domain, suggesting a role for calcium signalling in protein degradation or plant homeostasis (33). UBP12 and UBP13 play a key role in plant immunity and development. They are upregulated during infection and share redundant functions in plant defence, as the double mutant is lethal (34,35). They have deubiquitinating activity, localize in various cellular compartments, and are ubiquitously expressed, suggesting broader functions. They regulate flowering time, circadian rhythms, and the jasmonate signalling pathway (36,37). Moreover, UBP12 and UBP13 contribute to heterochromatin gene silencing (38). UBP14 is essential for embryo development. The mutant plants (*ubp14*) where the activity of UBP14 was removed halted the development of the embryo (39). It also plays a role in root development under phosphate deprivation and regulates the cell cycle through its interaction with other proteins,

influencing cell and organ growth (39–41). None of the UBPs are structurally determined experimentally except the UBA domains of UBP14 (PDB: 1VEK and PDB: 1WIV). However, Alphafold-predicted UBP protein structures are available in the Alphafold (AF) Protein Structure Database (https://alphafold.ebi.ac.uk). The superposition of the structure of UBP14 and UBA domains of UBP14 is shown below (Figure 1.1).

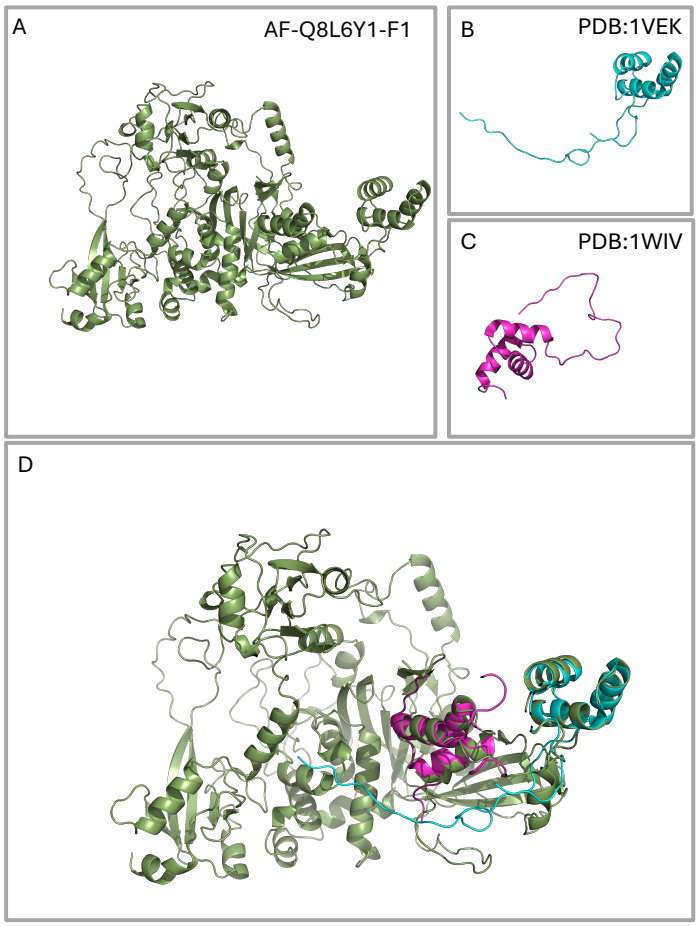

Figure 1. 1 Structure of UBP14 and superposition of Alphafold structure of UBP14

A; AF-Q8L6Y1-F1 (smudge) and UBA domains of UBP14 [B; PDB: 1VEK (cyan) and C; PDB: 1WIV (magenta)] and D; superposition structures of Alphafold protein and UBA domains of UBP14. All structural images were visualized using PyMol v2.5.

UBP15 regulates plant size, leaf development, and seed size. It is localized in both the cytosol and nucleus and expressed more highly in leaves and flowers (24). Interestingly, UBP15 seems to partially overlap in function with UBP16 despite having a stronger sequence

similarity to UBP17 (23). UBP15 also promotes seed size by influencing cell proliferation in the seed coat (42). Beyond plant development, UBP16 plays a role in salt stress tolerance. Mutations in UBP16 lead to hypersensitivity to salt and an imbalance of sodium and potassium levels in the plant. UBP16 stabilizes a protein involved in salt tolerance and directly affects sodium-hydrogen and potassium transport. It also regulates cell death through a pathway involving reactive oxygen species (30,43). Another subfamily member, UBP19, is likely essential for plant development as mutants are found to be embryo-lethal (30). UBP24 contributes to abscisic acid signalling, as well as salt and drought tolerance, by affecting stomata closure. It can also cleave ubiquitin chains into monomers (44). UBP26 may be involved in transcriptional control through deubiquitinating histone tails and shows functional similarity to UBP12 and UBP13 (38). Moreover, UBP26 involves H2Bub1 deubiquitination in *Arabidopsis* (45), and it plays a critical role in controlling flowering time. It functions by silencing the FLOWERING LOCUS C (FLC) gene. This silencing is achieved through deubiquitination of the H2Bub1 protein on the FLC chromatin (46). Consequently, ubp26 mutant plants flower earlier and exhibit elevated global levels of H2Bub1. Interestingly, the methylation patterns of histones associated with FLC are also altered in the ubp26 mutant. The levels of H3K36 methylation decrease, while H3K27me3 methylation increases. These findings suggest that UBP26 might regulate FLC expression by reducing the repressive H3K27me3 mark through H2B deubiquitination. Furthermore, studies have shown that the expression of a Polycomb Group (PcG) target gene, AT1G80160, is also upregulated in the ubp26 mutant. PcG genes are known to be involved in gene silencing (38). Finally, UBP27 is potentially involved in shaping mitochondria. It localizes to mitochondria and cleaves polyubiquitin chains, but its role remains unclear as mutants show no obvious phenotype. Overexpression alters mitochondrial morphology (47).

1.1.2 Ubiquitin C-terminal hydrolases (UCH)

The Arabidopsis UCH family consists of just three members: UCH1, UCH2, and UCH3. While all three share similar N-terminal and catalytic domains, only UCH1 and UCH2 have highly similar C-terminal sequences (48). This C-terminal extension, found in human UCH enzymes, might influence substrate specificity by limiting the processing of multimeric ubiquitin chains (49).

UCH2 can disassemble ubiquitin chains from targets linked as both peptides and isopeptides *in vitro*. Interestingly, UCH1 and UCH2 play a significant role in shoot development, influencing inflorescence architecture (48). This is likely due to their impact on AUX/IAA protein turnover, which regulates auxin signalling. Analyses of the *uch1-1* and *uch2-1* double mutant plants revealed increased AUX/IAA protein turnover, affecting shoot architecture due to altered auxin signalling patterns. Conversely, UCH1 overexpression produced the opposite effect. Notably, both UCH1 and UCH2 are ubiquitously expressed, though UCH2 levels are higher. They also localize to both the cytoplasm and nucleus in Arabidopsis cells (50).

Unlike their counterparts in yeast and humans, UCH1 and UCH2 do not appear to be part of the Arabidopsis 26S proteasome complex. However, truncated versions of these proteins can interact with 26S proteasome subunits *in vivo* (48). Additionally, UCH1 and UCH2 can form heterodimers with each other and interact with subunits of the TREX-2 complex, which mediates mRNA export (51). Human UCHL1 is the most studied DUB of the UCH family and predicted Alphafold structure of UCH1 superimposed with the structure of UCHL1 (Figure 1.2). In addition to deubiquitinase activity, UCHL1 is involved in ubiquitin binding, conjugation and transnitrosylation (52,53) and predicted *A. thaliana* UCH1 may also possess these activities. Further research is needed to understand the specific functions of the third

UCH family member (UCH3) in Arabidopsis and other plants. As UBP family DUBs, none of the UCH family protein structures have been experimentally determined from Arabidopsis. Only Alphafold predicted structures are available (Figure 1.2).

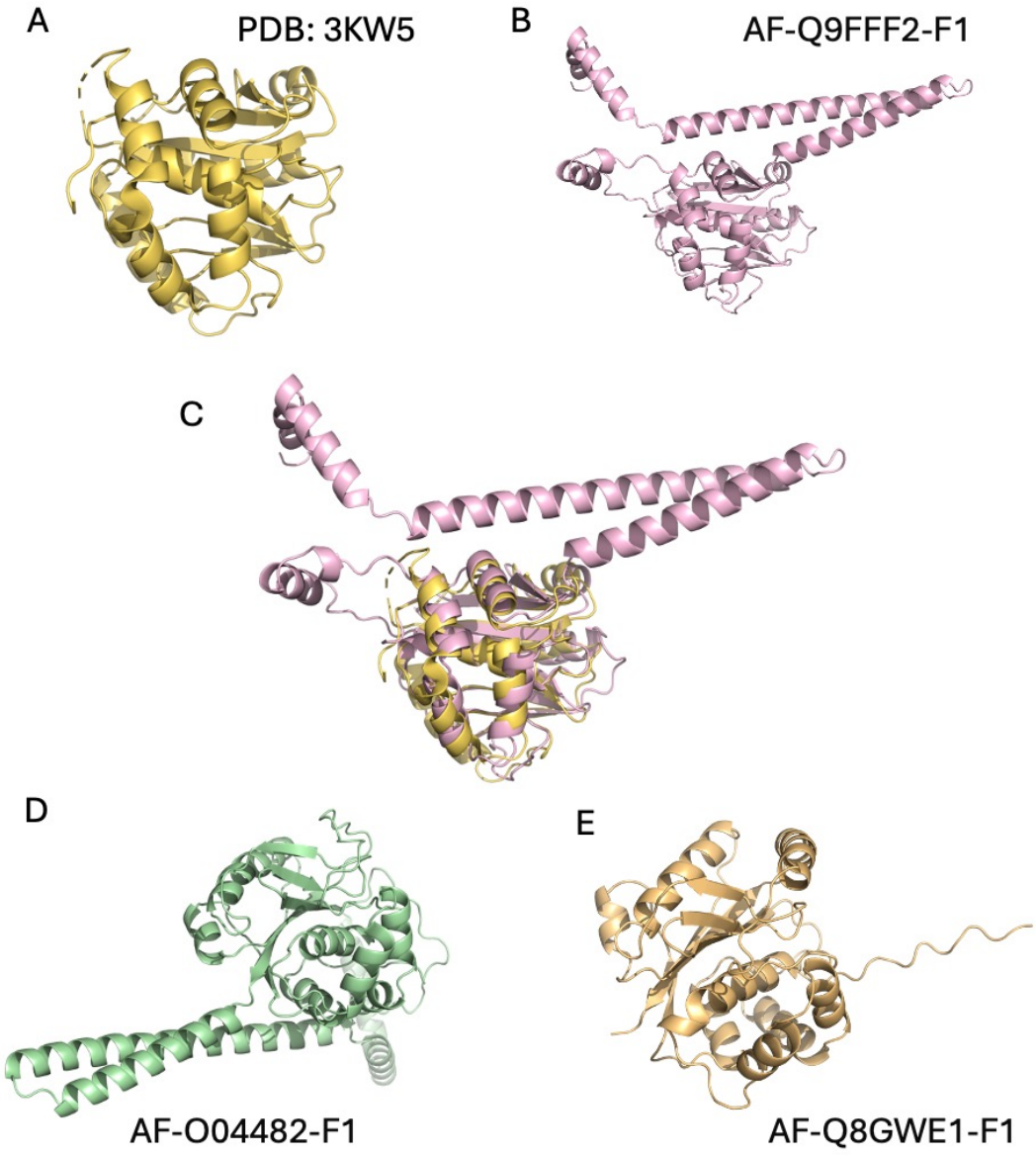

Figure 1. 2 Alphafold structures of UCH family proteins in *A. thaliana* and human UCHL1 deubiquitinase structure

A: HsUCHL1 (PDB:3KW5), B: UCH1 (light pink), C: superposition structure of A and B, D: UCH2 (light green) and E: UCH3 (light orange). All structural images were generated using Pymol v2.5.

The UCH protein family likely regulates a histone H2A monoubiquitination (H2Aub1). In Drosophila, the UCH protein CALYPSO, part of the PR-DUB complex (polycomb repressive-DUB), is responsible for H2Aub1 deubiquitination. (54,55). Mutations in PR-DUB lead to H2Aub1 accumulation and misregulation of genes, highlighting its importance in maintaining H2Aub1 dynamics. The human counterpart of CALYPSO is BRCA-1-associated protein 1 (BAP1), which also functions as a tumour suppressor (56). Interestingly, Arabidopsis lacks a clear CALYPSO ortholog and no H2A deubiquitination complexes have been identified (23). However, the presence of the conserved H2Aub1 mark suggests a similar regulatory mechanism involving as yet unidentified Arabidopsis DUB proteins or complexes. Given the conserved UCH domain in all three Arabidopsis UCH members, it is possible that one of these proteins has assumed the regulatory role of BAP1/CALYPSO in this plant (21). Future research is needed to explore this possibility.

1.1.3 Ovarian tumor protease (OTU)

The OTU family of proteases is named after the ovarian tumour (otu) gene discovered in Drosophila (57). These enzymes are present in eukaryotes, viruses, and bacteria (58). Arabidopsis has 12 genes encoding OTU domain proteins, similar to those found in other metazoans (23). Some Arabidopsis OTU proteins have isoforms with a non-functional OTU domain due to alternative splicing (21).

Arabidopsis OTU proteases often contain additional domains beyond the OTU domain, which contributes to their diverse functions. For example, OTUBAIN-LIKE DEUBIQUITINASE 1 (OTLD1) isoforms possess a UBA-like domain, while OTU5 isoforms have a coiled-coil domain, and OTU7a has a putative nucleic acid binding SEC-C motif (23).

OTU domain proteases can exhibit a range of substrate specificities. OTU1, 2, 3, 4c, 7a, 9, and 10 can cleave both K48-linked and K63-linked ubiquitin chains *in vitro*. K48-linked chains target proteins for degradation by the proteasome, while K63-linked chains are involved in various other processes like endocytosis, DNA repair, and complex assembly. Interestingly, OTU1 can also hydrolyze linear dimers, trimers, and tetramers of ubiquitin, while OTU3 and 4c are limited to trimers and tetramers (59).

OTLD1 is the only Arabidopsis OTU protease extensively studied at the molecular level. Overexpression of OTLD1 in Arabidopsis leads to various phenotypes, including increased flower number and enhanced plant growth due to larger cells. Mechanically, OTLD1 represses genes involved in these processes, such as WUS, OSR2, and ABI5, by deubiquitinating H2Bub1 at their loci. This deubiquitination also leads to decreased H3K4me3 levels at these genes (60). Besides H2B deubiquitination, OTLD1 is involved in gene activation and gene repression (61). However, none of the OTU DUBs from Arabidopsis have been experimentally determined, and only Alphafold predictions were available (Figure 1.3).

The presence of a conserved catalytic triad of amino acids (Cysteine, Histidine, and Aspartate) in Arabidopsis OTU DUBs classifies them as cysteine proteases, similar to their counterparts in humans and yeast (59,62) for which X-ray crystal structures are available (63,64). Mutations in the conserved catalytic triad of Cys 92 and His288 of OTU1 completely abolished their ability to cleave K48 and K63-linked ubiquitin tetramers, and these mutations also generally eliminated the cleavage of linear ubiquitin polymers by OTU1 and OTU4c. Also, these mutations abolished their ability to cleave ubiquitin and RUB (related ubiquitin-like protein) fusion proteins (59). The central role of the active site cysteine in OTU1 has also been confirmed chemically using His-tagged OTU1, where cleavage of K48-linked and K63-linked

ubiquitin tetramers by OTU1 was inhibited by cysteine and thiol-modifying reagents (UB aldehyde and N-ethylmaleimide) but not by metalloprotease or serine protease inhibitors (59).

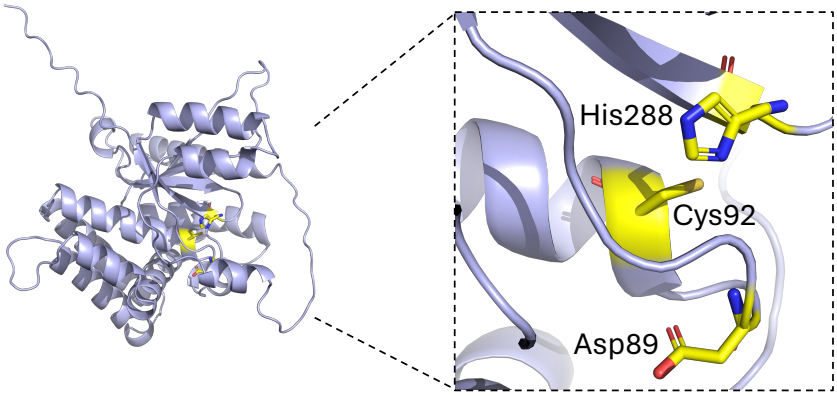

Figure 1. 3 Alphafold predicted structures of OTLD1 of *A. thaliana*

The predicted catalytic residues of AF-Q9DB92-F1 (right); Asp89, Cys92 and His288 are shown as sticks (left).

Interestingly, a mutation in OTU1 (D89E) that reduced the cleavage of isopeptide bond-linked ubiquitin tetramers surprisingly did not affect its ability to cleave linear ubiquitin polymers (59). Initially, this Asp residue (D89) was predicted to be part of the catalytic triad in Arabidopsis OTU DUBs and human OTUB1/2 (65). However, structural studies revealed that a different aspartic acid (D290 in OTU1) located one residue away participates in triad formation (66). While not directly involved in catalysis, the backbone amide of the originally predicted Asp residue (D89 in OTU1) appears to be crucial for stabilizing a key intermediate during the reaction (67).

1.1.4 Machado-Joseph Domain containing deubiquitinase (MJD)

The Machado Joseph disease (MJD) protease family, which includes human proteins like Ataxin-3 (ATXN3), Ataxin-3like (ATAXIN-3L), JOSD1 and JOSD2 (68) and has yet to

be identified in Arabidopsis. However, evolutionary analysis suggests the presence of at least two Arabidopsis genes with high sequence similarity to human ATXN3 (Figure 1.4).

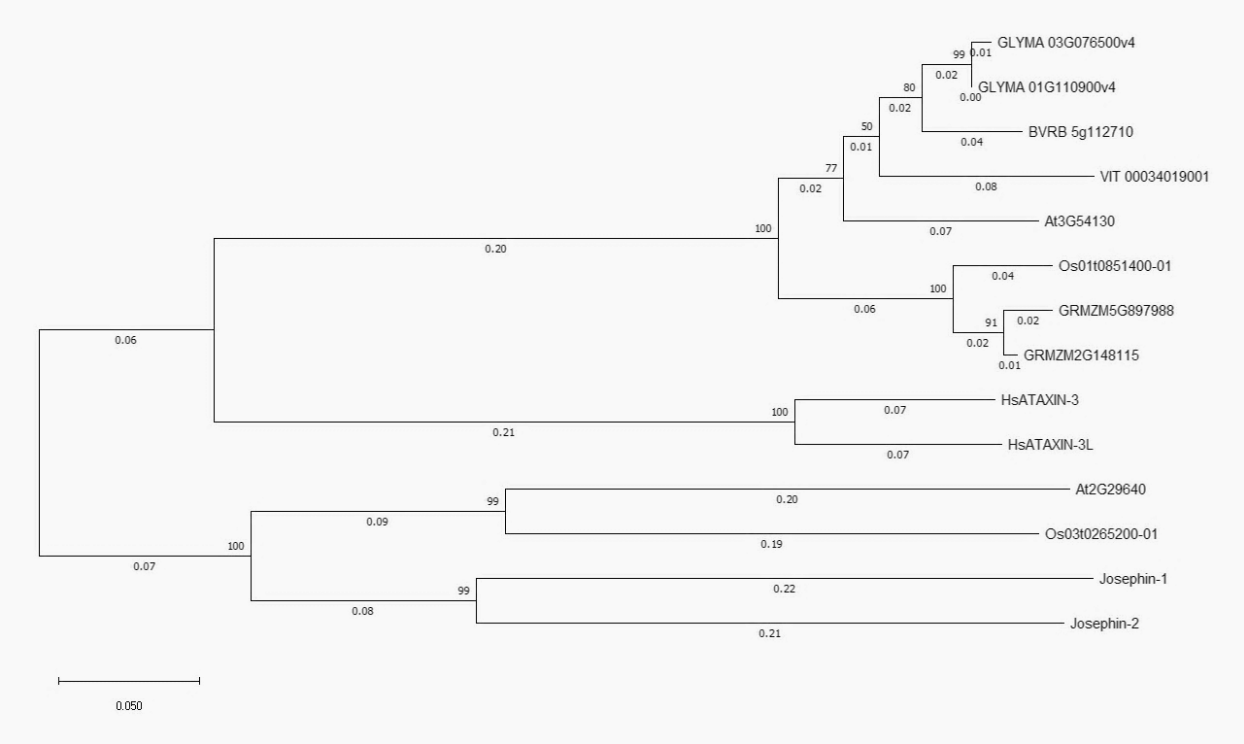

Figure 1. 4 Phylogenetic relationship of MJD family DUBs of human and predicted plant DUBs

The analysis was conducted using the MEGA 11 software, and the tree was constructed using the Neighbor-Joining method with bootstrap resampling (5000 replicates). The numbers in the nodes represent bootstrap values, and distance indicates the divergence or mismatch of these amino acid sequences with each other. The scale bar represents units of the number of amino acid substitutions per site. (Hs: *Homo sapiens*, Os: *Oryza sativa*, At: *Arabidopsis thaliana*, GRMZM: *Zea mays*, VIT: *Vitis vinifera*, BVRB: *Beta vulgaris*, GLYMA: *Glycine max*)

In humans, Ataxin-3, a member of the Machado Joseph disease (MJD) protein family, exhibits deubiquitinating activity *in vitro*, cleaving both K48 and K63-linked ubiquitin chains. However, shorter chains (six or fewer ubiquitin molecules) are poor substrates for this enzyme (69). The K63-linked chains appear to be the preferred target for Ataxin-3 compared to K48 chains. Interestingly, similar to JOSD1, the catalytic activity of Ataxin-3 can be regulated by its own ubiquitylation (70).

Ataxin-3 functions in two key cellular processes: transcription repression and protein homeostasis (71). It interacts with various transcription regulators, including TAFII130

(involved in RNA polymerase II assembly), CREB-binding protein (CBP), which regulates genes responsive to cyclic AMP signalling, RAD23 (involved in DNA repair) and histone deacetylases (HDAC3 and HDAC6) which influence chromatin structure and gene expression (72). Notably, nuclear localization of Ataxin-3 is essential for its role in spinocerebellar ataxia type 3 (SCA3) disease development, highlighting the importance of its intracellular location (69).

Based on these findings from humans, Arabidopsis MJD proteins (At2G29640 and At3G54130) could potentially be involved in the epigenetic regulation of gene expression through interaction with histones. This intriguing hypothesis remains to be explored and requires further characterization of these Arabidopsis and other plant proteins related to MJD family DUB.

1.1.5 Zinc finger with UFM1-specific peptidase domain protein (ZUFSP)

A new subfamily of deubiquitinase, ZUFSP (zinc finger with UFM1-specific peptidase domain protein), was recently discovered in human cells by two independent research groups (15,73). ZUFSP demonstrates high selectivity towards K63-linked poly-ubiquitin chains (73–75) and possesses a unique domain structure (15). In addition to the catalytic domain at the C-terminus, it contains four neighbouring zinc finger (ZnF) motifs and a motif interacting with ubiquitin (MIU) at the N-terminus (21). The ubiquitin-binding zinc finger (UBZ) is essential for ZUFSP to interact with and cleave long K63-linked poly-ubiquitin chains (21,73). However, the role of MIU in ubiquitin chain binding and cleavage remains inconclusive. The interaction of ZUFSP with replication protein A (RPA) through immunoprecipitation suggests its potential involvement in DNA metabolism (74,75). Consistent with this, ZUFSP-deficient cells display increased sensitivity to DNA-damaging agents, formation of micronuclei, and DNA damage during the S phase (21,73).

The Arabidopsis genome encodes two ZUFSP homologs, At3g48380 and At5g24680. At3g48380 harbours all predicted ZUFSP domains, while At5g24680 lacks three tandem ZnF motifs (21). The catalytic cysteine residue essential for ZUFSP function is conserved in both Arabidopsis counterparts (21). There are two Alphafold-predicted structures [AF-Q9STL8-F1(At3g48380) and AF-A0A178U8G8-F1(At5g24680)] available in the Alphafold protein structure database. Based on the sequence alignment (18), At5g24680 possesses the same amino acid residues within UBZ and MIU domains of HsZUFSP, considered crucial for long K63-linked ubiquitin chain binding, but also contains neighbouring conserved histidine residues critical for catalysis. The close similarity in the active site region of superimposed structures of HsZUFSP (PDB: 6FGE) and AF-Q9STL8-F1 indicates that the predicted protein of At3g48380 might bind with the ubiquitin in a similar way as HsZUFSP (Figure 1.5). However, the biological and biochemical functions of ZUFSP family members in plants remain to be elucidated.

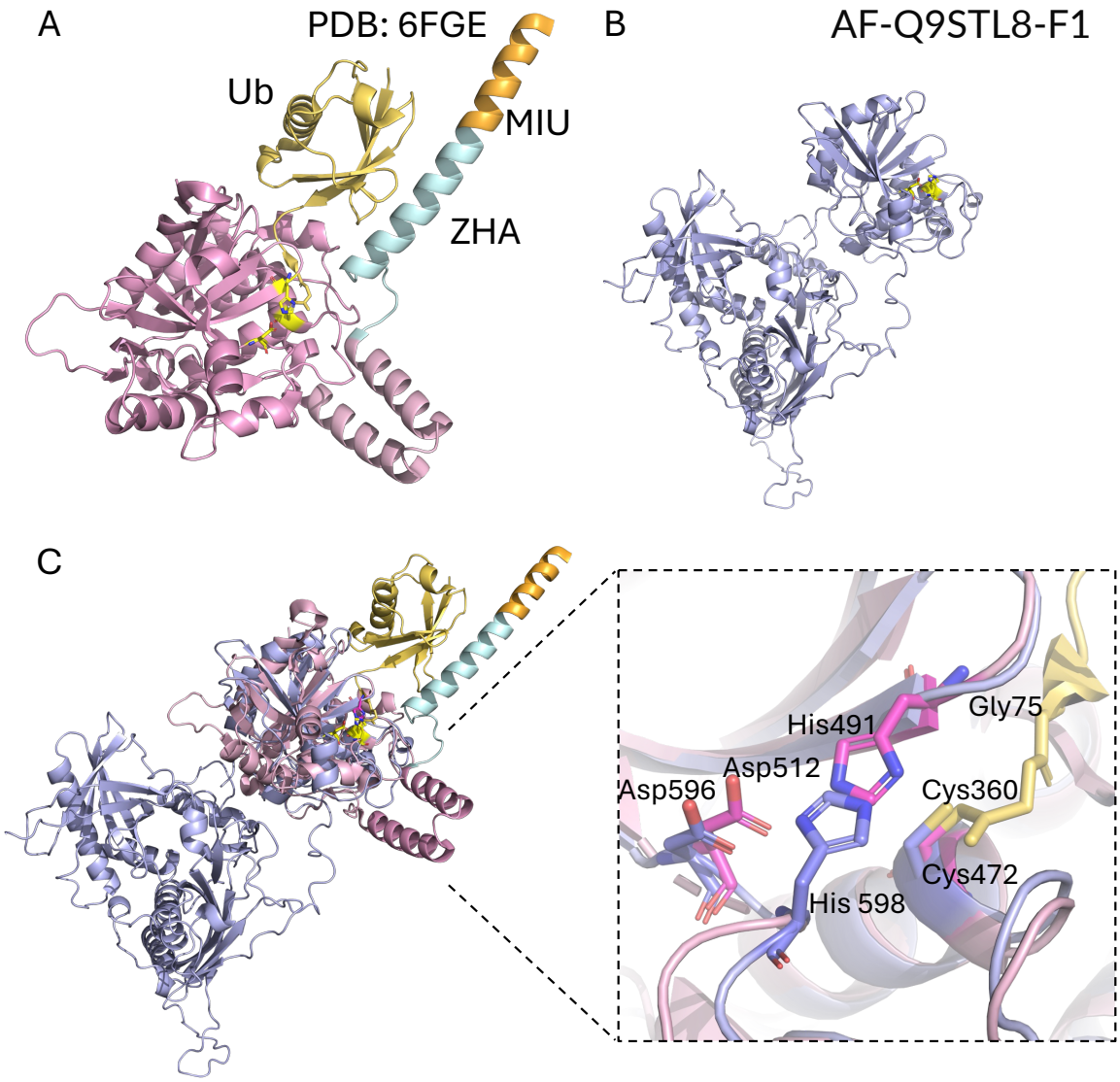

Figure 1. 5 Crystal structure of HsZUFSP bound to Ub (PDB: 6FGE) and compared with Alphafold predicted At3g48380

The HsZUFSP is shown in pink (light and dark), cyan and orange colour with dark yellow coloured Ub (A), and Alphafold predicted structure of At3g48380 (AF-Q9STL8-F1) is shown in light purple. The helical arm is labelled as ZHA (cyan), and the MIU motif is highlighted in orange colour. The superimposition of A and B shows that catalytic residues of Cys360, His 491 and Asp512 of HsZUFSP and Cys472, Asp596 and His 598 of At3g48380 (C). The covalent bond between the Gly75 residue of Ub and catalytic Cys360 of HsZUFSP is depicted in the close-up view.

1.1.6 Motif interacting with Ub-containing novel DUB family (MINDY)

MINDY proteins are a new group of enzymes that remove ubiquitin from proteins. The human MINDY proteins come in two groups, MINDY1/2 and MINDY3/4. MINDY1/2 targets longer ubiquitin chains (>5), and MINDY3/4 targets shorter ubiquitin chains (<6). Both cleave K48-linked chains (18,19,76,77).

These enzymes have a unique structure with a catalytic domain containing unique regions. MINDY1/2 also has a C-terminal Caax signature motif for the prenylation signal and an MIU motif for ubiquitin binding, whereas MINDY3/4 lacks these (18,21). Arabidopsis also has predicted MINDY proteins such as AT4G11860 and AT4G22960, similar to HsMINDY1 and AT1G43690, similar to HsMINDY3, but little is known about their function (Figure 1.6).

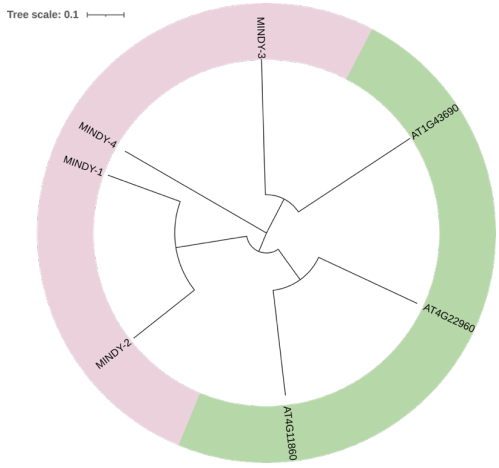

Figure 1. 6 Phylogenetic relationship of MINDY family DUBs of human and *A. thaliana*

Based on the sequence similarity, AT1G43690 is closely related to MINDY-3 and AT4G22960, AT4G11860 are related to MINDY-1 and 2.

1.1.7 JAB1/MOV34/MPR1 PAD1 N-terminal (MPN)(JAMM) domain proteins (JAMM)

The *A. thaliana*, a well-studied plant model, has eight JAMM DUBs classified into two subfamilies: JAMM/MPN+ and JAMM/MPN- (78,79). JAMM/MPN+ DUBs are the active members of the JAMM family, utilizing a zinc ion to cleave specific bonds within ubiquitin chains. They particularly target isopeptide bonds in K63-linked poly-ubiquitin chains (80).

JAMM/MPN- members lack catalytic activity and function as scaffolds within protein complexes (21,80). The yeast protein Rpn11 shares similarities with the Arabidopsis JAMM/MPN+ subfamily. However, Rpn11 requires another protein, Rpn8, to form a complex that alters its activity for cleaving ubiquitin from substrates regardless of the linkage (81). This differs from Arabidopsis JAMM/MPN+ DUBs, which seem to have more specific cleavage preferences. The component of 19s regulatory particle in *Arabidopsis* is identified as the homology of Rpn11 (82). The CSN5 (COP9 signalosome 5) is a JAMM/MPN+ DUB that cleaves a ubiquitin-like protein (Nedd8) (80,83,84) and plays a crucial role in various processes like auxin-dependent plant growth (85–87), seed development and cell elongation (88). The mutant csn5 suggested that CSN5A is required for auxin homeostasis and regulation of H34me3 histone methylation and heat stress (89–91).

An associated molecule with the SH3 domain of the STAM3 (AMSH3) exemplifies both K48 and K63-linked polyubiquitin. It interacts with other proteins involved in vacuole formation, autophagosome degradation, protein sorting within vacuoles (92) and endocytic plasma membrane protein degradation (93) During autophagy-mediated processes, AMSH3 interacts with ESCRT-III (94), and AMSH1 interacts with ESCRT-III subunits of VPS2.1 (94,95) Beyond growth and development, AtBRCC36, another JAMM DUB, plays a vital role in DNA repair processes. Located in the nucleus, it interacts with BRCA1 and is essential for homologous recombination and DNA cross-link repair (96).

As with previous AtDUBs, none of the AMSH DUBs of *A. thaliana* are structurally determined except Alphafold predicted structures. However, the Alphafold predicted structure for AtAMSH3 (AT4G16144: AF-D7MA75-F1) showed a structural similarity to human AMSH-like protein [AMSH-LP (PDB:2ZNV)], and Zn^{2+} recognized active site residues of

AMSH-LP are superimposed with the same amino acid residues of AF-D7MA75-F1 (Figure 1.7).

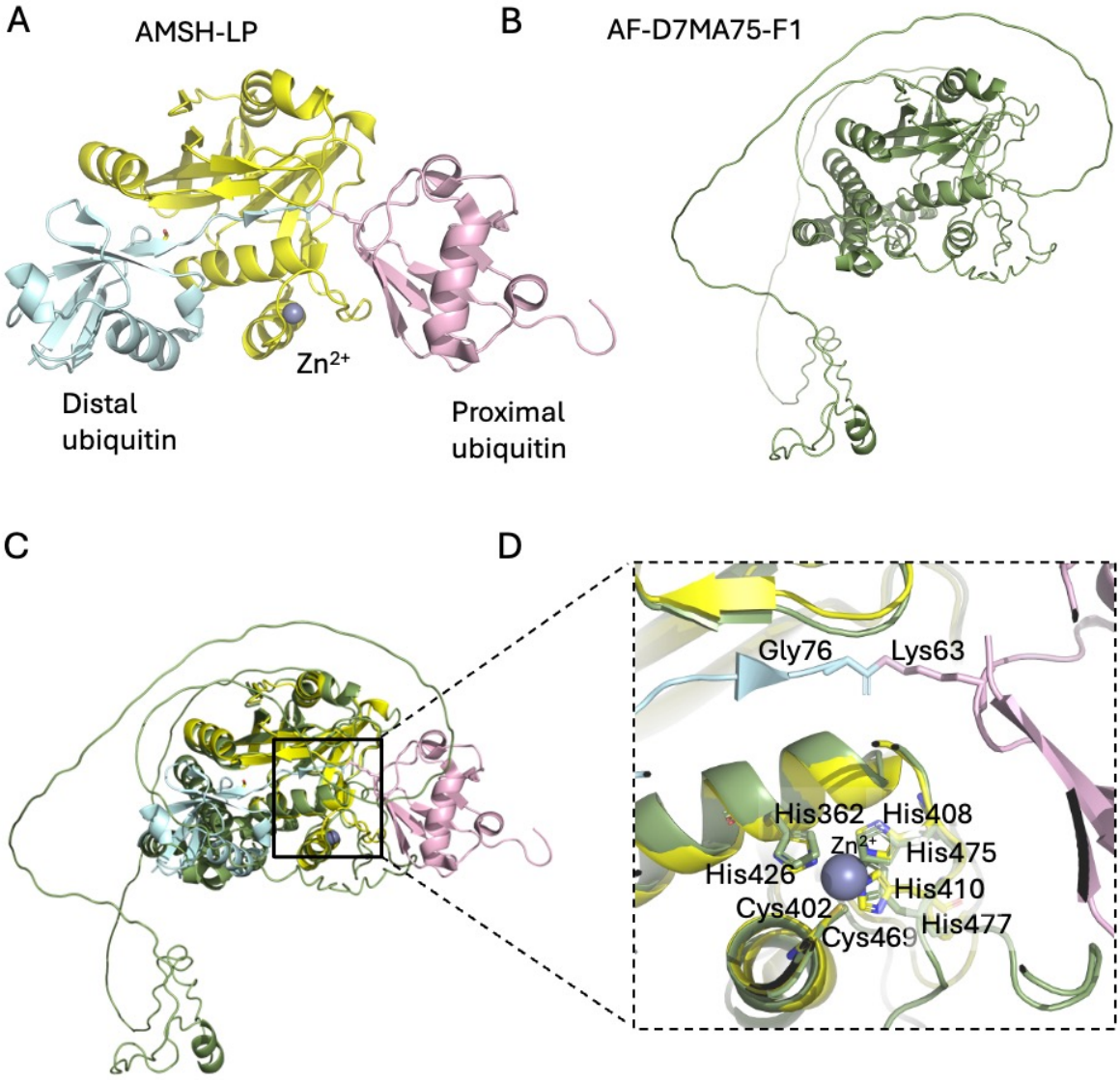

Figure 1. 7 Crystal structure of HsAMSH-LP bound to Ub (PDB: 2ZNY) and compared with Alphafold predicted AtG16144

The HsAMSH-LP is shown in yellow, cyan, and pink-coloured Ub, which present distal and proximal Ub, respectively (A). The Alphafold predicted structure of At4G16144 (AF-D7MA75-F1) is shown in smudge (B). The superimposition of A and B shows that Zn^{2+} recognized amino acid residues His362, Cys402, His408 and His410 of HsAMSH-LP and His426, Cys469, His475 and His477 of At4G16144 (C and D). The covalent bond between the Gly76 residue of distal Ub and the Lys63 residue of proximal Ub is depicted in the close-up view.

1.2 Role of virally encoded deubiquitinases

Viruses are essentially genetic material (RNA or DNA) wrapped in a protein and/or lipid coat and lack the machinery to reproduce on their own; because they cannot reproduce on their own, viruses rely entirely on hijacking the cellular machinery of a host (human, animal, or plant) to replicate (97,98). Despite their dependence on a host cellular molecular machinery for replication, viruses are equipped with their own specialized enzymes, such as viral protease, RNA-dependant RNA polymerase and viral helicase. These enzymes facilitate the production of new viral particles, perpetuating the spread of infection. Among these enzymes, viral protease has a key role in processing long viral polyproteins into functional units, and some of these viral proteases also act as deubiquitinases (20) (99,100). The following sections discuss recent discoveries and insights regarding how viral protease functions during infection. Also, the section discusses how these enzymes are involved in infection-related virulence and how they contribute to counteracting the host defence system.

Several eukaryotic viruses are known to exploit post-translational modification mechanisms of the host to degrade various cellular proteins and thus evade host defence mechanisms during their infection cycle (101,102). Numerous studies have found that both DNA and RNA viruses control the cellular ubiquitin-proteasome system (UPS) for degradation (103–106). Viruses can achieve this by producing deubiquitinases that can remove K48- linked ubiquitin chains and similar modifiers, such as interferon-stimulated gene 15 (ISG15), from cellular proteins. Also, viral DUBs can remove K63-linked chains to suppress Ub-mediated antiviral pathways (107). The deubiquitinating (DUB) activity of the adenoviral Avp protein marks the first occurrence of such a viral protease with such activity (108). The observed escalation in deubiquitinating activity upon adenovirus infection highlights the role of Avp as a cysteine protease, which is vital for viral polyprotein processing and mature viral particle formation. Alongside its DUB activity, the capacity of Avp to process pro-ISG15 into its

mature form establishes Avp as both a protease for viral polyproteins and a deISGylation enzyme (108). Later, in 2004, another group speculated on a potential deubiquitinating domain within the N-terminus of the Crimean-Congo Haemorrhagic Fever virus (CCHFV) massive L protein (109). They hypothesized this based on previous viral DUBs containing Ovarian Tumor Domain (OTU)-like protease motifs, suggesting potential deubiquitinating activity for CCHFV L protein due to its OTU-like domain harbouring zinc-finger-like motifs. Concurrently, the DUB activity of the SARS-CoV papain-like protease (PLpro) was speculated as its ability to deconjugate ISG15, thus aiding viral innate immune evasion (110). This speculation was confirmed in 2005 by Barretto et al. and Lindner et al., who independently verified the DUB activity of SARS-CoV PLpro (111,112). Furthermore, Ratia et al. (2006) elucidated the structural basis of SARS-CoV PLpro deubiquitinating activity, noting similarities with known host DUB proteins and highlighting the structural fold of its N-terminal domain to ubiquitin (113).

Expanding beyond SARS-CoV, Frias-Staheli et al. (2007) reported the DUB activity of two RNA virus OTU domain-containing proteases from disparate viral families. They confirmed the DUB and deISGylation activities of CCHFV L protein and related nairovirus Dugbe virus (DUGV) L protein, as well as arterivirus proteases (114). Subsequent structural studies by Akutsu et al. (2011) and James et al. (2011) further confirmed the DUB and deISGylation activities of the CCHFV OTU domain and explored its binding kinetics with Ub and ISG15 (115,116).

Bergeron et al. (2010) replicated previous findings indicating that the L protein of CCHFV possesses deubiquitinating and deISGylation capabilities. However, they also discovered that the OTU protease activity is not essential for its RNA-dependent RNA polymerase (RdRp) function (117). However, independent research by Tchesnokov et al. (2020) confirmed that the OTU activity of CCHFV RdRp can be inhibited without affecting its

RdRP function (118). Furthermore, the non-structural protein 3 (nsp3) of the porcine epidemic diarrhea virus (PEDV), Xing et al. (2013) discovered the presence of a papain-like protease 2 (PLP2) with DUB activity and inhibits IFN- β (interferon beta) production (119). Likewise, Sun et al. (2010) demonstrated that porcine reproductive and respiratory syndrome virus (PRRSV) encodes a protease with DUB activity in nsp2, which also inhibits IFN-β production (120). Through luciferase-based reporter assays, they further elucidated that PRRSV nsp2 negatively influences NFκB activation. This observation was supported by the inhibition of p65 translocation into the nucleus by nsp2, highlighting its role in modulating host immune responses (120). The DUB activity of papain-like proteases in milder human-infecting coronaviruses, including HCoV-OC43, HCoV-NL63, HCoV-229E, and HCoV-HKU1, has been recently elucidated (107,121,122). Moreover, research has shown that the PLPs of common-cold coronaviruses, along with the PLpros of more pathogenic strains, negatively impact innate immune signaling pathways (121). Notably, highly pathogenic viruses exhibit stronger immune suppression. This phenomenon may correspond to their higher affinity for ISG15 compared to less pathogenic strains, which exhibit stronger binding to Ub (123). In addition, the PLpro enzyme from the MERS coronavirus has also been discovered to possess deISGylation properties, indicating its capability to remove ISG15 from cellular substrates (124). Similarly, investigations have revealed comparable activities in the SARS-CoV-2 PLpro, encompassing polyprotein cleavage, DUB, and deISGylation activities (125–127). Considering that ISG15 binding to host proteins is a post-translational modification involved in antiviral immunity, this deISGylation activity indicates an additional mechanism for the protease to disrupt the innate immune response. Due to the multifaceted functions of the viral DUB enzyme, it has been identified as a highly promising drug target.

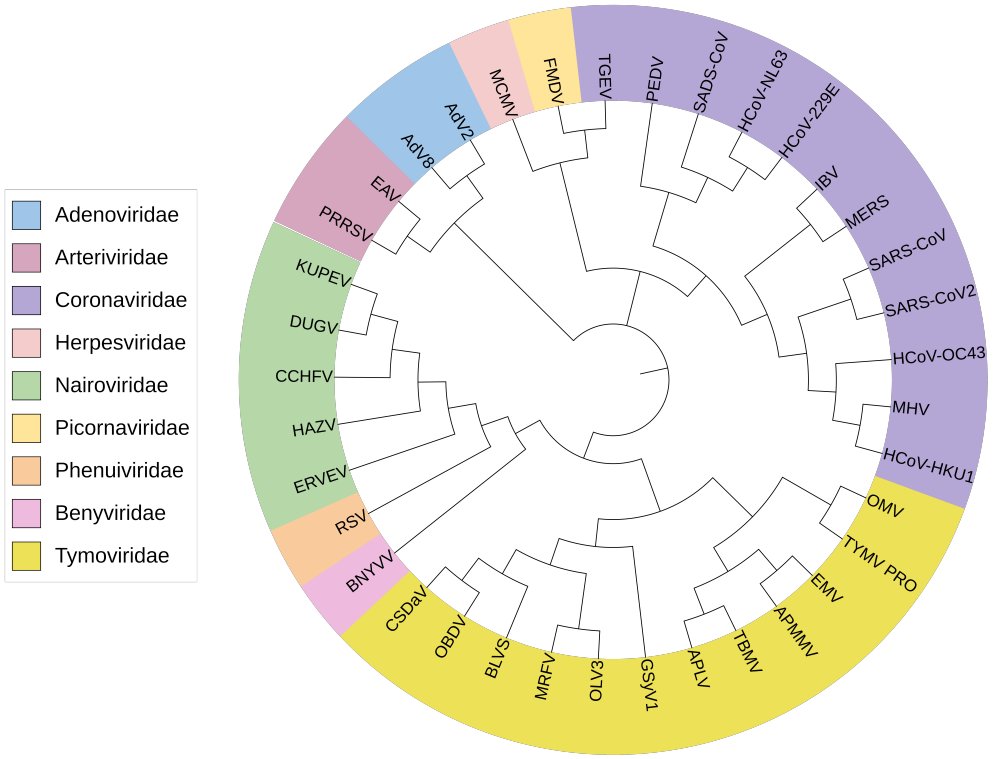

Figure 1. 8 The phylogenetic tree of viral proteases with deubiquitinating activity

The phylogenetic tree was constructed using MEGA 7 software using the maximum likelihood method with 1000 bootstrap replicates. The modifications of the phylogenetic tree were accomplished on the iTOL website, and all the amino acid sequences were obtained from NCBI and PDB websites. The viral DUBs of different viruses are labelled at the tip of the branches, and different colours of branches indicate the different virus families. The arrangement of branches and nodes reflects the inferred evolutionary relationships among these viral families. The HCoV-HKU1 is more closely related to the Adenoviridae family of vDUBs, and BNYVV and RSV families may have a common ancestor based on the node of these branches. Adenovirus 2 (AdV2, PDB:1AVP), Adenovirus 8 (AdV8, PDB:4PIQ), Severe acute respiratory syndrome coronavirus (SARS-CoV, PDB:4MM3), Severe acute respiratory syndrome coronavirus 2 (SARS-CoV2, PDB:6XAA), Human Coronavirus 229E (HCoV-229E, NCBI:NC_002645.1), HCoV-NL63 (NCBI:NC_005831.2), HCoV-OC43 (NCBI:NC_006213.1), HCoV-HKU1 (PDB:7WFC), Middle East respiratory syndrome coronavirus (MERS, PDB: 5W8U), Porcine epidemic diarrhoea virus (PEDV, PDB:6NOZ), Murine hepatitis virus (MHV, PDB:5WFI), Swine acute diarrhoea syndrome coronavirus (SADS-CoV, PDB:6L5T), Transmissible gastroenteritis virus (TGEV, PDB:3MP2), Avian infectious bronchitis virus (IBV, PDB:4X2Z), Foot- and -mouth disease virus (FMDV, PDB: 6FFA), Murine cytomegalovirus (MCMV, PDB:2J7Q), Equine arteritis virus (EAV, PDB:4IUM), Porcine reproductive respiratory syndrome virus (PRRSV, PDB:8EHO), Kupe virus (KUPEV, PDB: 6OAR), Hazara virus (HAZV, PDB: 7JMS), Dugbe virus (DUGV, PDB:4HXD), Crimean-Congo haemorrhagic fever virus (CCHFV, PDB:3ZNH), Erve virus (ERVEV, PDB:5JZE), Beet necrotic yellow vein virus (BNYVV, NCBI ID:NC_003514), Maize rayado fino virus (MRFV, PDB: 7MIA), Blackberry virus S (BLVS, NCBI: NC_038328), Citrus sudden death associated virus (CSDaV, NCBI: NC_006950), Grapevine Syrah virus 1 (GSyV1, NCBI: NC_012484), Oat blue dwarf virus (OBDV, NCBI:

NC_001793), Olive latent virus 3 (OLV3, NCBI: NC_013920), Turnip yellow mosaic virus (TYMV, PMID: 32732284, PDB: 6YPT), Andean potato latent virus (APLV, NCBI:NC_020470), Andean potato mild mosaic virus (APMMV, NCBI:NC_020471), Eggplant mosaic virus (EMV, NCBI:NC_001480), Okra mosaic virus (OMV, NCBI:NC_009532), Tomato blistering mosaic virus (TBMV, NCBI:NC_021851), Rice stripe tenuivirus (RSV, NCBI ID: NC_003755).

Interestingly, several plant viruses also have been found to encode proteases possessing DUB activity, much like the DUB proteases found in +ssRNA animal viruses (Figure 1.8). These plant virus DUBs, similar to their animal virus counterparts, function as proteases, cleaving viral polyproteins into essential functional protein units during replication (128). Additionally, they cleave ubiquitin from host proteins, aiding viral replication by suppressing host antiviral responses (129–131). Plant viral DUBs appear to target host proteins involved in immunity, thus interfering with pathways triggering antiviral defences (132). The presence of DUBs in both plant and animal viruses underscores the advantageous role this enzymatic function plays in virus replication.

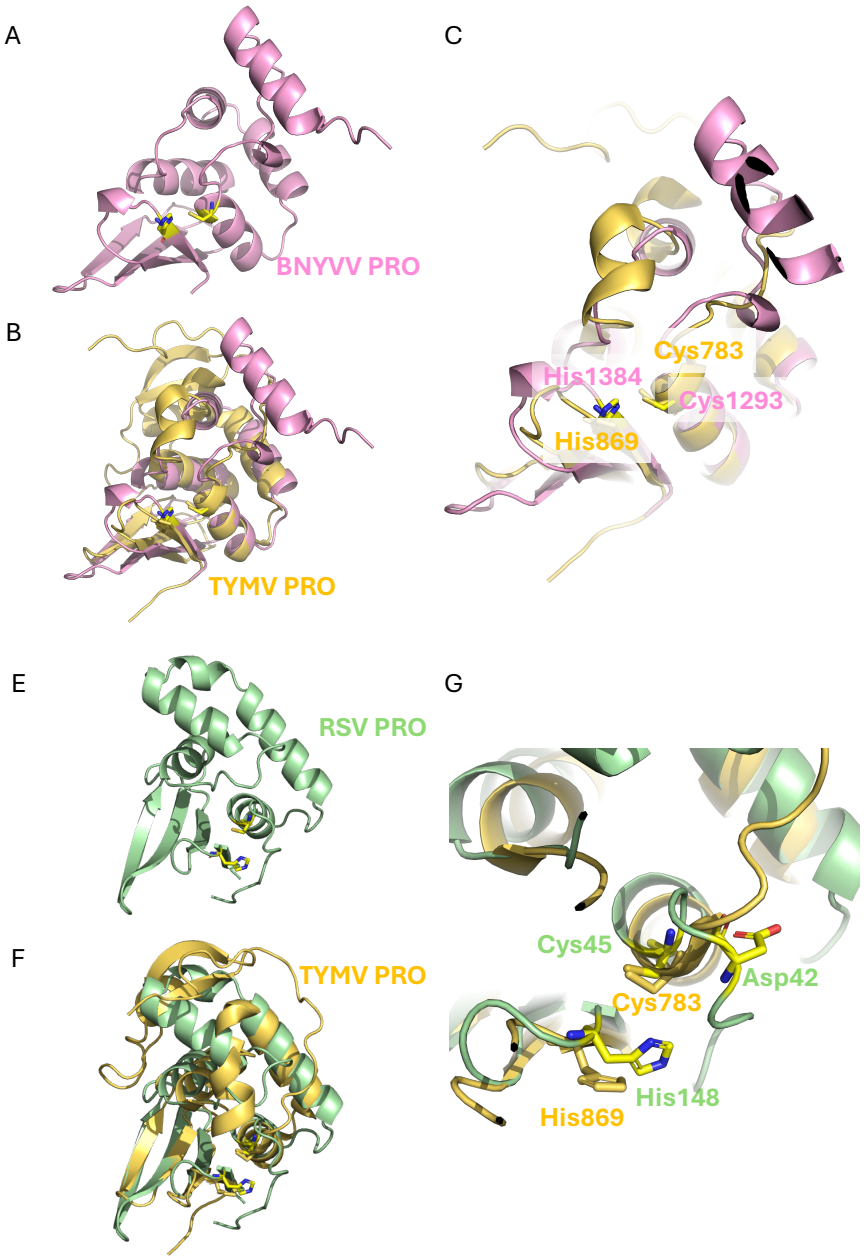

Figure 1. 9 Alphafold structures of BNYVV and RSV proteases and superposition with TYMV PRO

The predicted structures of BNYVV PRO and RSV PRO are depicted in A and E. The superposition structures of BNYVV PRO and RSV PRO with TYMV PRO are shown in B and F. The predicted catalytic site residues are shown in C and G. Predicted structures are generated by ColabFold v1.5.5.

Among the plant viruses that encode DUB proteases, those from the Tymoviridae family are the most extensively characterized. The Tymoviridae family comprises three genera:

Tymovirus, Marafivirus, and Maculavirus (133). Turnip yellow mosaic virus (TYMV) from the Tymovirus genus was the first plant virus demonstrated to contain a protease with DUB activity (134). TYMV has a monopartite positive-strand RNA genome of 6.3kb with three ORFs, one of which encodes a polyprotein of 206 kDa containing the methyltransferase (MET), protease (PRO), helicase (HEL), and RNA-dependent RNA polymerase (RdRP) domains. The viral PRO enzyme cleaves both the RdRp and HEL from the rest of the viral polyprotein (135). Similarly to animal viruses, both proteases are OTU-like deubiquitinating enzymes, and TYMV PRO enhances viral replication by stabilizing the viral polymerase. This is achieved by removing K48-linked poly-Ub chains from the polymerase, preventing its degradation by the plant ubiquitin-proteasome system (132,136,137).

Beet necrotic yellow vein virus (BNYVV) is a member of the Benyviridae family, which causes rhizomania in sugar beets. Since its discovery, it has been one of the most economically damaging diseases worldwide, and it directly affects the sugar production from beets (138). BNYVV is a +ssRNA virus with a multipartite genome consisting of up to five RNA species. BNYVV RNA-1 encodes a polyprotein responsible for replication complex expression and contains a putative papain-like cysteine protease domain (139). This PCP acts as an endopeptidase. However, it has been hypothesized that it may possibly have a deubiquitinating (DUB) activity (140), similar to the papain-like protease domain of the Hepatitis E virus (141). Preliminary AlphaFold structural analysis has shown a high degree of similarity between BNYVV PRO and Turnip yellow mosaic virus (TYMV) PRO, notably in the catalytic site (Figure 1.9). TYMV ovarian tumour (OTU)-like protease has been shown to have DUB activity and is able to switch between the PRO/DUB functions via a mobile loop near the active site (136). Our lab still working on finding deubiquitinase activity of BNYVV protease, and the results showed the BNYVV protease recognized the K63-linked polyUb chains and acted as a deubiquitinase *in vitro* (142).

The rice stripe virus (RSV) is a member of the Phenuiviridae family and causes severe outbreaks in rice cultivation, mainly in China, Japan and Korea (143). RSV genome is composed of four single-stranded RNA and encodes seven proteins (144). The largest polyprotein of vRNA1 encodes RNA-dependent RNA polymerase enzyme and endonuclease (predicted protease). The preliminary Alphafold structural analysis (Figure 1.9) has shown a similar resemblance with the OTU domain of TYMV PRO, and the same catalytic residues (Asp42, Cys45 and His148) suggest that this predicted protease may act as a deubiquitinase during RSV infection. To confirm the prediction of having deubiquitinase activity, Zhao et al., 2021 determined the deubiquitinase activity of the RSV pc1 isolate (145). Three mutants (D42A, C45A and H148A) of RSV protease were constructed and determined that mutations on the catalytic site resulted in the loss of deubiquitinase activity. This demonstrated these residues are required for the deubiquitinase activity of RSV protease. However, understanding how these Tymoviridae, Phenuiviridae and Benyviridae family DUBs manipulate the plant cell to the viral advantage remains a significant area for exploration.

1.2.1 Family Tymoviridae and Role of TYMV PRO

The genomes of TYMV and MRFV were sequenced in the late 1980s and early 2000s, respectively (146,147). Interestingly, their genome sizes are remarkably similar, both around 6.3 kb, with only a 13 nt difference between the two isolates first sequenced (147,148). Structurally, both genomes are 5' capped and arranged similarly, featuring one predominant ORF spanning approximately 90-95% of the genome (147,148). This major ORF undergoes direct translation by the host cell ribosome, yielding the replicase complex consisting of four subdomains: the methyltransferase domain (MET), PLCP domain (PRO), helicase domain (HEL), and RdRp (149).

Both MRFV and TYMV possess movement proteins called p43 and p69, respectively, enabling the viruses to spread from cell to cell and throughout the tissues of the infected host (150). Interestingly, Marafiviral genomes encode two distinct coat proteins, a major and minor version (CP and CP*, respectively). CP is translated from the primary ORF responsible for replicase production, resulting in a large polyprotein where the replicase is fused to CP at the C-terminal of the RdRp. On the other hand, CP* is generated from its own ORF via subgenomic RNA, utilizing a core sequence called the marafibox as its transcriptional promoter (150–152). This approach to structural protein production differs from tymoviruses, where only one coat protein is produced similarly. Marafiviral genomes utilize subgenomic RNA (sgRNA) and a promoter known as the tymobox to generate CP* (153). Conversely, tymoviral genomes lack this mechanism and instead feature a tRNA-like secondary structure at their 3' end in place of a poly-A tail, a characteristic absent in marafiviruses (154). Initially identified in TYMV, this tRNA-like structure has since been observed in numerous other plant-affecting viruses (155). Structurally resembling eukaryotic tRNA, it is thought to interact with eukaryotic elongation factor 1A, enhancing translation efficiency for TYMV (155,156). Additionally, the PRO domain of MRFV self-extracts from the viral polyprotein through *cis* cleavage at the PRO|HEL junction, differing from TYMV, where cleavage at the PRO|HEL junction appears to occur in both *cis* and *trans* (135,157).

Structural characterization has been performed on proteases from TYMV and MRFV (PDB: 6YPT and PDB: 7MIA). In contrast to their closest structural homologues within the ovarian tumour domain, MRFV PRO and TYMV PRO only possess catalytic dyads (MRFV PRO: Cys61, His144, TYMV PRO: Cys783, His869). Superposition of the proteases from TYMV and MRFV bound to Ub reveals exploitable similarities for inhibitor design (Figure 1.10).

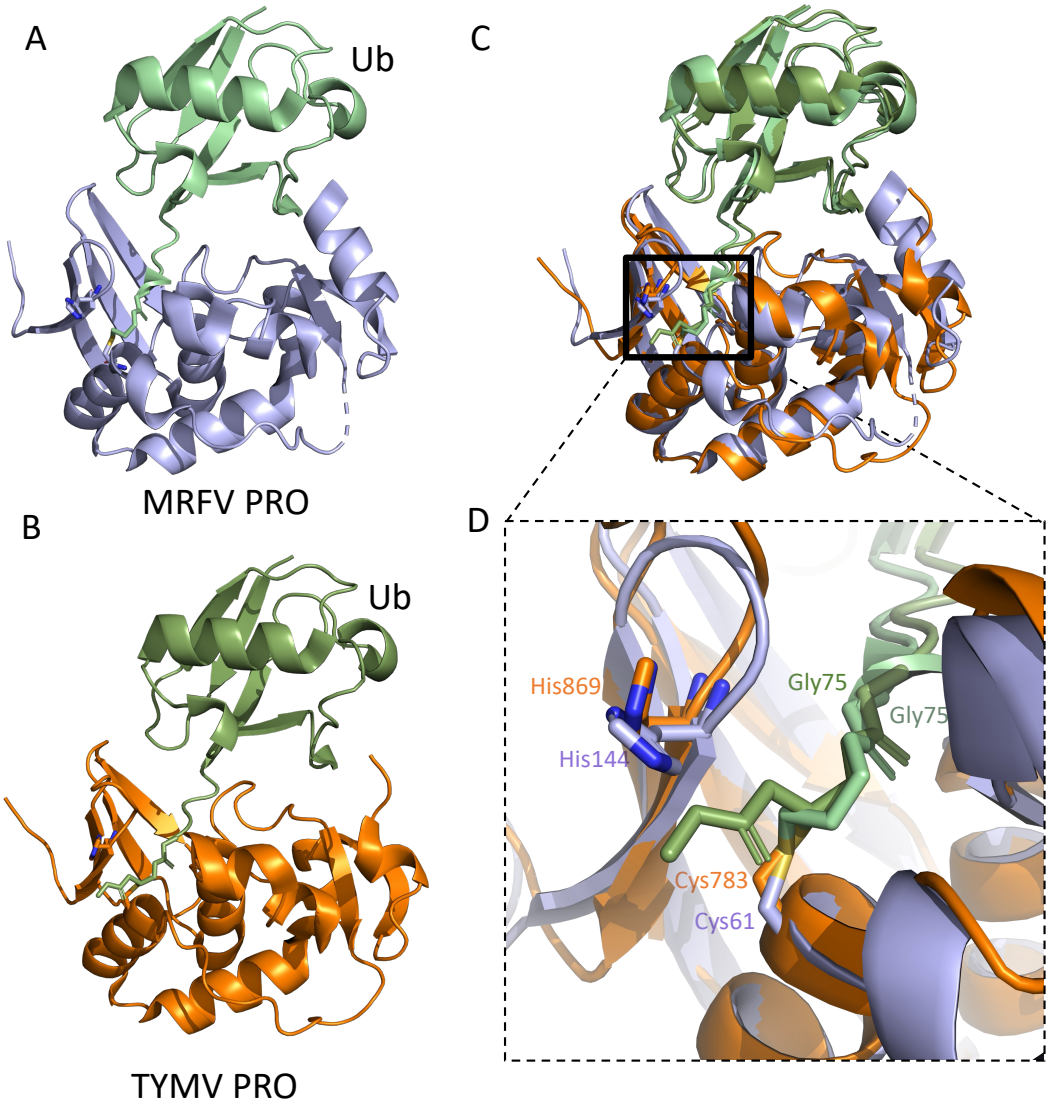

Figure 1. 10 Superposition of the MRFV PRO-Ub and TYMV PRO-Ub

The MRFV PRO is shown in orange, and the TYMV PRO is shown in pale purple. The catalytic residues of TYMV (Cys783 and His869) and MRFV (Cys41 and His144) are depicted in the close-up view.

The sequence similarity suggests that proteases from Andean potato latent virus (APLV), Andean potato mild mosaic virus (APMMV), eggplant mosaic virus (EMV), okra mosaic virus (OMV), and tomato blistering mosaic virus (TBMV) may also possess DUB activity. A recent study revealed that six Marafiviruses, including maize rayado fino virus (MRFV), Blackberry Virus S (BLVS), citrus sudden death-associated virus (CSDaV), Grapevine Syrah virus 1 (GSyV1), oat blue dwarf virus (OBDV), and olive latent virus 3

(OLV3), harbor deubiquitinating activity (157). The predicted structures of APLV PRO and OMV PRO show a close resemblance to TYMV PRO, and catalytic residues of Cys and His are shown in Figure 1.11. This shows that the predicted PRO would act as a deubiquitinase.

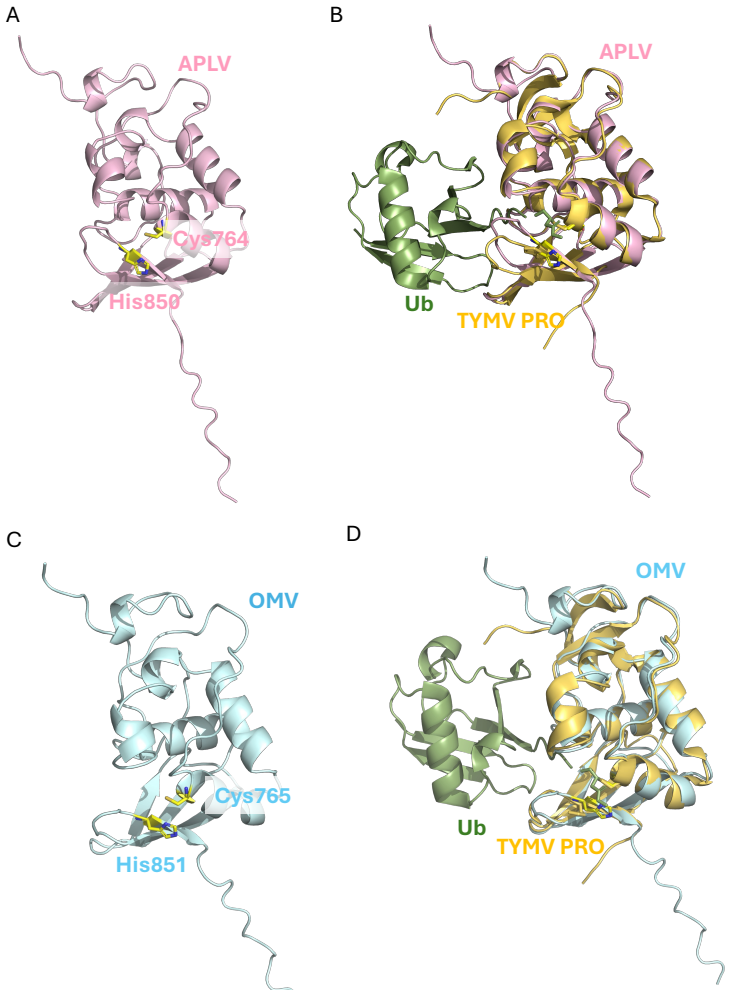

Figure 1. 11 Predicted structures of APLV and OMV and superposition with TYMV PRO

The structures are predicted using AlphaFold2 Colab. The predicted catalytic site residues of APLV (A: Cys764 and His850) and OMV (B: Cys765 and His851) and the superposition structures are depicted in the figures of B and D. Predicted structures are generated by ColabFold v1.5.5.

While approximately half (~45%) of all plant viruses encode proteases (128), little has been done to exploit them as targets for infection control. Most agronomically essential plant viruses, including Potyviridae, Tymoviridae, and Bromoviridae, utilize cysteine proteases as part of their replication and infection mechanism. Thus, these viral proteases could serve as promising antiviral targets.

1.3 Inhibitors targeting the DUB domain of viruses

Most of the proposed inhibitors target cellular DUBs or only main viral proteases. For an example, the inhibitor GRL0617 binds to the Plpro of SARS-CoV and neutralizes its DUB activity *in vitro*. The cell viability assay also showed diminished viral infection (158). Following the emergence of SARS-CoV-2, researchers revisited the potential of a naphthalene-based inhibitor originally developed against SARS-CoV PLpro and proven to restrain the PLpro activity by interfering with its DUB activity (159). This renewed interest led to the discovery of promising candidates like XR8-23 and XR8-24, which exhibited *in vitro* efficacy despite binding to a novel site in the catalytic site of PLpro called “BL2 groove” (160). Further research explored alternative derivatives of GRL0617. One study identified compounds "7" and "14" that displayed superior inhibitory activity against SARS-CoV-2 compared to GRL0617 itself. These compounds bound to the PLpro active site, but concerns remained regarding their stability (161). Another series, named "Jun", showed promising results but shared similar instability issues (162,163). Other promising candidates emerged, such as VIR250 and VIR251, which demonstrated excellent inhibitory activity against both SARS-CoV and SARS-CoV-2 PLpro with good selectivity (127). However, none of these potential inhibitors have yet reached the market. Interestingly, none of the inhibitors are made to target plant viral protease or DUB domain.

A major obstacle in the development of inhibitors is the structural similarity between coronavirus PLpro enzymes and human ubiquitin-specific proteases (USPs) (164). This similarity raises concerns about the potential adverse effects of targeting the viral PLpro. Researchers have attempted to address this challenge by screening potential inhibitors against human USP panels to identify selective candidates (165,166). However, some studies using this approach identified SARS-CoV-2 PLpro drug candidates that also inhibited human USP21, highlighting the ongoing challenge of achieving high viral specificity (167,168). The

ongoing pursuit of SARS-CoV-2 PLpro inhibitors necessitates the identification of compounds with high selectivity for the viral DUBs, minimizing any effect on structurally similar human DUBs.

1.4 Protein-based alternatives to small molecular inhibitors

We have been exploring an innovative approach using variants of ubiquitin to develop protein-based inhibitors against viral DUB enzymes (169). The method utilizes phage-display libraries containing ubiquitin amino acid sequence variants (UbVs) that have been developed by our collaborator Dr. Sachdev Sidhu and his research group (170,171). Using this technique, scientists have successfully identified UbVs that potently and specifically inhibit PLpro from MERS-CoV and SARS-CoV-2, as well as the OTU domain from CCHFV (170,171). These UbVs act as highly specific mutants of ubiquitin, exhibiting remarkably tight binding to their respective viral PLpros (Figure 1.12). Studies have shown that these UbVs effectively inhibit the DUB activity of targeted viral proteases. Additionally, they block polyprotein processing and viral replication of MERS-CoV and SARS-CoV-2 PLpro in cell culture (170,171). Notably, the UbV against SARS-CoV-2 PLpro inhibit its deISGylation activity (170). Compared to traditional small molecule inhibitors against SARS-CoV-2 PLpro, UbVs offer several advantages. Their large surface area and extreme specificity significantly reduce the likelihood of off-target effects (172). However, this specificity also limits their use as broad-spectrum antivirals. On the positive side, UbVs can be rapidly developed if new coronaviruses emerge.

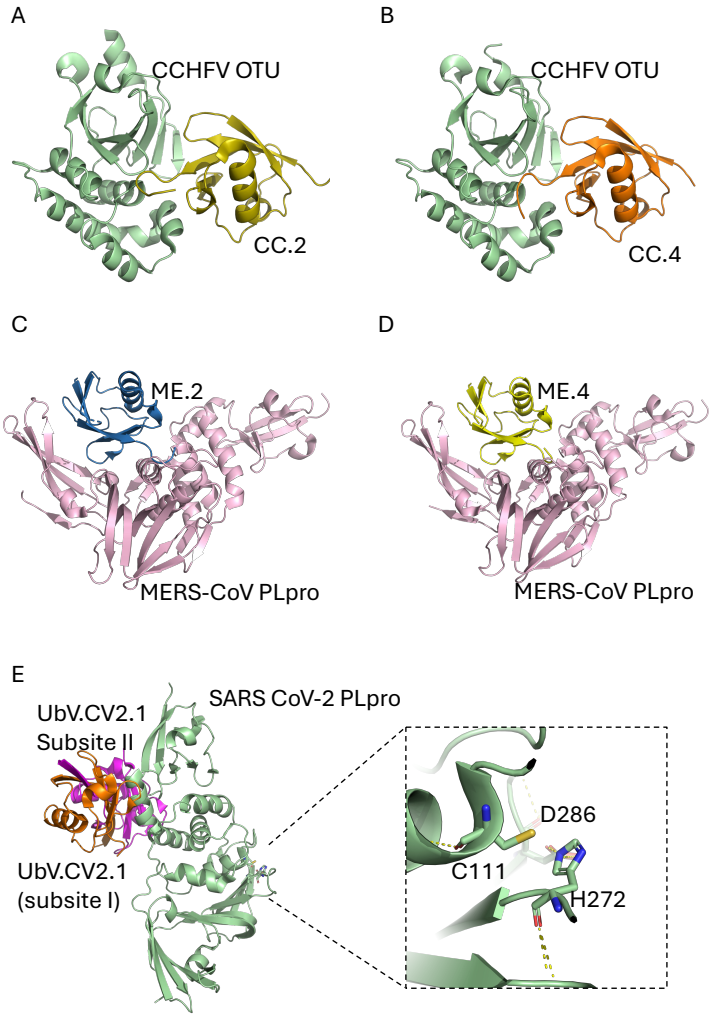

Figure 1. 12 X-ray crystal structures of ubiquitin variants in complex with CCHFV OUT, MERS-CoV PLpro and SARS-CoV-2 PLpro

The Crystal structure of (A) the CCHFV OTU-CC.2 complex (PDB: 5V5H), (B) the CCHFV OTU-CC.4 complex (PDB: 5V5G), (C) the MERS-CoV PLpro-ME.2 (PDB: 5V6A), and (D) the MERS-CoV PLpro-ME.4 (PDB: 5V69). (E) the complex of SARS-CoV-2 revealed that UbV.CV2.1 bound to PLpro as an asymmetric strand-swapped dimer (PDB: 8CX9). The close-up view of the catalytic residues (C111, His272, Asp286) of SARS-CoV-2 PLpro showed that UbV.CV2.1 bound to a novel site distal to the catalytic site. The hydrogen bonds are depicted in yellow dotted lines.

A major hurdle of UbV inhibitor approach is the lack of efficient delivery methods for introducing them into the cytosol of human cells. Given this current limitation, while human applications may not be currently feasible, exploring transgenic approaches in plants could provide proof-of-concept for the use of UbVs to protect cash crops from viral disease (1). Genetic engineering techniques may offer promising tools, such as inserting genes

encoding antiviral UbVs into the genome, potentially creating resistance against critical viruses threatening plant crops and perhaps even animal livestock. Our research is actively exploring these avenues, mainly focusing on the development of a potential approach to introduce UbVs against various plant viruses. By utilizing the model plant *A. thaliana* systems, I aimed to develop genetically engineered *A. thaliana* plants against the Turnip yellow mosaic virus. My research demonstrates the potential to establish UbV-based DUB inhibitors as potent, selective antiviral agents for use in plants.

1.5 Thesis Objectives

Before this work, the UbV inhibitor strategy was studied and demonstrated to effectively inhibit vDUBs of several viruses, including the MERS-CoV, CCHFV and SARS-CoV-2. The delivery of UbVs to human cells or animal bodies is still in progress, however, even though the strategy is working well in cell culture assays. Interestingly, several families of plant viruses also code protease with deubiquitinase activity and it is plausible to develop transgenic plants that express UbVs against plant viruses. Therefore, I started working on plant viruses, mainly TYMV as a model virus, to determine whether this strategy works in the model plant *A. thaliana*. In addition to the main project, I also studied the biochemical characterization of MJD family DUBs of *A. thaliana* and papain-like protease of PRRSV. The detailed objectives are as follows:

1. To generate UbV expressing transgenic *A. thaliana* to determine the efficiency of the UbV strategy *in vitro* and *in vivo* and to evaluate the specificity of UbVs for TYMV protease versus plant deubiquitinase.
2. To identify and characterize the predicted Machado-Josephin Domain family deubiquitinases of *A. thaliana*.
3. To determine the enzyme kinetics of papain-like protease of Porcine Reproductive and Respiratory Syndrome virus.

CHAPTER 2: BIOCHEMICAL ANALYSIS OF TYMV PRO AND UbV3

Contributions Statement:

Dr. Jihyun Hwang constructed the artificial substrate where the cleavage site from the TYMV polyprotein between the PRO domain and helicase and performed the polyprotein cleavage activity of TYMV PRO with the presence of UbV3, Dr. Kihun Kim performed the X-ray structure determination of the complex of TYMV PRO and UbV3 and Dr. Higor Pereira performed the Small-angle X-ray Scattering data analysis.

2.1 Introduction

Ubiquitination is a cellular process that adds one or more copies of the 76 amino acid protein ubiquitin (Ub) to cellular target proteins (173). This protein modification system plays a crucial role in regulating many essential cellular processes, such as protein degradation, hormonal signaling, cellular immunity and abiotic stress signaling and responses (174). It is reversed by DUBs that remove Ub from cellular proteins (175). Interestingly, plant and animal viruses have developed strategies to manipulate the Ub system to promote their ability to infect and replicate in host cells through the use of virally encoded proteases that have DUB activity (100,106). Viral DUBs deubiquitinate cellular proteins to suppress Ub-dependent antiviral responses of the cell, which contributes significantly to viral pathogenesis during infection *in vivo* (102,132,176). Viral DUBs also play an essential role in virus replication by processing viral polyproteins during virus replication (124,177–179), making them promising targets for developing antiviral strategies.

Given the role of viral DUBs (vDUBs) in polyprotein processing in addition to suppressing Ub-mediated antiviral responses (20), antiviral strategies targeting these enzymes might be helpful to protect plants and animals from viruses that encode these enzymes. However, their structural and functional similarity to host deubiquitinases poses a challenge when designing vDUB-specific inhibitors. To address this challenge, the Mark laboratory, in collaboration with the laboratory of Sachdev Sidhu (University of Waterloo), has employed a strategy capable of identifying remarkably specific protein-based inhibitors of vDUBs from phage-displayed libraries of ubiquitin variants (UbV) (180). Using this approach, several UbVs have been isolated that selectively and potently block the vDUB activity from several viruses, including the Middle East Respiratory Syndrome coronavirus (MERS-CoV) (171), Crimean Congo Hemorrhagic Fever Virus (CCHFV) (171) and Severe Acute Respiratory Syndrome

Coronavirus 2 (SARS-CoV-2) (170). UbVs targeting these viruses block their DUB activity and polyprotein processing, which, in turn, block virus replication in cells (170,171).

Though UbVs are effective inhibitors of vDUBs, a remaining challenge is how to deliver these small proteins into animal cells. In contrast, transgenic expression of UbVs in plants could provide a powerful new strategy to protect plants against infection by viruses that encode vDUBs. While not all plant viruses encode viral proteases with deubiquitinase activity, five major plant virus genera *Tymovirus, Marafivirus, Tenuivirus, Benyvirus and Carlavirus* contain viruses that encode proteases with bona fide or putative DUB activity (157). Several viruses from the genera can cause significant crop yield losses, such as *Maize Rayado Fino Virus* (*Marafivirus*) (181), *Turnip Yellow Mosaic Virus* (*Tymovirus*) (131), *Beet Necrotic Yellow Vein Virus* (*Benyviruses*) (182), *Rice Stripe Tenuivirus* (*Tenuivirus*) (183).

To explore the use of UbVs as a strategy to protect plants from viral infection, I joined the Mark laboratory to determine if UbVs could be used to block Turnip Yellow Mosaic Virus (TYMV) replication in plants. TYMV is a model plant virus that encodes a vDUB that suppresses Ub-dependent antiviral responses and is vital to virus replication as a protease that processes the viral polyprotein (20,134,135). TYMV is a single-stranded RNA plant virus that can cause significant damage to plants, particularly turnips and other members of the *Brassicaceae* family(184–186). It primarily infects the plant leaves via flea beetles, causing symptoms such as mosaic patterns, yellowing and leaf distortion. Infected leaves may also become necrotic as the virus replicates and spreads through the plant (187). TYMV can also reduce the yield and quality of crops by reducing the size and number of reproductive parts. It can also weaken plants and make them more susceptible to other pathogens and environmental stresses, such as drought or extreme temperatures (184). The vDUB encoded by TYMV is commonly known as PRO and was the first plant virus deubiquitinase to be characterized (188). TYMV PRO appears to suppress host antiviral immune responses by removing Ub from the

viral polymerase to avoid degradation of the viral polymerase (134). Crystal structures of TYMV PRO have revealed that the protease shares structural similarity with the Ovarian Tumor domain family (OTU) of deubiquitinases (58).

In this study, several UbVs that bound tightly to the deubiquitinase and their selectivity were determined. The most potent UbV inhibitor was chosen for further structural and functional characterization with TYMV PRO, revealing that the UbV exists as a domain-swapped dimer that binds to a single copy of the PRO enzyme. Consistent with UbVs targeting animal viruses, we found that the TYMV PRO UbV inhibitor was highly specific for PRO and did not appreciably inhibit a panel of functionally related plant DUBs from the model plant system *A. thaliana*. Our findings provide a promising new strategy to inhibit the replication of economically important plant virus replication that could provide important cash crop protection from viral infection through transgenic expression.

2.2 Materials and Methods

2.2.1 Construction of protein expression plasmids

Synthetic DNA (IDT: Integrated DNA Technologies) coding for the catalytic domain of the TYMV PRO and the catalytic domain of AtAMSH3 (92) as purified by PCR using primers listed in Table 2.1 and ligated into pGEX-6P-1 (GE Healthcare) using BamHI and XhoI restriction sites (5' and 3', respectively). Synthetic DNA coding for the catalytic domain of TYMV PRO, AtUCH2, AtOTLD1 and AtAT3G was purified by PCR using primers listed in (Table 2.1) and ligated into pET19b (Novagen) and pET28a using NdeI and BamHI restriction sites.

Table 2.1 DNA Constructs

Oligo Name	NCBI Reference Number	Primers (5' to 3')
GST-TYMV PRO	NC_004063.1	Forward Primer: GATATAGGATCCGGCTCCTCACAATTACTGCC Reverse Primer: GGTAAACGTCTCTTAGGCTCTTAACTCGAGGATATA
His6-TYMV PRO	NC_004063.1	Forward Primer: GATATACATATG GGCTCCTCACAATTACTGCC Reverse Primer: GGTAAACGTCTCTTAGGCTCTGGATCCGATATA
GST-AtAMSH3	NM_148342.8	Forward Primer: GATATAGGATCCAAAATCGATCTTAATAAAGTGG Reverse Primer: CCTTCTGCATGTAATTTCTTAACTCGAGGATATA
His6-AtOTLD1	NM_001202687.2	Forward Primer: GATATACATATGACCCGCATTTTAGTC Reverse Primer: GTAAAGGAAAAGCCACAGAAGGATCCTATATC
His6-AtUCH2	NM_105238.3	Forward Primer: GATATACATATGTCCTGGTGCACTATTGAAT Reverse primer: GACCGAATCATCCACGGGATCCTATATC
His6-AtAT3G	NM_115273.4	Forward Primer: GATATAGGATCCGAACGCACCAGCAAC Reverse Primer: GAAACCGAAAAACAGAAAGGATCCTATATC

2.2.2 Selection of Ubiquitin Variants

The phage-display technique was used in this study to develop ubiquitin variants (180). Protein immobilization and the following UbV selections were made according to established

protocols (170,171,189). Briefly, purified viral protease (GST-tagged TYMV PRO) was coated on 96-well MaxiSorp plates (Thermo Scientific 12565135) by adding 100 µL of 1 µM proteins and incubated overnight at 4 ºC followed by five rounds of selections using the phage-displayed UbV library as described (189,190). The selected UbV sequences were inserted into the pET DEST plasmid. Plasmids named pET53 DEST-UbV1, pET53 DEST-UbV2, pET53 DEST-UbV3 were transformed into $CaCl_2$-competent *Escherichia coli* BL21 (DE3) Gold cells to allow for T7 polymerase-driven expression of N-terminally His_6-FLAG-tagged UbVs.

2.2.3 Construction of mutants of UbV3 using site-directed mutagenesis

Single point mutations (V10G, R6K, R6A) were generated in the UbV3 expression construct pET53 DEST-UbV3 using the Q5 site-directed mutagenesis kit (NEB, cat. E0554S). *E. coli* BL21(DE3) Gold cells were transformed with a mutated plasmid.

2.2.4 Protein expression and purification of TYMV PRO, plant DUBs and UbVs

Expression plasmids described above were used to transform *Escherichia coli* BL21 (DE3) GOLD cells (Stratagene) for subsequent recombinant protein production. Transformed *E. coli* were grown overnight at 37 °C in LB (lysogeny broth) containing appropriate antibiotics (Ampicillin,150µg/mL or Kanamycin, 50µg/mL). The overnight culture was then used to inoculate 1 l of fresh LB with appropriate antibiotics (1:50 dilution) and was grown at 37 °C with shaking to an OD_{600} of 0.7 to 0.8. Expression of GST-tagged enzymes (from pGEX-6P-1 constructs) or His_6-tagged enzymes (from pET19b and pET28a) was induced by the addition of 0.5 mM IPTG and then incubated with shaking at 16 °C for an additional 18 h. After 18 hours of incubation, cells were pelleted by centrifugation.

Cell pellets of GST-tagged enzymes were resuspended in ice-cold lysis buffer (50 mM TRIS- HCl pH 8.0, 300 mM NaCl and two mM DTT) and lysed using an Avestin Emulsiflex

C3 high-pressure cell homogenizer. Cell lysates were purified by centrifugation (13,500 rpm at 4 °C for 40 minutes). The supernatant containing GST-tagged enzymes was mixed end-over-end for one h at 4 °C with GST-Bind resin (Millipore), pre-equilibrated in the lysis buffer. The lysate/resin slurry was poured into a gravity column and washed with two column volumes of the lysis buffer, followed by elution of the GST-tagged fusion proteins with the lysis buffer supplemented with ten mM reduced glutathione (pH 8.0 with NaOH). The GST tag was removed from each enzyme using GST-tagged HRV 3C PreScission Protease (GE Healthcare), which was incubated with the eluted fusion protein in dialysis tubing overnight at 4 °C with a two-litre of dialysis buffer (20 mM Tris HCl, pH 8.0, 150 mM NaCl, and 2 mM DTT). After dialysis, the enzymes were purified using a Superdex 75 (GE Healthcare) gel filtration column and Superdex 200 (GE Healthcare) gel filtration column.

Cell pellets of His_6-tagged enzymes were resuspended in ice-cold lysis buffer (50 mM Tris HCl, pH 8.0, 300 mM NaCl, 2 mM DTT, and 5 mM imidazole) and lysed identically to the GST-tagged enzymes. Cell lysates were purified by centrifugation (13,500epm at 4°C for 40 minutes), and supernatants containing proteins were mixed end-over-end for 1 h at 4°C with nickel-nitrilotriacetic acid resin (Qiagen), pre-equilibrated in the lysis buffer. The mixture of lysate and resin slurry was then poured into a gravity column and washed with 20 column volumes of the lysis buffer, followed by ten column volumes of the lysis buffer supplemented with 15 mM imidazole, followed by ten column volumes of the lysis buffer supplemented with 30 mM imidazole and finally eluted with the lysis buffer supplemented with 450 mM imidazole. The eluted proteins were dialyzed against 2 L of dialysis/gel filtration buffer (20 mM TRIS-HCl pH 8.0, 150 mM NaCl and 2 mM DTT) overnight at 4°C and then further purified using a Superdex 75 gel filtration column and Superdex 200 gel filtration column.

2.2.5 EC_{50} and IC_{50} Assays

To measure the half-maximal binding concentration (EC50) of UbVs binding to viral proteases, the concentration of UbVs or wild-type Ub was varied from 0 to 4 μM (24 points, 1:2 dilution), while the concentration of target proteins immobilized on the plate remained at 1 μM. EC_{50} values were calculated using the GraphPad Prism software with the built-in equation formula (non-linear regression curve). Three potential UbVs (UbV1-3) were identified.

The initial rates of each reaction were calculated to measure the IC_{50} values. Assuming the enzymes follow Michaelis-Menten kinetics, the initial velocity (intensity) was plotted against UbV3 concentrations using GraphPad Prism. The data was fitted to a four-parameter sigmoid Hill curve model (Sigmoidal, 4PL), and IC_{50} values were calculated using GraphPad Prism.

2.2.6 ELISA assays to evaluate the binding and specificity of UbVs and deubiquitinases

The ELISA assay was used to determine the binding specificities of the UbVs towards a panel of plant DUBs and TYMV PRO. As previously described (171), proteins were immobilized on a MultiScreen 96-well polystyrene flat bottom clear ELISA high binding plate (Millipore) at 2 mg/mL and incubated overnight at 4 ºC. Then, 300 nM of FLAG-tagged UbVs was added and bound UbV protein was detected by the addition of an anti-FLAG HRP antibody (GenScript). The colourometric assay was initiated by the addition of the TMB (3', 5, 5' tetramethyl benzidine) peroxidase substrate (mixture of equal volume of TMB substrate A and B, BioLegend). The reaction was stopped by adding a BioLegend Stop Solution (Cat. No. 423001), turning the colour from blue to yellow. The absorbance of the plate was read at 450 nm using SpectraMax iD5 Multi-Mode Microplate Reader (Molecular Device, USA), and the mean of the absorbance was represented in a heat map on a white (minimum value)–black

(maximum value) gradient using GraphPad Prism software (v.9.5.1). The data is in Appendix, Table A19.

2.2.7 Ub-AMC deubiquitinase assay

All deubiquitinases, including TYMV PRO, were assayed against the fluorogenic substrate analogue 7-amino-4- methyl-coumarin (AMC)–Ub (Ub-AMC) (Boston Biochem). The reaction buffer for all assays consisted of 50 mM Tris-HCl (pH 8.0), 150 mM NaCl, and 2 mM DTT. The substrate in the reaction buffer was placed in a black, flat-bottom 96-well microplate (Corning Life Sciences), and the different concentrations of the enzyme were added immediately before readings (113). The final reaction volume was 100 µl. Time-course kinetics assays were carried out using a SpectraMax iD5 microplate reader (Molecular Devices). The monochromators of the instrument were set to excitation of 360 nm and emission of 460 nm. The PMT gain was medium, and reads were taken every 20s. The graph of deubiquitinase activity for each deubiquitinase was plotted using the relative fluorescence units (RFU) against time (sec) using GraphPad Prism.

2.2.8 Michaelis-Menten Kinetic of TYMV PRO

Enzyme kinetics assays were performed at 25 °C in black-round bottom 96-well microtiter plates (Corning Inc.) using Ub-AMC (R&D Systems) as substrate. Reaction progress was monitored by fluorescence using a SpectraMax iD5 Multi-Mode Microplate Reader (Molecular Devices), and data were collected using SoftMax Pro Software. Reactions were carried out at 25°C for 3,600s in 50mM Tris HCl pH 8.0, 100mM NaCl and 5mM DTT with 500nM of TYMV PRO with Ub-AMC substrate ranging from 0-50µM. Fluorescence was monitored at $\lambda_{Ex}/\lambda_{Em}$=360/460nm. Data were analyzed using SigmaPlot and GraphPad Prism 9.0. The initial velocity was determined using linear regression analysis, and the data was

plotted against the different Ub-AMC substrate concentrations (0-50μM). Initial rates were calculated as a previously established method (191) , and the Km and V_{max} were determined using the Michaelis-Menten model in GraphPad Prism (v.9.5.1).

2.2.9 Inhibition Assays

The deubiquitinase activity of TYMV PRO and *A. thaliana* plant DUBs using Ub-AMC (1μM) as substrate was measured in the presence of increasing concentrations of UbV3 to measure the ability of the UbV to inhibit the proteases. Progress curves were fitted to a non-linear regression equation to determine the initial rate of each reaction using SigmaPlot software. Initial rates were plotted against UbV3 concentrations using GraphPad Prism (v.9.5.1). To measure inhibitor potency; V/V_o were plotted against different concentrations of UbV3. The data was fitted to a four-parameter sigmoid Hill curve model (Sigmoidal, 4PL, X is the inhibitor concentration) (192), and IC_{50} values were calculated using GraphPad Prism. If no data point achieved 50% inhibition, then the absolute IC_{50} was reported as >X nM or X μM (where X is the highest tested concentration) (193).

2.2.10 K48- and K63-linked polyUb chain cleavage assay with the presence of UbV3

Using recombinant human polyubiquitin chain [K48- linked (UC-220), K63- linked (UC-320) Boston Biochem)] as substrates, the ability of UbV3 to inhibit TYMV PRO activity against these substrates was measured in 50 mM Tris-HCl, pH 8.0, 100 mM NaCl, 1 mM DTT containing 1μg of polyUb substrate, 2 μM TYMV PRO and 0-2 μM UbV3. After incubation at 25°C for 30 min, reactions were stopped by adding 2X Tris-Tricine SDS PAGE sample buffer. Protein samples were denatured at 40°C for 20 minutes. Reactions were visualized by carrying out TRIS-Tricine SDS PAGE (10%) and subsequent detection using a Pierce Silver Stain Kit (Thermo Fisher Scientific).

2.2.11Cleavage of the Pro↓Hel site from the TYMV polyprotein by PRO and its inhibition by UbV3

A fusion protein containing the PRO cleavage site Pro↓Hel from the TYMV polyprotein was constructed as follows: The open reading frame (ORF) of PRO and the first 10 amino acids of Hel were fused to the N-terminus of the glycosidase NagZ (GenBank ID: OEOG01000025) (194,195)(196). The Pro↓Hel cleave site is located between the open reading frames of PRO and Hel (Figure 2.4). NagZ was used to replace Hel to ensure expression of a soluble fusion protein. This fusion construct was synthesized by IDT and cloned into pET Duet using AsiSI and XhoI sites. The ORF encoding UbV3 was cloned into the partnering cassette of pET Duet using BamHI and SalI sites. Two pET Duet constructs were created, one with UbV3 and one without (Figure 2.4).

The resulting plasmids were used to transform *E. coli* BL21(DE3) for subsequent protein expression. Transformed *E. coli* were incubated in LB medium with 100 μg/mL of ampicillin at 37°C, 180 rpm. When the OD600 reached 0.5, IPTG 0.5 μM was added to the medium. The temperature was lowered to 18 °C, and the culture medium was harvested overnight. The cells were lysed by homogenizer in a lysis buffer (20 mM Tris-HCl pH 7.5, 150 mM NaCl, 10mM beta-mercaptoethanol). After centrifugation at 13000rpm, 4 °C for 50 minutes, supernatant was collected for analysis.

Protein in clarified lysates were separated on 12% tricine-SDS-PAGE and then transferred to PVDF membrane. The membrane was stained with Ponceau S to verify consist of sample loading (Figure S3). The membrane was blotted using anti-Flag antibody-HRP(GenScript, A01428), and anti-HIStag antibody-HRP (Thermo, PI15165). The cleavage or inhibition of cleavage of the PRO-NagZ fusion protein was determined by visualizing the cleavage products and intact fusion protein.

2.2.12 Gel filtration protein coupling of TYMV PRO and UbV3

Purified TYMV PRO was mixed with a 2-fold molar excess of UbV3 at room temperature for 1 h, with the addition of TCEP [Tris (2-carboxyethyl) phosphine

hydrochloride] to a final concentration of 5mM in order to stabilize the enzyme reaction. To verify protein-protein interactions and purify the resulting complexes, the TYMV PRO:UbV3 complex was separated from excess UbV3 by gel filtration. The resulting complex mixture was purified using a Superdex 75 gel filtration column (GE Healthcare), eluting in 20 mM Tris pH 8.0, 150 mM NaCl and 2 mM DTT.

2.2.13 Covalent linkage of UbV3 and TYMV PRO

The open reading frame for UbV3 (lacking the N-terminal 6xHis and FLAG tag) was ligated into vector pTYB2 using restriction enzymes *NdeI* and *SmaI* to generate pTYB2-UbV3. *E. coli* BL21(DE3) Gold cells were transformed with pTYB2-UbV3 and cultured in LB media (Ampicillin added) at 37°C. Upon reaching an OD_{600} ~0.6, the culture was cooled to 18°C and supplemented with 0.5mM IPTG to induce recombinant protein expression for 18 hours with shaking. Cells were harvested by centrifugation and lysed in the lysis buffer (50mM HEPES pH 6.5 100mM sodium acetate) by using an Emulsiflex cell disruptor. After lysis, cell debris was removed by centrifugation and the supernatant was mixed with chitin resin (NEB, cat. S6651L) at 4°C for 1 hour. Resin was washed with lysis buffer and MES-Na (mercapthanesulfonate sodium salt) was added up to 50mM. After 16 hours of incubation at 37°C, resin was washed with lysis buffer and the flowthrough was collected.

As previously described (197), 200mM 3-bromopropyl hydrobromide and 0.2 equivalent volume of 2M NaOH was added. After 20 minutes the reaction was quenched by adding 0.2 equivalent volume of 2M HCl. Final sample was dialyzed in the 50mM sodium acetate pH 4.5 150mM NaCl at 4°C for 2 hours. The sample was further dialyzed in buffer (20mM Tris pH 8.0 150mM NaCl), and then purified by size exclusion chromatography (Superdex 75). 1:1 molar ratio mixture of purified UbV3-Br and TYMV PRO was incubated

at 37°C for 2 hours. After incubation, it was purified by size exclusion chromatography (Superdex 75) with same buffer.

2.2.14 Crystallization and Structure Determination

A single peak corresponding to the dimer of UbV3 was pooled from the size exclusion chromatography and concentrated to 8 mg/mL for crystallization trials. Initial crystals were observed from preliminary screens (PEGs, PEGs II suite, NeXtal Cat. #130904, #130916) then optimized conditions were set up for sitting drop vapour diffusion crystallization at 20°C. The total drop volume was 2μL, containing equal volumes of the protein and the crystallization solution. Diffraction quality crystals of dimeric UbV3 appeared in 15% PEG 1000, 0.5M Ammonium Sulfate after 7 days. Crystals were cryoprotected with mother liquor supplemented with 15% glycerol and flash cooled in liquid nitrogen. X-ray diffraction data were collected using a Rigaku MicroMax-007 HF X-ray generator and R-axis detector. Data were indexed and integrated by XDS package (198), merged, and scaled by Aimless (199). The structure was determined by molecular replacement using Phaser (200) and ubiquitin (PDB: 1UBQ) as the search model. Atom coordinates of the exchanged loop β1-β2 region were manually fitted and refined by Phenix-refine (201).

Covalently linked TYMV PRO:UbV3 dimer complex was concentrated to 12mg/mL, and crystallized by mixing an equal volume of protein sample and crystallization mother liquor (1.5M ammonium sulphate 100mM Bis-Tris pH 6.5 100mM NaCl) using the sitting drop vapour diffusion method. Crystals appeared 2 weeks after set up, and were cryoprotected in the mother liquor supplemented with 22.5% ethylene glycol before flash cooling in liquid nitrogen. The X-ray data collection strategy was the same as described above. Collected data were indexed and merged using XDS and scaled by Aimless. The structure was determined by molecular replacement using Phaser, using TYMV PRO (PDB: 6YPT) and the UbV3 dimer

determined before as search models. The complex was further fitted into the resulting electron density manually and refined by Phenix.refine.

2.2.15 Small-angle X-ray Scattering Analysis

Purified UbV3 dimer from size exclusion chromatography was sent to B21 BioSAXS beamline at Diamond Light Source (Didcot, Oxfordshire, UK). A complex of UbV3 dimer and TYMV PRO was purified by size exclusion chromatography before being sent to DLS. All samples were in the same buffer (20mM Tris pH 8.0, 150mM NaCl, 2mM DTT). Samples were concentrated to ~5mg/mL, 80uL of samples were loaded on the Shodex KW402.5-4F column at the beamline B21. The ATSAS suite version 2.8 (202) and Chromixs (203) were used to analyze the scattering data, with Chromixs used to correct for buffer baseline on the samples' peak intensity. Guinier analysis (q2vs. ln(I(q))) (204) was employed to determine the quality of the samples and the radius of gyration (R_g). The folding was characterized by generating a dimensionless Kratky plot (qR_g vs. qR_g^2*I(q)/I(0)) (205). Real-space R_g and the maximum particle dimension (D_{max}) were calculated using a paired distribution function (P(r)). The P(r) plot served as input data for DAMMIN, which produced twenty models in each condition using different seeds for each model and equal parameters to ensure symmetry (206). An average model was obtained using DAMAVER, and a filtered representative structure model was created using DAMFILT (206,207).

2.3 Results

2.3.1 Screening of UbVs that bind with TYMV PRO

The TYMV PRO enzyme was expressed as a soluble and active DUB in *Escherichia coli* with its N-terminus fused to a removable (HRV-3C cleavage site) His_6 affinity tag or GST affinity tag (Appendix, Figure A1). The GST-TYMV PRO fusion protein was panned against

phage-displayed UbV as previously described for other DUB proteins (170,171,180) in the laboratory of Dr. Sachdev Sidhu, University of Toronto (since relocated to the University of Waterloo). By screening phage-displayed peptide libraries, three UbVs (UbV1, UbV2, UbV3) were identified that exhibited selective and potent binding to the TYMV PRO. Based on preliminary binding data from our collaborators (Figure 2.1), I subsequently characterized the binding of the UbVs to TYMV PRO using gel filtration and enzyme activity assays (Figure 2.2).

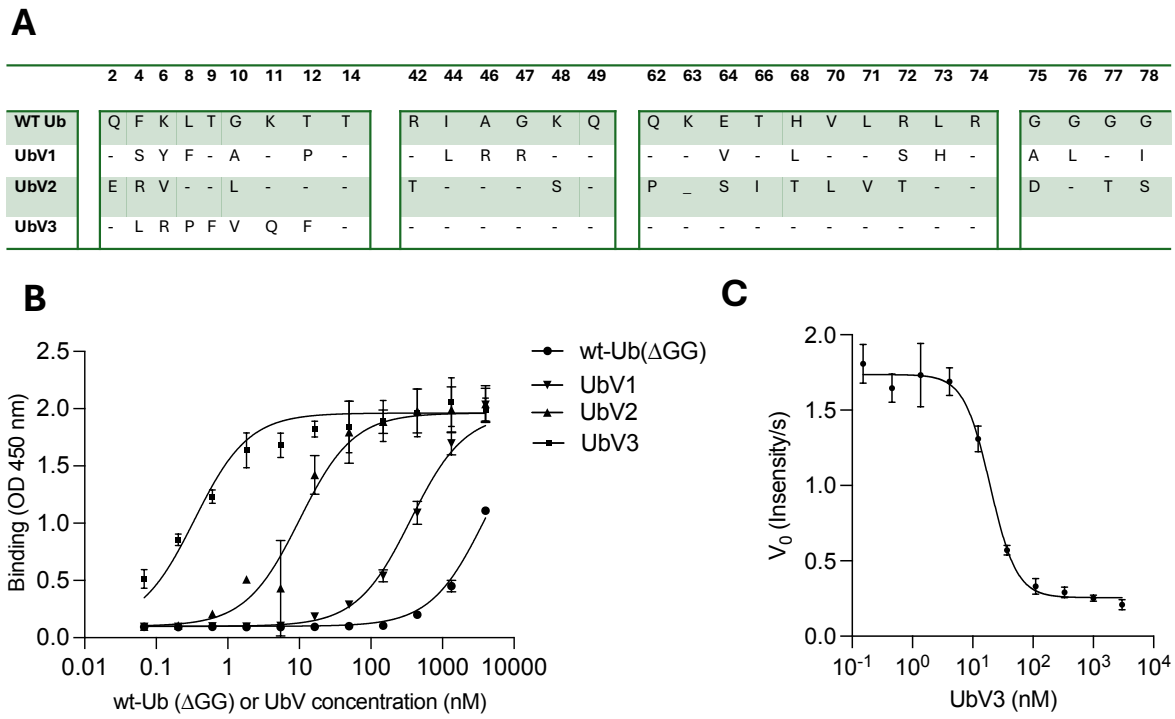

Figure 2. 1 Binding of UbVs to TYMV PRO

(A) Sequence alignment of WT Ub with UbVs 1, 2 and 3. Dashes indicate identity with the WT. (B) The following half-maximal binding concentrations (EC_{50}) of UbVs to TYMV PRO were determined as described (189) : >1000 nM (WT Ub, circles), 560 nM (UbV1, inverted triangles), 11 nM (UbV2, triangles), 0.3 nM (UbV3, squares). (C) Inhibition of TYMV PRO by UbV3 shown as a dose-response curve using Ub-AMC as a substrate. The IC_{50} value (19.5 ± 2.7 nM) was determined as the concentration of UbV that reduced deubiquitination activity by 50%.

To determine the binding stoichiometry of TYMV PRO with UbV3 and generate a protein-protein complex for subsequent crystallization trials, purified TYMV PRO and UbV3 were mixed with an excess of UbV3 (1:2 molar ratio) and purified by gel filtration

chromatography (Figure 2.2). Interestingly, according to gel filtration, the UbV3 protein appeared to form a homodimer that bound two copies of TYMV PRO, which we later confirmed by X-ray crystallography and small-angle X-ray scattering.

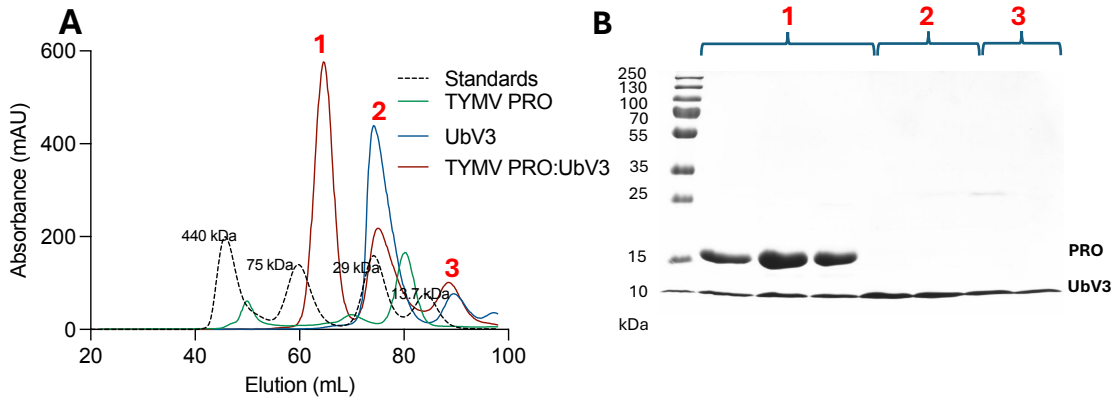

Figure 2. 2 UbV3 interacts with TYMV PRO

(A) Gel filtration of TYMV PRO bound to UbV3 is shown in red (TYMV PRO and UbV3 were mixed at a 1:2 ratio). The elution profile of UbV3 in the absence of TYMV PRO is shown in blue. UbV3 appears to exist primarily as a homodimer (peak 2) in equilibrium with its monomeric form (peak 3). The elution profile of TYMV PRO without UbV3 is shown in green. Molecular mass standards are shown in the black dashed line. (B) 12% SDS-PAGE of the peaks collected by gel filtration in panel A. Lanes (1) is TYMV PRO bound to UbV3 (peak 1 at ~65 ml, shown in red in panel A). Lanes 2 and 3 are proteins from peaks 2 and 3 in red at ~75 ml and ~88 ml, respectively, and are dimeric and monomeric UbV3, respectively.

2.3.2 UbV3 inhibits the DUB and polyprotein cleavage activity of TYMV PRO

Previous studies demonstrated that proteins coded by TYMV, including the viral RNA-dependent RNA polymerase, are prone to K48 polyubiquitination by the host cell and subsequently destroyed by the Ub-proteasome system (UPS) both *in vitro* and *in vivo* (137,188,208). This cellular defense mechanism is suppressed by the K48 polyUb DUB activity of TYMV PRO (132), presumably to enhance replication of the virus, which TYMV PRO also assists in by processing of the viral polyprotein (135,209).

To further examine the ability of the UbV3 dimer to block the DUB activity of PRO, we measured its ability to inhibit K48-linked polyUb chain cleavage by PRO (Figure 2.3). Indeed, this DUB activity was inhibited in a dose-dependent manner by UbV3, with DUB

activity completely abrogated with a 2:1 molar ratio of TYMV PRO and UbV3. Also, the UbV3 dimer inhibits the K-63 linked polyUb chain cleavage by PRO (Figure 2.3).

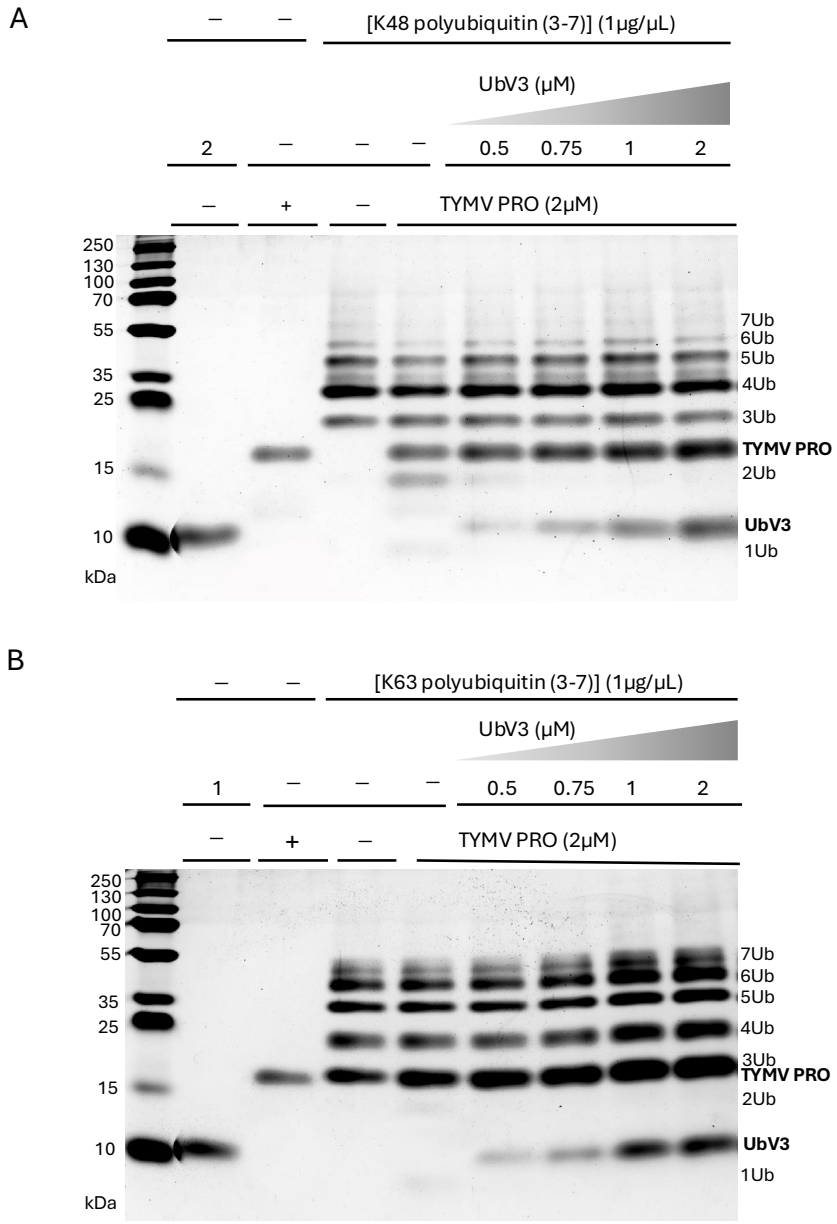

Figure 2. 3 UbV3 inhibits the K48- and K63-linked poly Ub chain cleavage

Purified TYMV PRO was incubated for 30 minutes at 25°C with 1µg of K48-linked (A) K63-linked polyUb chains (B) in the presence of increasing amounts of UbV3 in a final volume of 12µL. UbV3 inhibition of TYMV PRO occurred in a dose-dependent manner. PolyUb chains were visualized using TRIS-Tricine SDS PAGE (10%) and detected using a Pierce Silver Stain Kit. *Although it did not affect the experiment, we found the bright edge on the band in lane 1 to a repeatable but unusual artifact of this silver-stained SDS-PAGE gel

PRO cleaves the TYMV polyprotein at two sites to release the viral helicase and polymerase (135,210), We wanted to determine if UbV3 blocks this polyprotein cleavage activity *in vitro* (Figure 2.4). To achieve this, we created an artificial substrate that included the cleavage site in TYMV polyprotein between the PRO domain and helicase (Pro↓Hel site). The Pro↓Hel site was inserted between a copy of PRO and the glycosidase NagZ (195) and was expressed in the presence or absence of UbV3 (Figure 2.4A). The PRO-NagZ fusion protein served as a reasonable substrate to assess cleavage of the Pro↓Hel site by PRO and the inhibition of this activity by UbV3, since its cleavage by PRO could be readily monitored by the appearance of intact PRO-NagZ (~59 kDa), or free PRO (~20 kDa) and NagZ (~39 kDa) by Western blot (Figure 2.4B).

We confirmed the Pro↓Hel site within the PRO-NagZ fusion protein is cleaved by PRO to release free PRO and NagZ proteins (Figure 2.4B-1). Whether this occurs in *cis* or *trans* was not determined. Notably, co-expression of the PRO-NagZ fusion with UbV3 inhibited cleavage of the Pro↓Hel site as noted by the presence of intact PRO-NagZ protein (Figure 2.4B-2), indicating that UbV3 blocks PRO-mediated processing of the viral polyprotein during virus replication.

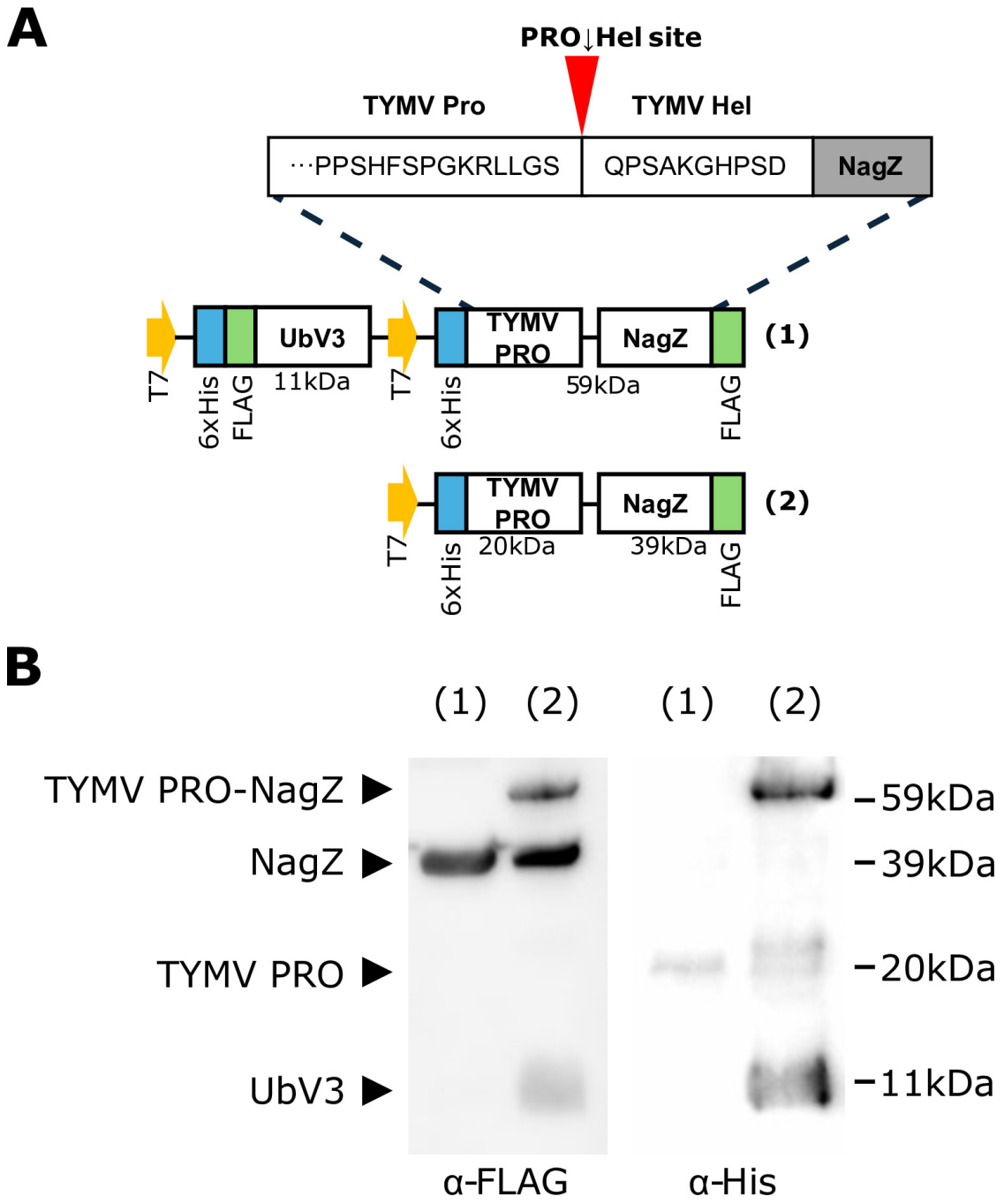

Figure 2. 4 Inhibition of TYMV PRO mediated cleavage of PRO↓Hel by UbV3

A) Construct design for demonstrating cleavage of the Pro↓Hel site by PRO (A-1) and its inhibition by UbV3 (A-2). (B) Western blot analysis of cell lysates from *E. coli* BL21(DE3) expressing PRO-NagZ(A-1) alone, or co-expressing PRO-NagZ with UbV3 (A-2). The gels are representative of 3 independent replicates. Ponceau stains of the blots are shown in Figure 2.5 to demonstrate protein loading consistency for each experiment

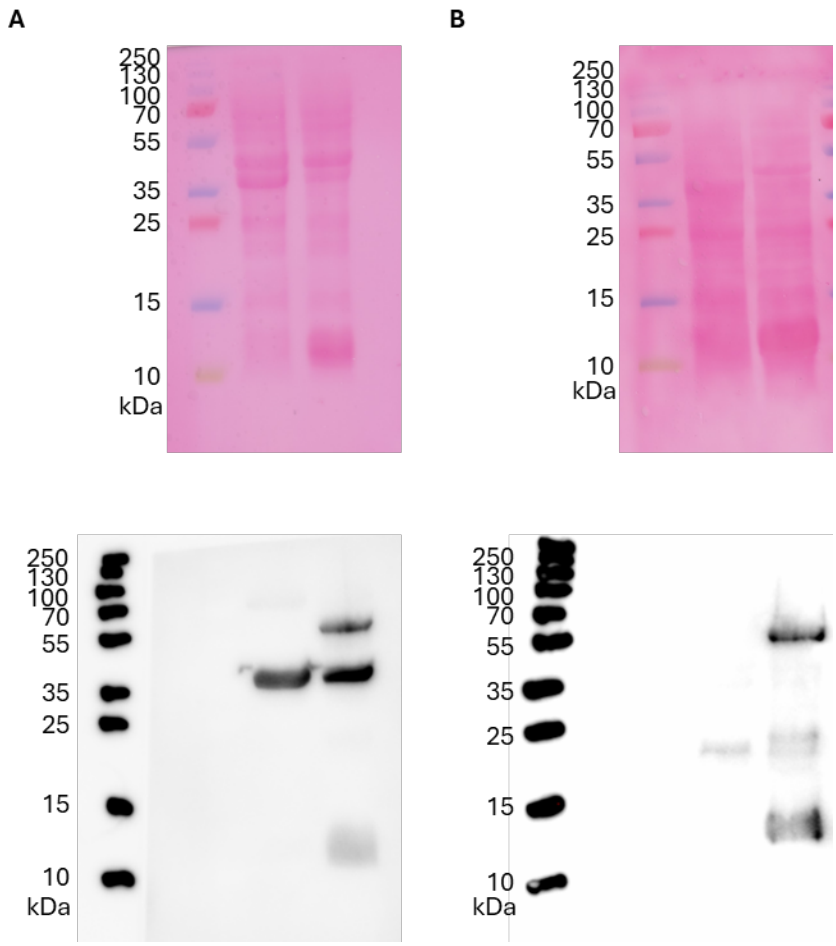

Figure 2. 5 Western blot analysis of UbV3 inhibition of Pro↓Hel cleavage

(A)Ponceau S staining of the blots is shown to control for equal protein loading (60 µg). Cell lysates were analyzed by Western blotting using anti-FLAG tag antibody(A), and anti-Histag antibody (B)

2.3.4 Evaluating off-target inhibition of cellular plant DUBs by UbVs.

To determine if UbVs selected by phage display exhibited any non-specific interaction with cellular DUBs, the UbVs were assessed against a panel of recombinant plant DUBs cloned from the model plant species *Arabidopsis thaliana*. Synthetic open reading frames of *A. thaliana* DUBs were ligated into pGEX 6PI, pET19b or pET28a vectors for expression and subsequent purification from *E. coli*. The recombinant *A. thaliana* DUBs were purified to homogeneity (Figure 2.6A) to generate a representative panel of plant DUBs that included AtAMSH3 (JAMM family)(92), AtAT3G/predicted plant deubiquitinase (MJD family)(21), AtUCH2 (UCH family)(211), and AtOTLD1 (OTU family)(61). The panel represented 4 of

the 5 major DUB families found in plants. While attempts were made to include representatives from the UBP family, we were unable to express members from these families as soluble proteins in *E. coli*. Of the families for which representative plant DUBs were produced, each was confirmed to be active using Ub-AMC as substrate (Appendix, Figure A2). Notably, the MJD family DUB AtAT3G (NCBI: At3G54130) was only predicted to be DUB based on sequence alignments (21); however, we verified it to be a functional DUB and included it in our *A. thaliana* DUB panel.

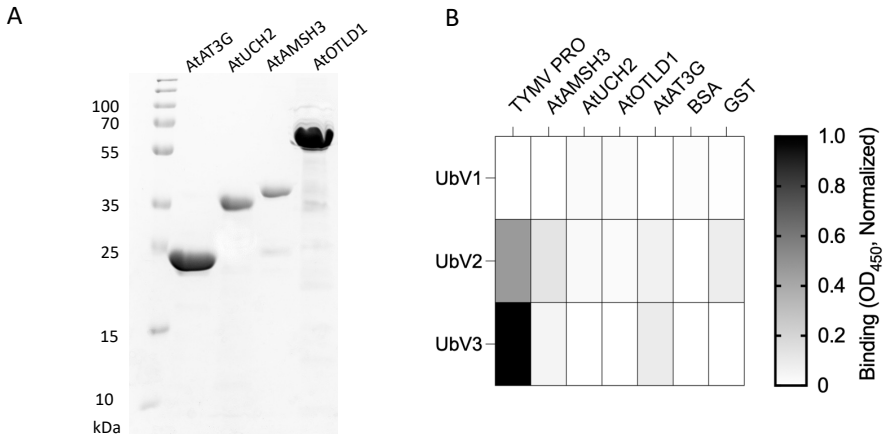

Figure 2. 6 The binding potency of UbVs against TYMV PRO and *A. thaliana* DUBs

(A) SDS-PAGE gel of purified DUB domains of 4 different groups of *Arabidopsis* plant DUBs, AtAT3G (26kDa), AtUCH2 (40kDa), AtAMSH3 (47kDa) and AtOTLD1 (57kDa). The binding specificities of FLAG-tagged UbVs (y-axis) are shown across a group of 5 DUBs (x-axis), including four plant DUBs [AtAMSH3, AtOTLD1, AtUCH2 and AtAT3G], TYMV PRO and two negative controls (GST and BSA), as assessed by protein ELISA. Purified His6-FLAG-UbVs were added to immobilized target proteins as indicated, and the anti-FLAG-HRP and colorimetric development of TMB peroxidase substrate detected bound UbVs. The mean value of absorbance at 450 nm is shaded in a grayscale.

The ability of the UbVs to bind to members of the *A. thaliana* derived panel of DUBs, or to TYMV PRO and negative controls GST and BSA was measured by ELISA. Consistent with the high selectively we previously observed for UbVs selected against animal vDUBs (171), we found that the UbVs (1 - 3) selected against TYMV PRO also did not bind appreciably to any of the DUBs from *A. thaliana,* or negative control proteins (Figure 2.6B).

In addition to ELISA-based binding assays, we also probed enzymatically the selectivity of UbV3 for TYMV PRO versus the panel of *A. thaliana* DUBs. Using Ub-AMC as substrate, the activity of each DUB was measured in the presence of increasing amounts of UbV3. Kinetic profiles were then fitted to a non-linear regression equation ($y= y_0+ae^{bx}$) to obtain initial rates for each reaction. The initial rates were plotted against UbV3 concentrations to determine IC_{50} values. Also, K_m for TYMV PRO (K_m=68 μM) was measured to interpret the Ub-AMC substrate specificity of TYMV PRO (Appendix, Figure A10) Consistent with the ELISA protein binding assays above, activity-based assays demonstrated that even at very high concentrations (>40x that needed to reduce TYMV PRO activity by half), UbV3 had minimal effect on the activity of the *A. thaliana* DUBs, yet it potently blocked TYMV PRO activity (Figure 2.7). Together, the above binding and inhibition assays confirmed that UbV3 is a highly specific and potent inhibitor of TYMV PRO and suggested that its transgenic expression in *A. thaliana* could potentially suppress TYMV replication without perturbing the cellular Ub system, and thus not adversely affect plant physiology.

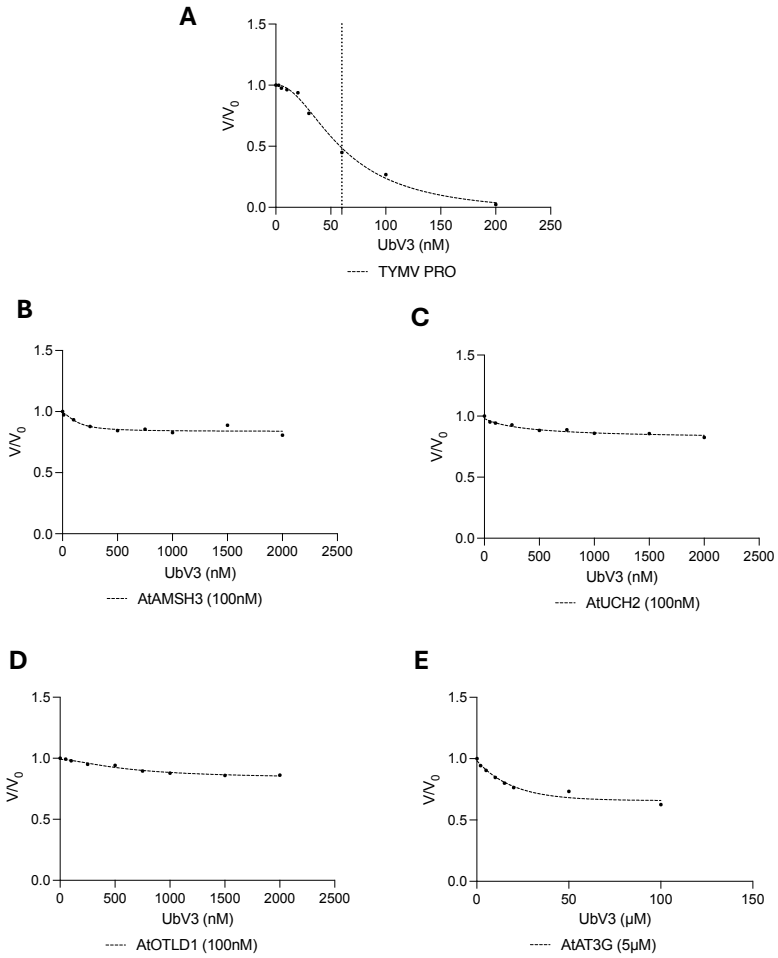

Figure 2. 7 The DUB activity of TYMV PRO and *A. thaliana* DUBs in the presence of UbV3

(A) inhibition curve of TYMV PRO (100nM) with 0-200nM concentrations of UbV3. (B-D); inhibition curves of AtUCH2 (100nM) (B), AtAMSH3 (100nM) (C), AtOTLD1 (100nM) (D) with 0- 1000nM concentrations of UbV3. (D) inhibition curve of AtAT3G with 0-50μM concentrations of UbV3. The predicted AtAT3G enzyme is only a moderately active deubiquitinase against Ub-AMC; therefore, 5μM of enzyme concentration and 0-100μM concentrations of UbV3 were used to analyze the inhibitory effect of UbV3 against AtAT3G. The IC_{50} values were calculated as follows TYMV PRO (IC_{50}=60±0.06nM), [AtUCH2, AtAMSH3 and AtOTLD1 (IC_{50}= >2000nM) and predicted DUB AtAT3G (IC_{50} = >100μM).

Table 2. 2 Non-liner regression analysis of fitting the kinetic profiles of Ub-AMC hydrolysis by TYMV PRO and *A. thaliana* DUBs in the presence of different concentrations of UbV3 to equation $y=Y_0+ae^{bx}$

UbV3 (M)	Parameter[a]				
	Y_0	a	b	Initial rate (ab)	R^2
TYMV PRO					
0.0×10^{-9}	$(2.81\pm0.23) \times 10^{5}$	$(4.15\pm0.11) \times 10^{6}$	$(1.27\pm0.03) \times 10^{-4}$	527.98±01.69	0.9997
2.5×10^{-9}	$(2.91\pm0.29) \times 10^{5}$	$(4.53\pm0.22) \times 10^{6}$	$(1.15\pm0.01) \times 10^{-4}$	522.48±32.96	0.9997
5.0×10^{-9}	$(2.65\pm0.29) \times 10^{5}$	$(4.31\pm0.13) \times 10^{6}$	$(1.20\pm0.07) \times 10^{-4}$	510.35±24.93	0.9997
1.0×10^{-8}	$(1.80\pm0.38) \times 10^{5}$	$(4.16\pm0.29) \times 10^{6}$	$(1.23\pm0.14) \times 10^{-4}$	509.26±03.73	0.9996
1.5×10^{-8}	$(1.65\pm0.05) \times 10^{5}$	$(4.18\pm0.18) \times 10^{6}$	$(1.21\pm0.06) \times 10^{-4}$	507.06±01.85	0.9997
2.0×10^{-8}	$(1.59\pm0.09) \times 10^{5}$	$(4.43\pm0.10) \times 10^{6}$	$(9.21\pm0.00) \times 10^{-5}$	406.50±06.10	0.9997
4.0×10^{-8}	$(1.41\pm0.33) \times 10^{5}$	$(3.63\pm0.14) \times 10^{6}$	$(6.54\pm0.01) \times 10^{-5}$	237.94±09.24	0.9996
8.0×10^{-8}	$(1.36\pm0.17) \times 10^{5}$	$(2.45\pm0.09) \times 10^{6}$	$(5.79\pm0.03) \times 10^{-5}$	142.19±06.46	0.9992
2.0×10^{-7}	$(1.28\pm0.62) \times 10^{5}$	$(4.81\pm0.91) \times 10^{7}$	$(2.82\pm0.08) \times 10^{-7}$	012.26±04.22	0.9445
AtUCH2					
0.0×10^{-9}	$(3.94\pm3.18) \times 10^{4}$	$(2.58\pm0.53) \times 10^{6}$	$(1.41\pm0.29) \times 10^{-4}$	358.03±01.41	0.9995
5.0×10^{-8}	$(7.56\pm0.86) \times 10^{4}$	$(2.99\pm0.03) \times 10^{6}$	$(1.39\pm0.37) \times 10^{-4}$	343.32±02.11	0.9993
1.0×10^{-7}	$(7.29\pm0.33) \times 10^{4}$	$(2.85\pm0.20) \times 10^{6}$	$(1.18\pm0.08) \times 10^{-4}$	338.43±00.31	0.9996
2.5×10^{-7}	$(4.27\pm3.38) \times 10^{4}$	$(2.98\pm0.31) \times 10^{6}$	$(1.12\pm0.10) \times 10^{-4}$	333.21±03.29	0.9998
4.0×10^{-7}	$(7.46\pm1.58) \times 10^{4}$	$(3.03\pm0.17) \times 10^{6}$	$(1.04\pm0.04) \times 10^{-4}$	316.86±03.69	0.9997
5.0×10^{-7}	$(8.36\pm0.60) \times 10^{4}$	$(2.78\pm0.07) \times 10^{6}$	$(1.14\pm0.01) \times 10^{-4}$	318.96±12.24	0.9997
7.0×10^{-7}	$(7.72\pm0.24) \times 10^{4}$	$(2.90\pm0.10) \times 10^{6}$	$(1.06\pm0.03) \times 10^{-4}$	308.53±02.36	0.9996
8.0×10^{-7}	$(5.12\pm1.83) \times 10^{4}$	$(2.76\pm0.54) \times 10^{6}$	$(1.13\pm0.20) \times 10^{-4}$	307.49±04.72	0.9997
1.0×10^{-6}	$(6.56\pm0.42) \times 10^{4}$	$(3.05\pm0.02) \times 10^{6}$	$(0.96\pm0.02) \times 10^{-4}$	296.26±06.49	0.9997
AtAMSH3					
0.0×10^{-9}	$(2.07\pm0.57) \times 10^{3}$	$(7.40\pm0.43) \times 10^{4}$	$(2.20\pm0.12) \times 10^{-4}$	16.26±0.06	0.9991
5.0×10^{-8}	$(1.97\pm0.22) \times 10^{3}$	$(7.70\pm0.61) \times 10^{4}$	$(2.25\pm0.11) \times 10^{-4}$	17.39±2.26	0.9992
1.0×10^{-7}	$(1.69\pm0.27) \times 10^{3}$	$(8.49\pm0.03) \times 10^{4}$	$(2.14\pm0.03) \times 10^{-4}$	18.22±0.19	0.9992
2.5×10^{-7}	$(1.83\pm0.08) \times 10^{3}$	$(7.83\pm0.82) \times 10^{4}$	$(2.09\pm0.10) \times 10^{-4}$	16.36±0.89	0.9992
4.0×10^{-7}	$(3.07\pm1.51) \times 10^{3}$	$(8.09\pm0.91) \times 10^{4}$	$(1.96\pm0.02) \times 10^{-4}$	15.73±0.55	0.9991
5.0×10^{-7}	$(1.66\pm0.05) \times 10^{3}$	$(8.13\pm0.05) \times 10^{4}$	$(1.96\pm0.02) \times 10^{-4}$	15.94±0.31	0.9992
7.0×10^{-7}	$(1.60\pm0.31) \times 10^{3}$	$(7.53\pm0.82) \times 10^{4}$	$(2.04\pm0.07) \times 10^{-4}$	15.43±2.24	0.9991
8.0×10^{-7}	$(3.72\pm2.58) \times 10^{3}$	$(7.83\pm0.82) \times 10^{4}$	$(2.11\pm0.16) \times 10^{-4}$	16.54±0.96	0.9989
1.0×10^{-6}	$(1.14\pm0.41) \times 10^{3}$	$(7.56\pm0.03) \times 10^{4}$	$(1.98\pm0.16) \times 10^{-4}$	15.03±1.14	0.9987
AtOTLD1					
0.0×10^{-9}	$(6.73\pm1.96) \times 10^{4}$	$(3.11\pm0.17) \times 10^{6}$	$(1.77\pm0.10) \times 10^{-4}$	548.75±04.85	0.9996
5.0×10^{-8}	$(6.53\pm1.56) \times 10^{4}$	$(3.14\pm0.08) \times 10^{6}$	$(1.69\pm0.04) \times 10^{-4}$	533.61±00.74	0.9998
1.0×10^{-7}	$(5.86\pm4.15) \times 10^{4}$	$(3.09\pm0.15) \times 10^{6}$	$(1.74\pm0.08) \times 10^{-4}$	538.01±01.29	0.9997
2.5×10^{-7}	$(4.98\pm0.22) \times 10^{4}$	$(3.18\pm0.08) \times 10^{6}$	$(1.65\pm0.03) \times 10^{-4}$	525.45±07.14	0.9998
4.0×10^{-7}	$(5.24\pm0.43) \times 10^{4}$	$(3.11\pm0.04) \times 10^{6}$	$(1.64\pm0.05) \times 10^{-4}$	510.59±10.62	0.9998
5.0×10^{-7}	$(4.51\pm1.13) \times 10^{4}$	$(3.03\pm0.03) \times 10^{6}$	$(1.59\pm0.04) \times 10^{-4}$	484.73±01.96	0.9990
7.0×10^{-7}	$(4.46\pm0.91) \times 10^{4}$	$(3.12\pm0.04) \times 10^{6}$	$(1.53\pm0.04) \times 10^{-4}$	480.14±06.36	0.9999
8.0×10^{-7}	$(5.05\pm2.17) \times 10^{4}$	$(3.06\pm0.07) \times 10^{6}$	$(1.53\pm0.02) \times 10^{-4}$	470.86±03.75	0.9998
1.0×10^{-6}	$(5.37\pm1.60) \times 10^{4}$	$(3.10\pm0.06) \times 10^{6}$	$(1.48\pm0.02) \times 10^{-4}$	460.96±03.14	0.9998
AtAT3G					
0.0×10^{-6}	$(4.31\pm0.12) \times 10^{5}$	$(1.80\pm0.06) \times 10^{6}$	$(4.47\pm0.15) \times 10^{-4}$	889.85±00.65	0.9504
5.0×10^{-6}	$(6.04\pm0.39) \times 10^{5}$	$(2.10\pm0.03) \times 10^{6}$	$(4.20\pm0.35) \times 10^{-4}$	884.63±59.40	0.9544
1.0×10^{-5}	$(5.11\pm1.34) \times 10^{5}$	$(1.83\pm0.03) \times 10^{6}$	$(4.58\pm0.00) \times 10^{-4}$	839.38±18.60	0.9494
2.0×10^{-5}	$(5.47\pm0.17) \times 10^{5}$	$(1.88\pm0.07) \times 10^{6}$	$(3.87\pm0.06) \times 10^{-4}$	804.81±00.90	0.9559
4.0×10^{-5}	$(6.92\pm1.22) \times 10^{5}$	$(2.03\pm0.06) \times 10^{6}$	$(4.38\pm0.15) \times 10^{-4}$	731.34±16.19	0.9077
8.0×10^{-5}	$(5.76\pm0.28) \times 10^{5}$	$(2.04\pm0.27) \times 10^{6}$	$(3.63\pm0.28) \times 10^{-4}$	737.08±41.42	0.9523
1.0×10^{-4}	$(4.71\pm0.38) \times 10^{5}$	$(1.73\pm0.10) \times 10^{6}$	$(3.93\pm0.14) \times 10^{-4}$	680.88±13.72	0.9532

[a]Parameter values represent averages of at least three technical replicates, and ±values represent the standard deviation.

2.3.5 UbV3 dimerization drives binding potency toward TYMV PRO

To gain insight into how UbV3 blocks TYMV PRO activity, I have collaborated with Dr. Kihun Kim to determine the high-resolution structure of UbV3 alone and bound to TYMV PRO using X-ray crystallography (Appendix, Table 2.3). According to size exclusion chromatography, purified UbV3 exists in an equilibrium that strongly favours homodimerization (~24kDa) versus remaining monomeric (~12kDa) in solution (Figure 2.2A). UbV3 dimerization is consistent with other previously characterized UbV proteins (212,213), where the substitution of glycine at position 10 to valine or alanine causes the N-terminal β-sheet of ubiquitin to unfold and participate in dimerization interactions (212). G10 is located in a loop between strands β1 and β2 of Ub, and its substitution to valine or alanine destabilizes the β1-β2 loop, causing strand β1 to engage with strands β2 and β5 of an independent UbV3 monomer to form a stable dimer with β1 strands exchange (212). Substitution of V10 to glycine in UbV3 abolished dimerization to yield a monomeric protein (Figure 2.8), verifying that G10V is a substitution crucial for maintaining UbV3 in a dimeric state.

UbV3 crystallized readily, and its X-ray structure revealed a dimeric structure, as expected from the chromatography studies (Figure 2.8B). Strand β1 of each UbV3 monomer was exchanged to form hydrogen bonds with strand β2 and strand β5 of the partnering UbV3 monomer within the dimer. The resulting β-sheet formed by these strands holds the dimer together (Figure 2.8C). The extended loops between strands β1 and β2 that link the monomers together do not show any appreciable interactions with each other, suggesting structural flexibility in this region (Figure 2.8D). There are 7 amino acid substitutions in UbV3 with respect to WT Ub (F4L, K6R, L8P, T9F, G10V, K11Q, T12F) (Figure 2.1A). In WT Ub, the sidechains of F4 and K6 project outward from the protein, and the conservative substitutions at these positions in UbV3 (F4L, K6R) do not affect the fold and would only minimally affect hydrophobicity or polarity in this region (Figure 2.8E top). Just downstream of strand β1, L8

substituted to proline in UbV3, where the proline has a cis-peptide bond that enables the backbone atoms to adopt similar positions to that found for the T7-L8 peptide bond of Ub. However, the backbone dihedral angles of F9 of UbV3 were changed dramatically (φ = -83.1°, ψ = 141.3°), compared to that of T9 (φ = -101.4°, ψ = 14.9°) in WT Ub, and those of V10 in UbV3 were also changed (φ = -92.3°, ψ = 129.3°) compared to G10 (φ = 77.4°, ψ = 16.5°) of WT Ub (Appendix, Figure A3). These angular changes reflect the change of the β1-β2 loop from a type I b-turn in WT Ub to an extension that reaches out to engage with the partnering monomer in the UbV3 dimer (Figure 2.8B). Substitutions K11Q and T12F did not affect backbone geometry, nor did their sidechains interact with other atoms of the UbV3 dimer (Figure 2.8E, bottom).

Finally, the sidechain of F9 of each monomer of UbV3 packs closely with several hydrophobic sidechains of other nearby residues (I13, I30, I36, V70 and L71) (Figure 2.8F). Known as the I36 patch in wild-type Ub, this patch participates in protein-protein interactions (214), including binding of Ub to TYMV PRO (134). The site is conserved in UbV3, and prior to determining the X-ray structure of UbV3 bound to TYMV PRO, we speculated that its participation in binding the protease may be enhanced by the T9F substitution. Indeed, the pyrrolidine ring of P8 and aromatic ring of F9 are roughly ~3Å apart and appear to form a C-H/π interaction placing the F9 sidechain in an orientation that helps stabilize the extended conformation of the β1-β2 loop along with the G10V substitution to form the UbV3 dimer.

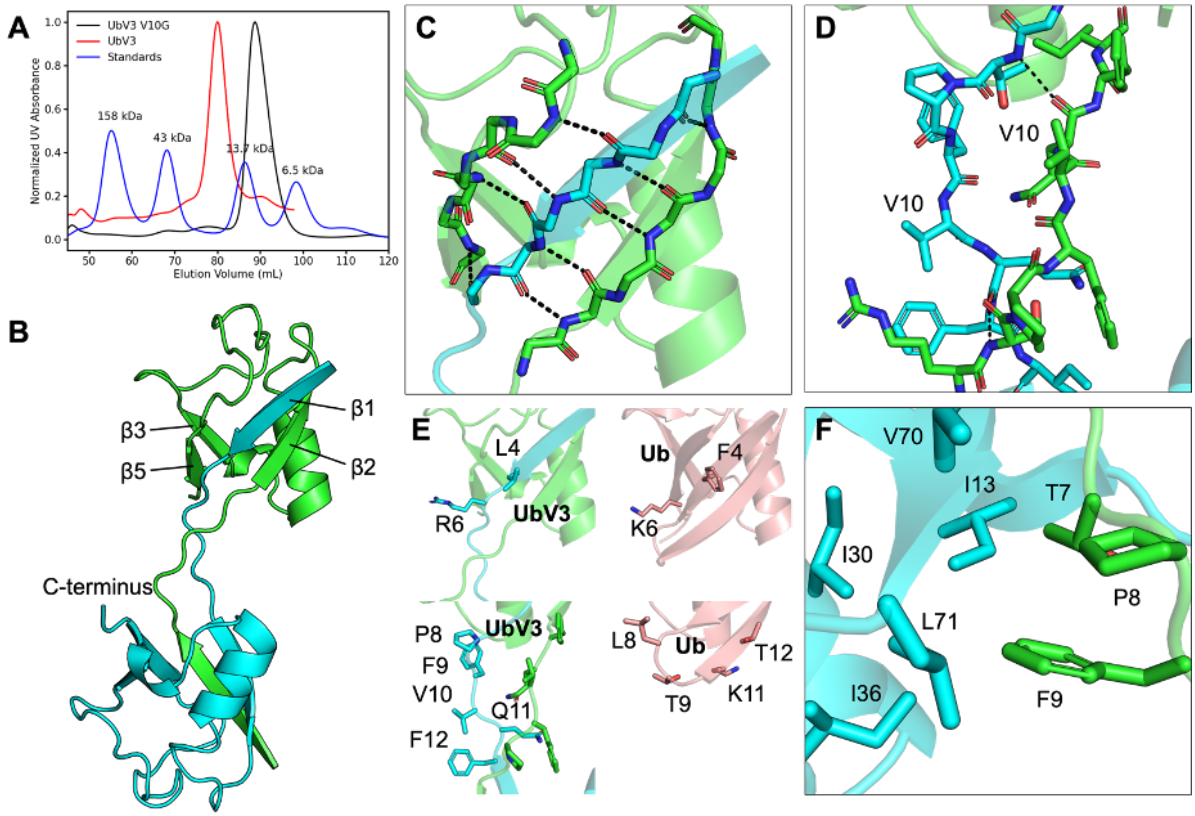

Figure 2. 8 Crystal structure of UbV3 dimer

(A) Size exclusion chromatography profile of UbV3 V10G construct and UbV3. With the aid of standards, UbV3 V10G was clearly identified as monomer instead of being a dimer like UbV3. (B) Cartoon representation of the UbV3 dimer. (C) Backbone hydrogen bond network near strand β1 that holds the UbV monomer together through strand exchange. (D) β1-β2 loop structure. (E) Substitutions in UbV3 compared to wild type Ub. UbV3 chains are colored as cyan and green, and ubiquitin (PDB ID: 1UBQ) is colored as salmon. Substitutions around strand β1 are described on top panel, and substitutions around β1-β2 loop are described on bottom panel. (F) Hydrophobic sidechains near I36 patch interact with β1-β2 loop region.

2.3.6 UbV3 dimerization drives TYMV PRO inhibition

TYMV PRO binds UbV3 in solution as a single complex that can be readily purified by size exclusion chromatography (Figure 2.2A), and its mass (~50kDa) suggested that two copies of TYMV PRO were bound to one UbV3 dimer (Appendix, Figure A4). This was not surprising considering that the UbV3 dimer has two solvent-exposed C-terminal tails (right after strand β5) to which independent copies of TYMV PRO could bind (Figure 2.8B) After several failed attempts to crystallize the complex, we ultimately met with success by covalently linking UbV3 to TYMV PRO by modifying the C-terminal glycines of UbV3 with 3-

bromopropylamine as we have done previously to generate stable complexes of vDUBs bound to Ub (197,215).

As verified below, the modification yielded covalent linkages between the C-termini of the monomers within UbV3 to the active site cystines (C783) of bound copies of TYMV PRO, which enabled crystallization of the complex for structural analysis (Figure 2.9A). An *ab initio* low-resolution envelope determined using the solution X-ray scattering (SAXS) method of the non-covalently bonded complex was also determined and revealed that the X-ray structure adopts an overall conformation that is consistent with the structure of the non-covalently bound complex in solution (Figure 2.9A).

The high-resolution structure clearly revealed two copies of TYMV PRO bound to one UbV3 dimer (Figure 2.9A). Each monomer of the UbV dimer binds a copy of TYMV PRO with a binding mode like that of wild-type Ub when comparing the complex to the previously determined structure of TYMV PRO bound to Ub (134) (PDB ID: 6YPT) (RMSD of Cα 0.48Å for UbV3 versus Ub, RMSD of Cα 0.97Å for TYMV PRO bound to UbV3 versus Ub) (Appendix, Figure A5). Dimerization of UbV3 does not interfere the interaction between TYMV PRO active site and C-terminal tail of UbV3, rather it led additional binding interface. Interestingly, reverting V10 to glycine made UbV3-(V10G) prefer to stay in a monomeric state (Figure 2.8A), and it significantly reduced the ability of UbV3-(V10G) to inhibit TYMV PRO activity (Figure 2.9B), demonstrating that V10 itself and/or UbV3 dimerization is necessary for potent inhibition of TYMV PRO activity by UbV3.

The C-terminal tail of each UbV3 monomer lies within the active site cleft of TYMV PRO, where the C-terminal propylamine is covalently linked to side chain of C783 of TYMV PRO as expected, and the interactions between the C-terminal tail of UbV3 (^{71}LRLRG^{75}) and TYMV PRO is consistent with how Ub binds the protease (Figure 2.9C). Most polar interactions between the C-terminal tail of UbV3 and TYMV PRO occur with backbone atoms

of UbV3. The amide N and carbonyl O atoms of L73 of UbV3 form hydrogen bonds with Oγ atom (3.1Å) and amide N atom of Thr824 (2.7Å) of TYMV PRO, respectively. The carbonyl O atom of R74 is close to the Oγ side chain atom of Ser868 (2.3Å) and Nε2 side chain atom of H862 (2.9Å). The sidechains of UbV3 R72 and TYMV PRO E816 also engage in hydrogen bonding interactions. Further, the sidechains of L71 and L73 of UbV3 pack against a hydrophobic surface of TYMV PRO comprised of V840, I847, F849 and F870 (Figure 2.9D).

Beyond the C-termini of the UbV3 monomers, the inhibitor makes additional polar contacts at 3 more sites on each copy of TYMV PRO (Appendix, Figure A6). The sidechain of UbV3 R6 forms a salt bridge with the sidechain of E759 TYMV PRO, whose active site binds to another UbV3 chain. The backbone amide N atom of V10 of UbV3 forms a 2.9Å hydrogen bond with the carbonyl O atom of TYMV PRO P846, and the sidechains of H68 of UbV3 and N760 of TYMV PRO also engage in a 2.9Å hydrogen bonding interaction.

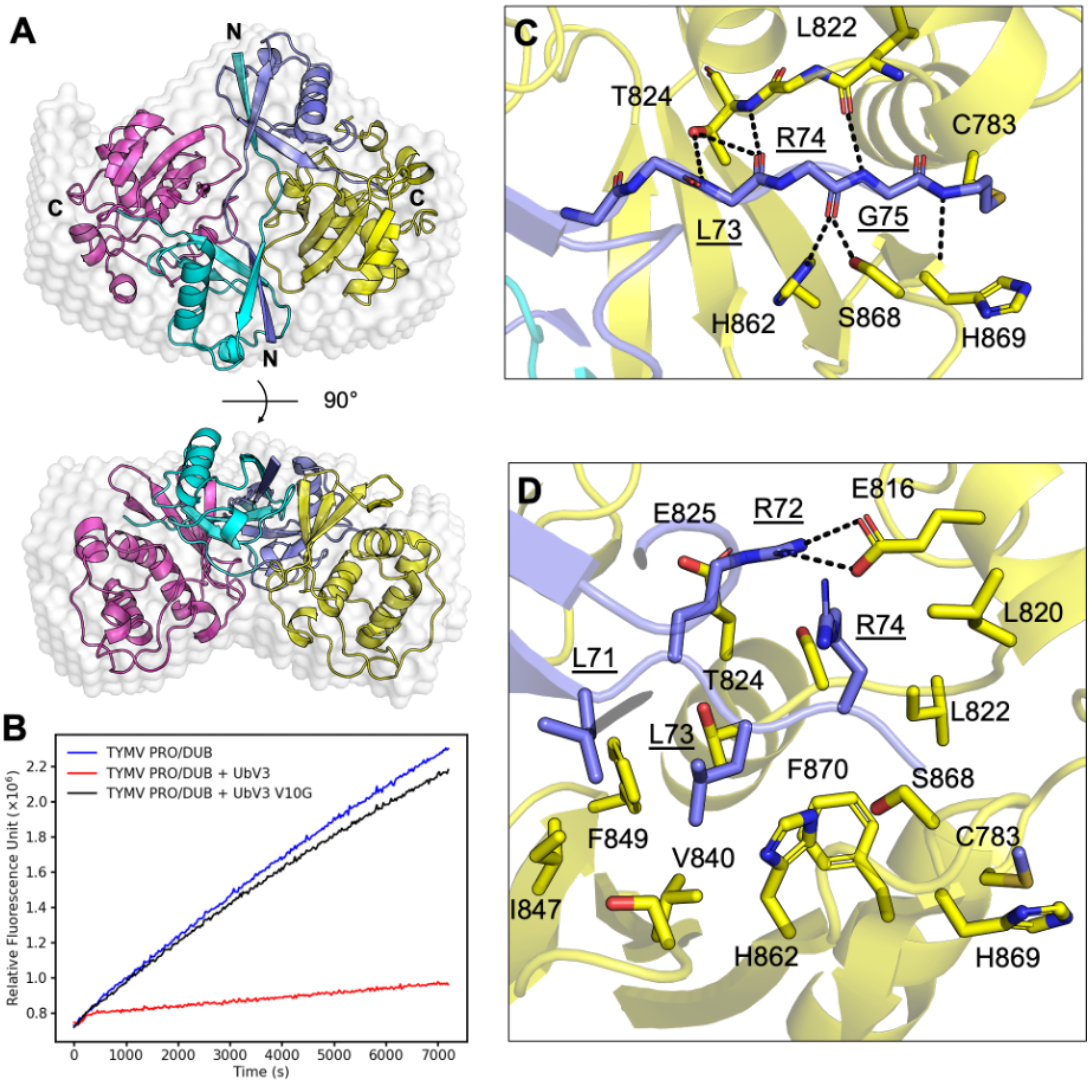

Figure 2. 9 Complex crystal structure of TYMV PRO and UbV3 dimer

(A) 2:2 complex of TYMV PRO and UbV3 molecules are present in 1 asymmetric unit. TYMV PRO chains are colored magenta and yellow, UbV3 chains are colored cyan and blue. N and C termini of UbV3 chains are labelled. *ab initio* SAXS envelope of the non-covalent bonded complex is represented as transparent white spheres and shows that the X-ray structure and solution structure are consistent. (B) UbV3 V10G has a dramatically reduced ability to inhibit TYMV PRO/DUB activity compared to the same amount of UbV3, as identified by a Ub-AMC cleavage assay. (C) Backbone atoms of the C-terminal tail of UbV3 (^{71}LRLRG^{75}) lie in the active site to form hydrogen bonds with TYMV PRO. (D) Polar interactions between UbV3 and TYMV PRO. Possible interactions are indicated by a dashed line with distance. Residues of UbV3 are labelled with underline, and the key residues of the TYMV PRO active site are labelled.

In addition to the polar contacts described above, the monomers of the UbV3 dimer make extensive hydrophobic contacts to each copy of TYMV PRO to which they are bound. With some substitutions in UbV3 resulting in additional hydrophobic sidechains, the hydrophobic region near β1-β2 loop (^{8}PFVQF^{12}) of each monomer of the UbV3 dimer makes extensive packing interactions with complementary hydrophobic regions of the TYMV PRO enzymes to which they are bound (Figure 2.10A). This hydrophobic packing involves the β1-β2 loop (^{8}PFVQF^{12}) of UbV3, C-terminal I36 hydrophobic patch of another UbV3 chain (I36, L69, L71), and TYMV PRO/DUB hydrophobic region (aliphatic carbons of T839, Y841, S842, R844, P846, I847 and L848). Similar to UbV3, Ub also interacts with TYMV PRO with its I36 hydrophobic patch as described (134). However, due to the lack of an extended β1strand in Ub compared to UbV3, TYMV PRO only utilizes a partial surface area for hydrophobic networking with Ub (Figure 2.10B). As a result, the total binding interface between TYMV PRO and Ub is ~884Å^2 according to PISA (216); whereas, this interface between TYMV PRO and UbV3 dimer is expanded to ~1318Å^2 (~961Å^2 for a UbV3 which interacts via C-terminal tail, ~356 Å^2 for another UbV3 which interacts via β1-β2 loop). Thus, the dimeric structure of UbV3 expands the hydrophobic binding interface with TYMV PRO compared with Ub and likely underlies its high affinity and selectivity for the protease. The data collection and refinement for UbV3 dimer and TYMV PRO-UbV3 complex structures are presented in Table 2.3.

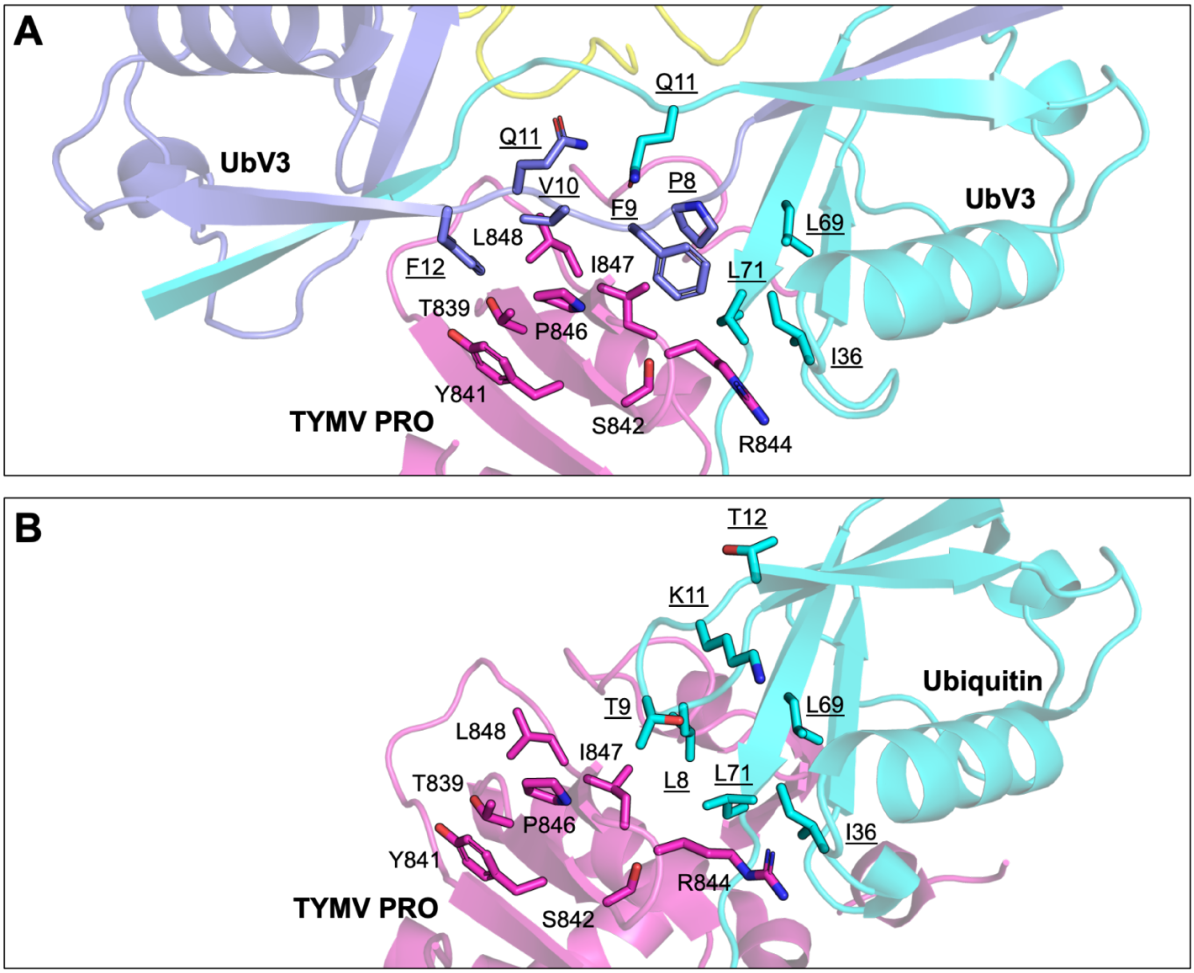

Figure 2. 10 Interaction between TYMV PRO and UbV3 other than its C-terminal tail

TYMV PRO are colored magenta and yellow, UbV3 are colored cyan and blue. Key residues are labeled and underlined for UbV3. (A) Key residues participating in the hydrophobic network of UbV3 and TYMV PRO. (B) Residues of TYMV PRO near the I36 hydrophobic patch of UB (PDB ID: 6YPT). TYMV PRO is colored magenta and Ub is colored cyan.

Table 2. 3 The data collection and refinement data for UbV3 and TYMV PRO-UbV3 complex

Crystal	**UbV3 dimer**	**TYMV PRO-UbV3 complex**
Crystal geometry		
Space group	I422	$C222_1$
Unit cell (Å)	a=b=75.698, c=121.5; α=β=γ=90°	a=72.01, b=89.66, c=137.46; α=β=γ=90°
Crystallographic data		
Wavelength (Å)	1.5418	1.5418
Resolution range (Å)	18.94 - 1.84 (1.91 - 1.84)	45.83 – 2.80 (2.9 - 2.80)
Total reflections	214790 (19516)	155365 (14024)
Unique reflections	15581 (1476)	11252 (1065)
Multiplicity	13.8 (13.2)	13.8 (13.2)
Completeness (%)	99.77 (97.87)	99.4 (95.8)
Mean I/σI	28.72 (2.86)	16.6 (4.4)
Wilson B-factor	27.05	36.2
R_{merge}	0.057 (0.931)	0.152 (0.597)
R_{meas}	0.059 (0.969)	0.157 (0.620)
R_{pim}	0.016 (0.262)	0.042 (0.166)
CC1/2	1 (0.838)	0.997 (0.896)
CC*	1 (0.955)	
Refinement statistics		
Reflections used in refinement	15579 (1476)	11226 (1211)
Reflections used for R_{free}	780 (66)	1122 (135)
R_{work}	0.1892 (0.2629)	0.2291 (0.3180)
R_{free}	0.2252 (0.3064)	0.2778 (0.3690)

Number of non-hydrogen atoms	1363	3456
macromolecules	1237	3448
ligands	5	8
solvent	121	0
Protein residues	149	436
RMS (bonds)	0.006	0.003
RMS (angles)	0.90	0.58
Ramachandran favored (%)	99.31	98.60
Ramachandran allowed (%)	0.69	1.40
Ramachandran outliers (%)	0.00	0.00
Rotamer outliers (%)	0.69	1.01
Clashscore	3.53	5.93
Average B-factor (Å^2)	32.17	35.16
macromolecules	31.38	35.14
ligands	74.72	44.29
solvent	38.49	
PDB ID	9CSF	9CSH

Statistics for the highest-resolution shell are shown in parentheses

2.4 Discussion

Having successfully identified several UbVs that selectively and potently block vDUB inhibitors from animal viruses, including SARS-1 and 2 and Crimean Congo Haemorrhagic Fever Virus (170,171), we wanted to demonstrate the utility of the approach to block susceptible vDUBs from plant viruses of agricultural importance, of which there are several (134,139,145,157). Though we have found UbVs straightforward to identify from phage-displayed Ub variant libraries when using stable recombinant vDUBs as bait, their ultimate delivery to the cytosol of virus-infected animal cells remains a compelling challenge to be overcome before they can be employed as antiviral therapeutics. Aside from recombinant lysosomal proteins that can be successfully sequestered into the lysosome of animal cells via mannose-6-phosphate receptor-mediated endocytosis to treat lysosomal storage disorders (217), mechanisms for intracellular delivery of recombinant proteins remain experimental (218). In contrast, transgenic expression of cytosolic proteins in plants is a proven technology that overcomes the challenges of exogenous protein delivery. Since UbVs are a protein-based antiviral strategy, we investigated if a UbV could protect plants from viral infection to provide a proof-of-principle example that the approach could serve to protect agriculturally important plants from infection.

UbV3 was identified as a selective and potent inhibitor of TYMV PRO (Figure 2.1 and 2.6), and in addition to blocking polyprotein cleavage activity as demonstrated for PRO↓Hel cleavage (Figure 2.4), which is essential for TYMV replication (135), UbV3 also blocked the DUB activity of PRO that is needed to usurp cellular Ub-dependent antiviral mechanisms (132,137). In particular, TYMV PRO has been found to deubiquitinate the RNA-dependent RNA polymerase (RdRp) of the TYMV replicase complex, thereby rescuing the polymerase from K48-polyubiquitin-mediated proteasomal degradation (132,137). The DUB activity of TYMV PRO thus appears to decrease RdRp turnover to enhance viral replication in plant cells

(132,137). We found that this activity is inhibited with increasing concentrations of low micromolar amounts of UbV3 (Figure 2.1-3). Together, we found that UbV3 could be used to block polyprotein cleavage and DUB activity, which was expected considering the UbV3 dimer occupied the active site and the majority of the Ub recognition site of PRO according to our structural studies of the complex formed by the proteins.

In the model plant *A. thaliana,* more than 1600 genes are involved in ubiquitin-related pathways, more than 1400 genes encode putative E3 Ub-ligase, and there are about 1415 E3 Ub-ligases (106,219). Given the presence of a DUB coded in the TYMV genome, this virus appears to disrupt the plant Ub system during infection (188,220). A previously determined X-ray structure of TYMV PRO revealed that the protease shares structural similarity to members of the Ovarian Tumor domain (OTU) family of DUBs (99). Since OTU DUBs comprise an important part of the Ub system in plants (221), prior to *in vivo* studies of the efficacy of UbV3 as antiviral in plants, we assessed the binding of the UbVs we identified from phage display to a panel of recombinant *A. thaliana* plant DUBs, and we found minimal binding of UbVs to the DUB panel even at very high concentrations (Figure 2.6-7), which is consistent with the remarkable selectively we found previously for UbVs that block animal virus vDUBs (170,171). Despite the structural similarity of the representative OTU family member AtOTLD1 (131) in the panel to TYMV PRO, it was not inhibited by UbV3 (Figure 2.7). Results of the *A. thaliana* DUBs panel assay suggested that transgenic expression of UbV3 in *A. thaliana* would not interfere with its Ub system.

Based on gel filtration and X-ray structure analysis, we found that UbV3 forms a dimer (Figure 2.8A) that is facilitated by a G10V substitution. Dimerization resulting from a G10V substitution has previously been found to enhance the affinity of a UbV for a specific ubiquitin interacting motif (212). This is consistent with the effect of this substitution in the UbV3 dimer described here, since reverting the substitution back to valine disrupts UbV3 dimerization and

dramatically reduces the binding affinity of UbV3 for the protease (Figure 2.9). Dimerization accompanied by the loss of β-turn may lead to the structural instability of UbV3 molecule, however, additional hydrophobic interactions between two UbV3 molecules involving P8 and F9 appear to compensate for this loss, as described above (Figure 2.8F).

As the X-ray crystal structure of the covalently linked TYMV PRO-UbV3 complex agrees with the SAXS *ab initio* envelope model of the non-covalent complex (Figure 2.9A), this suggests the binding conformation is not disturbed by the introduction of a covalent bond that was needed to crystallize the complex. Further, given the extensive interactions of the L71–R74 region of UbV3 within the active site cleft of TYMV PRO (Figure 2.9), it also suggests that the covalent linkage of G75 to the active site cysteine of TYMV PRO does not significantly affect the natural binding mode of UbV3 to the protease. Finally, no significant interactions exist between the two TYMV PRO chains of the asymmetric unit of the crustal structure, which indicates the complex is primarily held together by the interactions between UbV3 and TYMV PRO.

Compared with WT Ub, UbV3 dimerization creates a larger hydrophobic binding interface with TYMV PRO, where hydrophobic sidechains on this β1-β2 loop (F9, V10, F12) appear to form an extended hydrophobic network with TYMV PRO, thereby increasing affinity (Figure 2.10A). Utilizing this extended binding interface and its structural flexibility, the UbV3 dimer experiences conformational change, especially on the β1-β2 region when it binds to TYMV PRO, where most mutations lying on (Appendix, Figure A7). In summary, dimerization of UbV3 may not be caused by sole amino acid substitution, but rather by multiple substitutions acting together. Substitutions made additional binding interface for TYMV PRO/DUB, which include extended hydrophobic network. Further substitutions on other sites on UbV3 may promote its efficiency of inhibition.

A previously determined X-ray structure of TYMV-PRO bound to wild-type Ub suggested that although K6 of Ub was involved in crystal packing contacts with a neighbouring molecule, it might participate in binding TYMV PRO in solution by forming a salt bridge with E759 of the protease (134). However, a molecular dynamics simulation of the complex did not support this hypothesis due to distance constraints (134). Interestingly, K6 is substituted to R6 in UbV3, and the additional length provided by the arginine sidechain enables a convincing ~3.3Å salt bridge to form with the side chain of E759 (Figure 2.9D). Reverting the arginine substitution back to lysine or to alanine resulted in a measurable reduction in the ability of UbV3 to block TYMV PRO activity (Appendix, Figure A8). Given the previous observation that K6 of Ub was not quite close enough to engage productively with E759 of TYMV PRO, it was interesting that a UbV was selected from a phage display library with a substitution that closed the distance by using the of guanidinium group of Arg, the only choice available to form an adequate salt bridge.

The hydrophobic I44 patch on Ub is commonly found to participate in the binding of the molecule to other proteins (214). Surprisingly, the I44 patch of UbV3 (I44, L8, H68, V70) does not engage with TYMV PRO. L8 was substituted to P8 and it instead participates in a hydrophobic network extended from the I36 patch interface on TYMV PRO (Figure 2.10A). The region of TYMV PRO adjacent to the hydrophobic I44 patch of UbV3 primarily contains residues with polar sidechains (Appendix, Figure A9). It is, therefore, curious that UbVs with polar substitutions in the I44 patch were not selected by phage display, as it is conceivable that such substitutions could contribute to increased binding affinity between the proteins. Nonetheless, UbV3 is a potent inhibitor of TYMV PRO, and its low nanomolar binding affinity is consistent with UbVs we have identified for vDUB from other viruses (170,171).

CHAPTER 3: DEVELOPMENT OF TRANSGENIC *A. thaliana* THAT IS RESISTANT TO TYMV INFECTION

Contributions Statement:

All this transgenic study was performed by Anuradha De Silva following a discussion with Dr. Mohommed Mira (Postdoctoral fellow in Dr. Stasolla's lab). The infection study was performed by Dr. John Weiland (USDA group, ND), and Anuradha De Silva completed an analysis.

3.1 Introduction

Plant viruses are a significant challenge to global agriculture, causing substantial economic losses and compromising food security. The most common plant viruses worldwide (222)are alleged +ssRNA viruses. To accomplish successful infection, plant proteins are recruited (223) to cell movement of viral proteins (224) and prevention or shutdown of plant defence mechanisms (225). During the replication process, most plant proteins can recognize the components of viral replication factors (226) and initiate antiviral defences (227).

Throughout evolution, plants have developed nucleotide-binding site leucine-rich repeat protein (NBS-LRR) as cytoplasmic receptors to identify viral factors and initiate antiviral defence signalling pathways to prevent viral replication (228). Dicer-like proteins in plants can recognize the dsRNA to initiate the antiviral immunity mediated by RNA silencing pathways (229). Pathogen-triggered immunity (PTI) and viral-associated plants can utilize the pattern recognition receptors (PRR) to identify viral proteins in the cytoplasm (230).

There are two main types of counter-attack mechanisms employed by ssRNA viruses to prevent plant defence. The first is to manipulate plant proteins against the plant itself (231) and the second is to shutdown of plant defences using virally encoded proteins (232). For the first case, RNA viruses have evolved mechanisms by using plant proteins to shutdown antiviral defences: (1) the viruses recruit plant proteins to suppress RNA silencing (233), and (2) viruses may use heat shock proteins such as heat shock proteins 70 and 90 to induce viral replication by producing viral replication complexes (234). For the second case, plant viruses can use viral proteins to shut down plant protein regulation: viral deubiquitinase or viral protease can hijack ubiquitin mediated proteasomal pathways (235).

Traditional control methods, such as chemical pesticides and crop rotation, often prove inadequate or unsustainable (236). For years, genetic engineering has emerged as a promising strategy to develop plants resistant to viral infections (237). Initially, the cross protection was

known as the prevention of infection by a secondary virus based on prior infection with a similar primary virus (238). However, it was named as “coat protein-mediated resistance” lately considering the molecular mechanism of engineered viral coat protein in the plants (239) and successful viral resistant plants were achieved by this technique such as “Rainbow Papaya” against Papaya ring spot virus (240,241) and “HoneySweet”C5 Plum against Plum pox virus (242). Also, other viral protein-mediated resistance mechanisms were demonstrated, such as viral RNA-dependent RNA polymerase in transgenic tobacco plants (243) and replicase derived from cucomovirus, potato virus X and alfamovirus (244,245). Interestingly, this replicase approach was used to produce successful viral resistant plants to the ssDNA viruses of Gemini viruses, African cassava mosaic virus (ACMV) and Tomato yellow leaf curl virus (TYLCV) (246). Native or truncated forms of the replicase enzyme confer replicase-mediated plant resistance for several plant viruses (247,248). However, public pressure on introducing these viral-derived proteins into plants is concerning, and some of these transgenic plants were removed from the market (249). An alternative method and innovative approach which involves creating transgenic plants expressing protein-based inhibitors that interfere with the viral proteins and life cycle of a group of plant viruses would be worth studying.

The first objective of the thesis aims to explore the development of transgenic plants as a sustainable and effective solution to combat plant viral diseases using ubiquitin variants. As the above chapter mentioned, the delivery of UbVs to plants is plausible and expressing UbVs in plants could potentially inhibit the plant virus replication. As discussed, and confirmed in Chapter 2, UbV3 was selected as the tightest binding inhibitor for further transgenic studies using model plant *A. thaliana*.

Here, in collaboration with Dr. Claudio Stasolla and Dr. Mohommed Mira (Department of Plant Science, University of Manitoba), I have developed the transgenic plants and tested a transgenic approach to suppress the viral DUB activity of the protease (PRO) from TYMV

during its infection of *A. thaliana* with the collaboration with USDA group. Transgenic expression of the UbV in the cytosol of *A. thaliana* resulted in reduced TMYV replication *in planta* and was inversely correlated to the amount of UbV expressed in the plants. The results demonstrate the potential of using UbVs to protect plants from viruses that encode a protease with DUB activity.

3.2 Material and Methods

3.2.1 Molecular cloning and construction of UbV3 expressing transgenic plant lines

Synthetic DNA (Integrated DNA Technologies) of expression cassette consisted of the UbV3 open reading frame with a linker between attB1/attB2, a MASS (Met-Ala-Ser-Ser) motif to initiate translation and enhance protein stability (250), a 3x FLAG tag for protein detection, attB2, a linker between attB2 and T35s sequence. The expression cassette was amplified by PCR using primers listed in Table 3.1.

Table 3. 1 Primer used to construct binary vector pK2GW7

Oligo name	Binary Vector	Primers
UbV3	pK2GW7	5'GATATA**ACTAGT**GATATCACAAGTTTGTAC 3' 3'GATATA**AAGCTT**GGGCCCGACGTCCG5'

The resulting PCR amplicon was ligated into a pK2GW7 binary vector using restriction sites SpeI and HindIII to generate an N-terminally FLAG-tagged UbV3 expression cassette for integration into *A. thaliana* via *Agrobacterium*-mediated transformation (Appendix, Figure A11). The recombinant binary vector, pK2GW7-UbV3, was transformed to *Agrobacterium* GV3101::pMP90 strain via electroporation.

Cold stratification-treated sterile *Arabidopsis* seeds were kept at 4 °C for two days. Plates were then moved into a plant growth chamber (20-22 °C and 50% relative humidity) under a 16h light and 8h darkness cycle. Fluorescent bulbs provided white light (100 µmol m^{-}

^{2} sec^{-1}). Two-week-old seedlings grown under these conditions were transplanted from plates to soil and grown further under the same lighting and temperature conditions.

Arabidopsis thaliana Colombia (Col-0) was used as the wild-type strain for generating all transgenic lines. Transgenic *A. thaliana* was generated using *Agrobacterium*-mediated transformation by floral dip and a floral spray with *Agrobacterium tumefaciens* GV3101 (251). Kanamycin resistance was used to select transgenic plants and zygosity. The presence of the transgene was confirmed by PCR, and expression of UbV3 protein was detected by western blot analysis using an anti-FLAG antibody (BioRad). Three transgenic lines (*UbV3-1*, *UbV3-15* and *UbV3-18*) were subjected to phenotype analysis (Appendix, Figure A12).

3.2.2 Phenotype analysis

Half-strength Murashige and Skoog (MS) media containing 0.8% phytoagar and 2% sucrose at pH 5.8 was used for seed germination. Plates were placed in a growth chamber (16 h light/ 8 h darkness) and grown under light conditions until they reached 50% of the flowers to be produced. Five hundred seeds were used for the seed germination experiment.

Thirty wild-type and transgenic plants were analyzed for flowering time and shoot growth characteristics. Two weeks old, seedlings were transplanted from plates to the soil. For flowering time analysis, the total duration of flowering was measured. The height of the plant and dry mass weight after 21 days of seed germination were analyzed for shoot growth analysis. The data was obtained from three repeated experiments. Experimental data shown in this study are means with 95% confidence intervals (C.I). One-way ANOVA was used for data comparison. Probabilities of 0.05 or less were considered statistically significant. Graphpad Ver. 9.5.1 was used for data analysis.

3.2.3 Quantification and detection of FLAG-tagged UbV3

Total protein from 100 mg of foliar tissue (transgenic and wild-type) was isolated using lysis buffer (0.12M Tris-HCl pH6.8, 4% w/v SDS, 10% v/v beta-mercaptoethanol and 5% glycerol). The expressed UbV3 was quantified using a FLAG-tag (DYKDDDDK) detection ELISA kit following the protocol of the manufacturer (Cayman Chemical 501560).

Transgenic and wild-type tissue samples homogenized in protein loading dye (50mM Tris-HCl, pH 6.8, 100mM DTT, 2% SDS, 10% glycerol, $0.1gL^{-1}$ bromophenol blue) were boiled at 95 °C for 10 minutes. After vortexing followed by centrifuging, 20 µl of the supernatant was loaded and resolved on 12% SDS-PAGE gels. Proteins were then transferred to nitrocellulose membrane. The membrane was blocked with 5% Tris-Buffered Saline Tween-20 (TBST) skim milk for 1 hour at room temperature and then incubated with primary antibody (monoclonal Anti-FLAG M2) solution overnight at 4°C. The following day, the nitrocellulose membrane was transferred to the secondary antibody, Goat anti-mouse IgA: HRP and incubated for 2 hours at room temperature. Following the addition of the HRP substrate, the chemiluminescent signal was detected.

3.2.4 Subcellular fractionation of FLAG-tagged UbV3

For subcellular fractionation of FLAG-tagged UbV3, differential centrifugation was performed as described in (252). Protoplasts were isolated using a protoplast isolation kit (bioWorld, USA) and resuspended in homogenization buffer (0.4M sucrose, 3mM EDTA, 50mM Tris-HCl and 2mM DTT) and then disrupted with ~5 strokes of a Potter-Elvehjem homogenizer at 4°C (1:2 ratio of cells to buffer). The homogenate was then centrifuged at 800 x g for 15 min at 4°C, and the supernatant was separated from the cell pellet and further centrifuged at 10,000 x g for 15 min at 4 °C. The resulting supernatant, which contains mitochondria and plastids, was again separated from the pellet, and further centrifuged at 100,000 x g for 1 h at 4°C to generate a final supernatant that was the cytosolic fraction. As

previously described, the presence of UbV3 was visualized using FLAG-tagged detection western blot analysis.

3.2.5 Subcellular Localization

Fifteen-day-old transgenic seedlings were examined with Zeiss laser Confocal LSM 700 with Zeiss Imager M2 Microscope with Zen Black 2012 software. Leaf epidermal and inflorescence tissues of transgenic *A. thaliana* were fixed using 100% methanol. The cell walls were digested using 0.2 % cellulase and 0.15 % Macerozyme in 2 mM MES, pH 5.7. The membrane was permeabilized using the air dry, and tissues were blocked with BSA (253). Anti-FLAG tag antibody (ab245893) was used to detect the FLAG-tagged UbV3.

3.2.6 Inhibition of TYMV PRO with cytosolic extracts from transgenic *A. thaliana*

The inhibition assay using Ub-AMC (Boston Biochem) as a substrate was performed as described (171). Experiments were performed in assay buffer (50 mM Tris-HCl (pH 8.0), 150 mM NaCl, and two mM DTT) containing 1μM Ub-AMC substrate. The cytoplasmic fraction (~10-15kDa) was isolated using ultracentrifugation and centrifugal filtering techniques. The varying concentrations of cytoplasmic fractions of transgenic and wild-type *A. thaliana* were tested against 500 nM TYMV PRO. Inhibition activity was measured by monitoring the AMC fluorescence emission at 460 nm (excitation at 360 nm) for 30 minutes using a SpectraMax iD5.

3.2.7 Protoplast infection study

For the inoculation of *A. thaliana* protoplasts, plants were grown at 22 °C under fluorescent lighting with a 12 h day length to suppress bolting. Protoplasts were obtained using

a protocol for Chinese cabbage (254) and inoculated using electroporation (181) of synthetic, capped RNA transcribed from plasmid pTYMC (254). The washed protoplasts were transferred aseptically to the incubation medium (0.55M mannitol-MES pH 5.6 containing Muriashige and Skoog basal medium with vitamins). After 24 h and 48 h of incubation period, protoplasts were collected by centrifugation and frozen at -80 °C. The infected protoplasts were disrupted to extract the total protein content. The western blot analysis was performed to detect the TYMV coat protein as previously described (254). Evaluation of both inoculated whole plants and protoplast by ELISA followed the procedure recommended by the kit manufacturer (Kit# RT-0125; DSMZ-German Collection of Microorganisms and Cell Cultures GmbH, Braunschweig, Germany).

3.2.8 Inoculation of TYMV and infection study

Transgenic and wild-type Col-0 *A. thaliana* plants were grown at 19-21 °C under a 16h light/8h dark photoperiod in a growth chamber, and plants were inoculated with TYMV before and after the occurrence of floral transition using the foliar spray technique. After the inoculation, plants were allowed to grow in the same conditions, harvested at 28 of post-inoculation. The samples were frozen with liquid nitrogen and stored at -80 °C for further analysis. As previously described, the amount of UbV3 expressed in each infected transgenic plant was quantified using a FLAG-tag detection ELISA kit (Cayman Chemical 501560), and the accumulation of TYMV was determined using ELISA (TYMV Detection kit, Creative Diagnostics). Ten wild-type plants were used as a negative control.

Experimental data shown in this study are means with 95% confidence intervals (C.I). Quadratic regression analysis was used for data comparison, and probabilities of 0.05 or less were statistically significant. The Graphpad software Ver. 9.5.1 was used to analyze the data.

3.3 Results

3.3.1 Transgenic expression of UbV3 does not adversely affect *A. thaliana* physiology

Having demonstrated the ability of UbV3 to potently and selectively block TYMV PRO activity *in vitro*, we next determined if this ability could be used to suppress TYMV replication *in planta*. To explore this possibility, transgenic *A. thaliana* lines were developed that constitutively expressed the UbV3 protein via the 35S promoter derived from the CaMV (255,256). (Figure 3.1). Following *Agrobacterium*-mediated transformation (257), *A. thaliana* transformants were first screened by PCR to detect genomic insertion of the UbV3 expression cassette, followed by Western blot analysis to verify the expression of the UbV3 protein (Appendix, Figure A2). Three transgenic plant lines (*UbV3-1*, *UbV3-15* and *UbV3-18*) were confirmed to express UbV3 protein and thus selected for further studies (Figure A12). The zygosity of these transgenic lines was determined based on kanamycin antibiotic resistance, as the T-DNA binary vector pK2GW7 contains the neomycin phosphotransferase II gene (256).

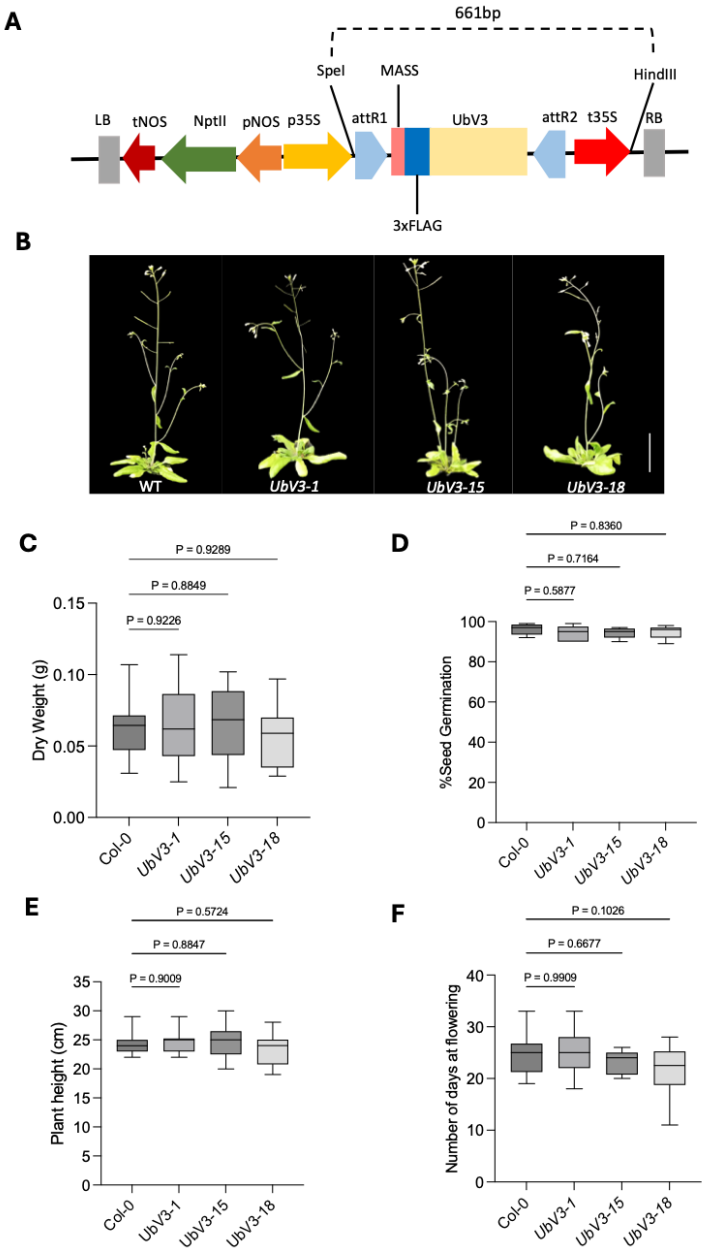

Figure 3. 1 Characterization of UbV3 expression in *A. thaliana* lines

A) T-DNA expression construct pK2GW7 (256): LB, left border; tNOS, terminator of NptII; NptII, neomycin phosphotransferase II gene; pNOS, promoter of NptII; p35S, CaMV 35S promoter; attR1 sequence; MASS, Met-Ala-Ser-Ser sequence; 3x FLAG tag sequence; UbV3, open reading frame; attR2 sequence; t35S, CaMV terminator sequence and RB, right border. (B) Phenotypic appearance of wild-type and three transgenic *A. thaliana* lines [*UbV3-1, UbV3-15* and *UbV3-18*] (scale bar, 30mm). (C) Dry weight after 21 days of seed germination; (D) Seed germination percentage; (E) Plant height; (F) Number of days at flowering of wild-type and transgenic *A. thaliana* lines (*UbV3-1*, *UbV3-15* and *UbV3-18*). Data in panels C, D, E and F represent three repeated experiments (Mean ± SD). The dry weight, number of days at flowering, and seed germination percentages of Col-0 and transgenic lines *UbV3-1*, *UbV3-15* and *UbV3-18* are not significantly different (p>0.05).

To evaluate whether UbV3 expression affected the phenotype of *A. thaliana*, comparative analyses were conducted between the three transgenic *A. thaliana* lines expressing UbV3 and the wild-type Col-0 parental line. Phenotypic analyses were conducted on all three transgenic lines (*UbV3-1*, *UbV3-15*, and *UbV3-18)*. Various growth parameters were evaluated, including seed germination, dry weight accumulation, flowering time, and plant height (Figure 3.1). The results of the phenotypic comparisons revealed no statistically significant differences ($p>0.05$) in terms of plant height, dry weight, flowering time, or seed germination percentage between the Col-0 and the transgenic lines. The findings suggested that the expression of UbV3 did not affect general plant physiology under the experimental conditions employed, which is consistent with UbV3 being highly selective for TYMV PRO (Figure 2.4).

3.3.2 UbV3 protein is present in the cytosol and organelle fractions of transgenic *A. thaliana*

Since TYMV replication occurs at the periphery of chloroplasts and protein maturation occurs in the cytosol of infected plants (148,176,220), we carried out subcellular fractionations of protoplasts isolated from leaf tissue of UbV3-expressing *A. thaliana* to determine where the UbV3 protein was localizing in plant cells. Protoplasts were isolated using a protoplast isolation kit (bioWorld, USA) and disrupted, followed by sequential centrifugation steps (800 x g, 10,000 x g and 100,000 x g) to obtain cytosolic and plastid fractions (the latter of which is enriched in mitochondria, chloroplast, and plastids) (252). Both the cytosolic and plastid fractions were found to contain UbV3 protein according to Western blot analysis (Figure 3.2A). This result was encouraging as it revealed the presence of UbV3 protein where it would be needed to block TYMV PRO activity and suppress TYMV replication in the host cell. We also quantified the amount of UbV3 expressed in inflorescence versus leaf parts of the transgenic

lines *UbV3-1*, *UbV3-15* and *UbV3-18* by ELISA and found that UbV3 was expressed primarily in leaf tissue and to a lesser extent in inflorescence parts (Figure 3.2B-D).

In addition to the subcellular fractionation study, the leaf and inflorescence protoplasts were examined using a confocal microscope after whole-mount immunolocalization (Figure 3.2E-J).

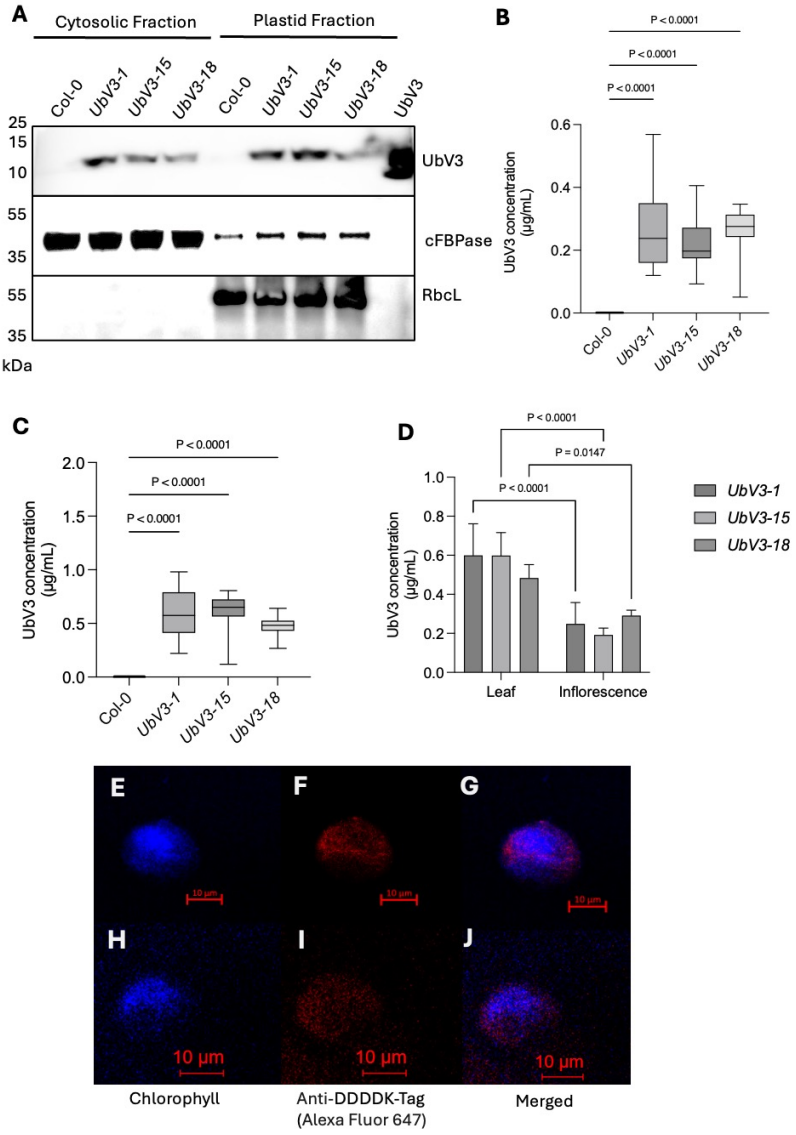

Figure 3. 2 Subcellular fractionation and quantification of transgene expression in leaf and inflorescence in wild-type and transgenic *A. thaliana*

A) Western blot analysis of differential centrifugations of protoplast lysates from transgenic *A. thaliana*. Lanes 1-4, supernatant fraction at 100,000xg (cytoplasmic fraction); lanes 5-8, pellet fraction (mitochondrial and chloroplast fraction) at 10,000xg; Lane 9, UbV3 protein standard. Western blot analysis of UbV3 detection was performed with monoclonal Anti FLAG M2 as the primary antibody and goat anti-mouse IgA:HRP conjugate as the secondary antibody. Polyclonal antibodies targeted against *Arabidopsis* cFBPase (cytosol) and RbcL (plastids) were applied to the same samples and the

goat anti-rabbit IgA:HRP conjugate as the secondary antibody to visualize via western blot analysis. The amount of UbV3 expression in inflorescence parts (B), foliage parts (C) and was quantified using a DYKDDDDK- tag detection ELISA kit. The data was obtained from two repeated experiments. Mean ± SD. (D) the amount of UbV3 expressed in leaf and inflorescence parts in transgenic *A. thaliana* are significantly different (p<0.05). The expression of UbV3 in the transgenic *A. thaliana* under confocal microscope. The subcellular localization of FLAG-tagged UbV3 in inflorescence tissues (E, F, and G) and leaf parts (H, I and J). E and H; chlorophyll, F and I; FLAG-tagged UbV3, G and J; merged image of Chlorophyll and FLAG-tagged UbV3. An anti-FLAG antibody was used to detect FLAG-tagged UbV3. The bar represents the 10µm distance.

Having identified UbV3 protein in the cytosol and plastid fractions of transgenic *A. thaliana* lines, we wanted to confirm if the expressed protein was functional and able to inhibit TYMV PRO activity. Indeed, we found that cytosolic extracts from transgenic *A. thaliana* contained functional UbV3, as these extracts were able to inhibit purified recombinant TYMV PRO in a concentration-dependent manner; whereas, cytosolic extracts from the parent Col-0 *A. thaliana* did not (Figure 3.3). Taken together, our structural and functional studies of UbV3 suggested the protein was well suited to inhibit TYMV PRO in plant cells and suppress TYMV replication *in vivo*.

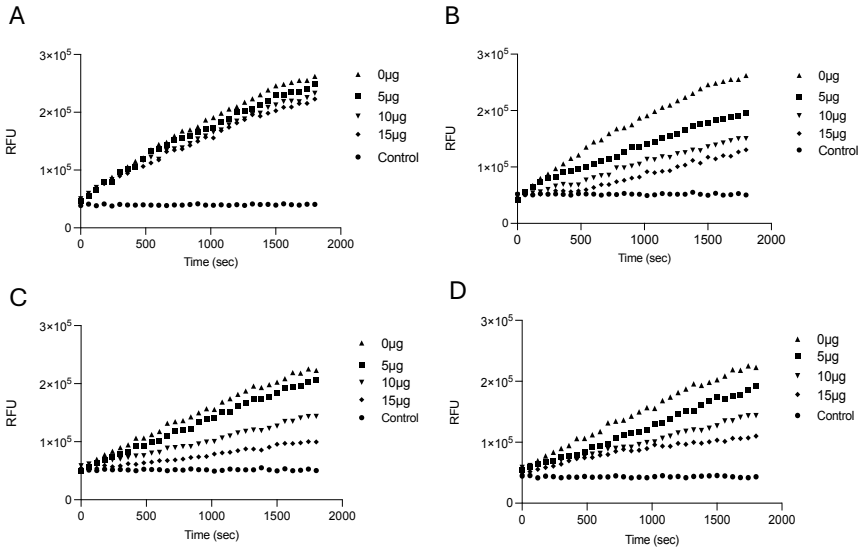

Figure 3. 3 Hydrolysis of 1µM Ub-AMC by 500nM TYMV PRO in the presence of varying concentrations of protoplast cytoplasmic fractions

(A) Wild-type *A. thaliana s* protoplast cytosolic fraction and transgenic *A. thaliana* protoplast cytosolic fraction UbV3-1 (B); UbV3-15 (C) and UbV3-18 (D). The line symbols represent the concentration of the cytoplasmic fraction (µg), and the black circle line represents the 1µM of Ub-AMC control).

3.3.3 UbV3 suppresses TMYV replication *in planta*

To gain insight into the ability of UbV3 to suppress cellular replication of infectious TYMV, protoplasts prepared from leaves of transgenic *A. thaliana UbV3-1* and the parent Col-0 line were infected with TYMV for 24 to 48 hours, followed by western blot analysis to detect the presence of TYMV coat protein (Figure 3.4A). Protoplasts were primarily comprised of mesophyll cells, which are the main photosynthetic cells of the plant leaf. After a 24-hour incubation in the presence of infectious TYMV RNA, the accumulation of TYMV coat protein was similar in transgenic protoplasts and wild-type Col-0. However, after 48-hour incubation, there was no longer any detectable coat protein in transgenic protoplasts, whereas coat protein continued to accumulate in the parent Col-0 protoplasts. This remarkable reduction in viral coat protein suggested that UbV3 interfered TYMV replication, where the lag phase may be due to the response time needed for the Ub-proteosome (UPS) system to clear viral protein from the protoplast generated directly off the initial infectious RNA transcripts.

To assess whether UbV3 expression could suppress TYMV replication in whole plants, we inoculated transgenic *A. thaliana UbV3-1* and wild-type Col-0 plants with infectious TYMV particles using an established foliar spray method (258) (Appendix, Figure A13). The infection was performed at two intervals before and after the bolting of *A. thaliana* plants using the foliage spray technique. The difference in TYMV replication between transgenic and WT plants was analyzed by determining the presence of TYMV coat protein in bulked leaves and inflorescences of inoculated plants by analysis with the TYMV ELISA kit, whereas the expression level of UbV3 in infected plants was determined using a FLAG-tag detection ELISA kit (Appendix, Figure A14, Table A20-21). We found that UbV3 expression levels varied between individual transgenic *A. thaliana UbV3-1* plants. However, transgenic plants expressing higher levels of UbV3 protein had the lowest levels of detectible TYMV protein. The observed negative correlation between the expression level of UbV3 and TYMV viral load

in transgenic *A. thaliana UbV3-1* demonstrated that the UbV3 protein was able to suppress TYMV replication *in planta* (Appendix, Figure A14). Though the presence of UbV3 was not able to completely clear the TYMV infection, as TYMV proteins were detected in all infected transgenic plants, this may be due to insufficient levels of UbV3 expression in the transgenic *UbV3-1* line that was used for this proof-of-principal study. Future transformation and breeding experiments aimed at increasing the expression level of UbV3 could potentially generate transgenic lines of *Brassica* species that are highly resistant to TYMV infection. The UbV inhibitor strategy could also be used to protect additional economically important plants from infection by Tymoviruses, as well as additional plant viruses that depend on proteases with DUB activity.

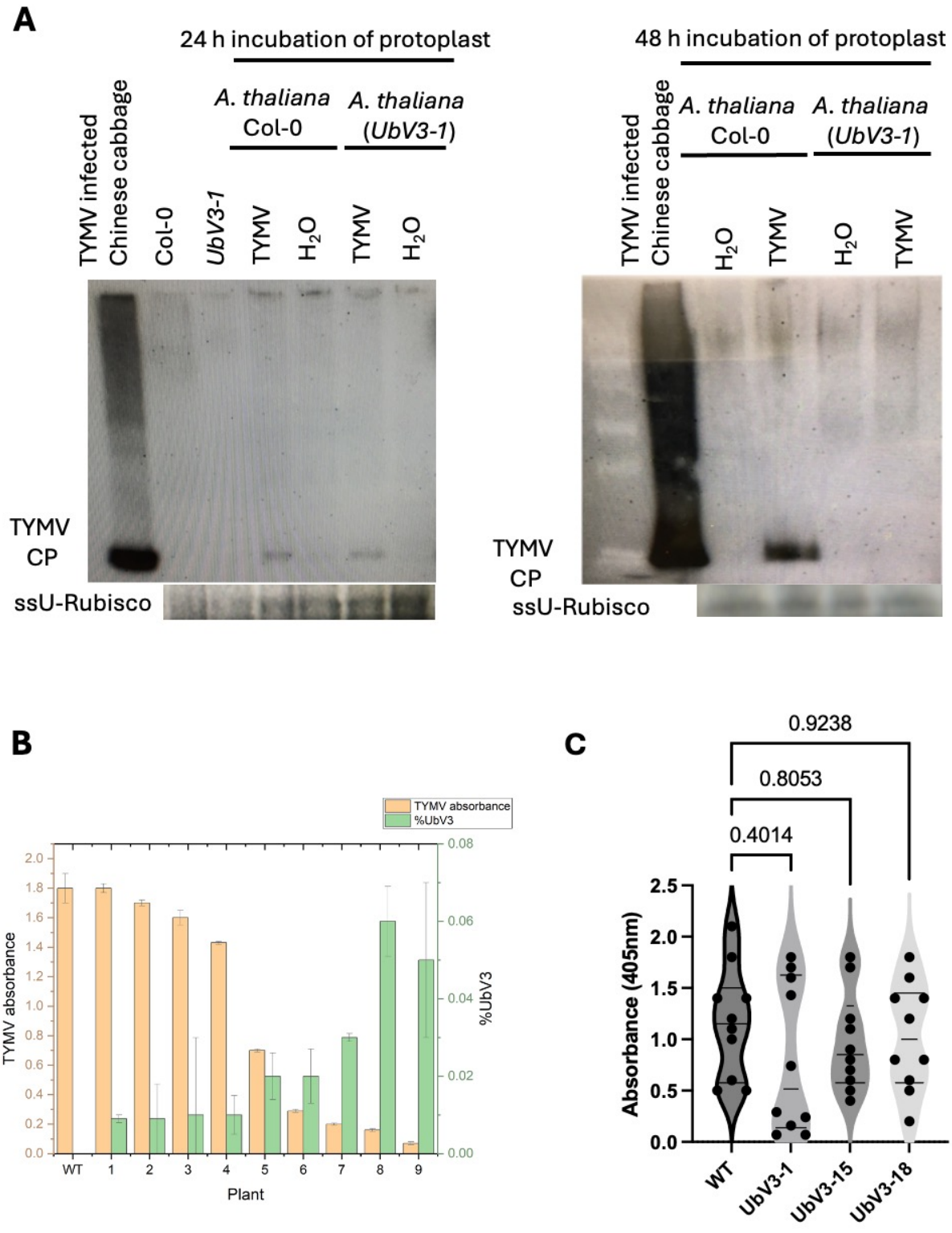

Figure 3. 4 UbV3-mediated suppression of TYMV replication *in planta*

(A) Protoplast infection study after 24-hour (left) and 48-hour (right) incubation with TYMV. Western blots were probed with anti-TYMV antiserum, and coat protein was detected under chemiluminescence. The small subunit Rubisco (ssU-Rubisco) was used as a loading control. (B) Detection of TYMV coat protein accumulation versus UbV3 expression level in the

transgenic *A. thaliana* UbV3-1 line and parent Col-0 plants. The accumulation of TYMV was detected using ELISA, and the expression of UbV3 was quantified using a FLAG-tag detection ELISA kit. The data were statistically analyzed using Quadratic regression analysis, and a strong negative correlation was observed in the Transgenic line UbV3-1 (Quadratic regression analysis, R^2=0.80; *see Figure A14*) (C) The Analysis of variance of TYMV coat protein detection (Absorbance at 405nm) of wild-type Col-0 and transgenic lines. The TYMV coat protein detection of the transgenic lines was not significantly different from Wild-type Col-0 ($p>0.05$). At least 10 plants from each independent line were inoculated with TYMV and analyzed for the analysis.

3.4 Discussion

TYMV infection can result in characteristic symptoms in the infected plants, such as mosaic patterns of light and dark green patches on leaves, yellowing, stunting, leaf distortion, deformed flowers and reduction in plant vigour (184). This results because the viral replication complex (VRC) is associated with the chloroplast envelope, particularly the peripheral vesicles and cytoplasmic invaginations in the chloroplast (259). Our funding that UbV3 was expressed in the cytosolic and plastid (chloroplast/mitochondria) of transgenic *A. thaliana* suggested that it would be available to co-localize with TYMV replication complexes that form at the periphery of chloroplasts (148,176,220), thereby blocking PRO and reduces TYMV replication. Indeed, this was confirmed in our subsequent infection studies (Figure 3.4). Interestingly, the amount of UbV3 expressed in the inflorescence and leaf parts of the transgenic plants, showed that UbV3 expressed in both inflorescence and leaf parts and UbV3 in leaves was twice higher than UbV3 in inflorescence parts (Figure 3.2). This phenomenon may arise from variations in transgene expression levels, even when driven by the constitutive CaMV 35S promoter (260). The subcellular fractionation analysis further revealed that UbV3 is, in fact, present in the cytosol where TYMV replication occurs (261) and also in other cellular compartments such as plastids and mitochondria.

To assess whether UbV3 affects TYMV accumulation *in vivo*, the transgenic lines were subjected to initial screening (Appendix, Figure A13) and *UbV3-1* transgenic line and wild-type *A. thaliana* Col-0 plants were selected for further TYMV infection. TYMV infection was quantified by the amount of viral coat protein present in the infected protoplasts or plants. Results from the protoplast infection study revealed that TYMV accumulation was dramatically reduced after 48 hours of incubation. However, we observed more variable results from our whole plant infection studies, possibly because TYMV does not infect *A. thaliana* aggressively. Also, the level of UbV3 expression was different between transgenic plants, which is possibly due to transgene copy number, site of the insertion in the plant genome, epigenetic mechanisms and repressor proteins in the plant. Despite this variability, we observed notable coat protein reduction that was negatively correlated Quadratic regression R^2= 0.80 (Appendix Figure A14)] to the level of UbV3 expression. The strong correlation demonstrated that higher levels of UbV3 expression were more effective at suppressing TYMV replication in plants. Thus, future efforts to maximize UbV expression could enhance the efficacy of this antiviral approach.

CHAPTER 4: BIOCHEMICAL ANALYSIS OF MACHADO-JOSEPH DOMAIN CONTAINING DEUBIQUITINASES IN *A. thaliana*

Contribution Statement:

All this work was performed by Anuradha De Silva following a discussion with Dr. Kihun Kim (Postdoctoral fellow in Dr. Mark's lab).

4.1 Introduction

The Machado–Joseph disease (MJD) protein domain family of DUBs is comprised of four members in humans—Ataxin3, Ataxin3L, JOSD1, and JOSD2. The name of this DUB family derives from a neurodegenerative disorder that is associated with mutations in the *ataxin-3* gene (262). Each MJD subfamily enzyme contains a conserved Josephin domain within their N-terminal region that is a cysteine protease that hydrolyzes polyUb linkages (71). Ataxin3 and Ataxin3L possess a Ub-interacting motif (UIM) at their C termini, facilitating binding to Ub conjugates, including ubiquitinated proteins. The flexible region between Josephin and UIMs acts as a folding arm, bringing the Ub chain into the proximal active site for efficient trimming of Ub signals (68,263). Initially described in the 26S proteasome subunit PSD4/RPN10, the UIM likely embeds as a short alpha-helix into various protein folds (69,264,265). Ataxin3 and Ataxin3L exhibit cleavage preference for K48- and K63-linked Ub chains, respectively, while JOSD1 targets monoubiquitinated substrates and JOSD2 prefers K11-, K48-, and K63-linked Ub chains (70,71,266). Ataxin3 also regulates transcription by mediating gene repression through interaction with essential transcription regulators (267).

In plants, knowledge about the MJD subfamily is limited. Three putative MJD proteases have been predicted in the Arabidopsis genome (NM_100604.3, NM_128518.2 and NM_115273.4). Only At2g29640 and At3g54130 share the conserved Josephin domain, challenging the classification of At1G07300 as an MJD subfamily member (21,268). Functional studies necessary to verify that these *Arabidopsis* genes are bona fide DUBs have not been carried out. Here, I report the cloning, expression, purification and functional characterization of recombinant At1g54130, At2g29640 and At3g54130 and confirm that At3g54130 possess DUB activity, as mentioned in Chapter 2. The At3g54130 was the only protein expressed as soluble.

4.2 Materials and Methods

4.2.1 DNA constructs

Synthetic DNA coding for AtAT1G, AtAT2G and AtAT3G was designed based on the predicted DUB domain coding sequence. The DUB domains were predicted using ScanProsite and NCBI Conserved Domain Search (Figure 4.1). Synthetic DNA was codon optimized for expression in *E. coli*, PCR amplified and ligated into pGEX-6p-1, pET28a and pET19b using standard restriction cloning (Table 4.1). The recombinant pET vectors were constructed for an X-ray crystallization study. The site-directed mutagenesis was used construct catalytically mutated AtAT3G (AtAT3G C20S). All constructs were transformed into *E.coli* BL21(DE3) cells following Sanger sequence verification for protein expression and purification.

Table 4. 1 DNA Constructs of MJD family DUBs

Oligo Name	NCBI Number	Primers	Purpose
AtAT1G (At1g07300)	NM_100604.3	5'GATATA**GGATCC**TCAGCAACCGGTATC3' 3'CAACAGCACCTCCTAA**CTCGAG**GATATA5'	AtAT1G in pGEX6PI
AtAT2G (At2g29640)	NM_128518.2	5'GATATA**GGATCC**GCCGATTCAGAGTC3' 3'GTGGTAGCAAAAGCTAA**CTCGAG**GATATA 5'	AtAT2G in pGEX6PI
AtAT3G (At3g54130)	NM_115273.4	5'GATATA**GGATCC**GAACGCACCAGCAAC3' 3'GAAACCGAAAAACAGAAATAA**CTCGAG**GATATA5'	AtAT3G in pGEX6PI
AtAT3GC20S	NM_115273.4	5'GAGTCAAATTTATCCGCTGTACATTG3' 3'GCATGCTCTACCACGAGGTTCAG5'	Site-directed mutagenesis
AtAT3G	NM_115273.4	5'GATATA**CATATG**GAACGCACCAGCAAC3' 3'GAAACCGAAAAACAGAAA**GGATCC**TATATC5'	AtAT3G in pET28a and pET19b

4.2.2 Protein expression and purification of AtAT3G

Transformed *E.coli* harbouring expression vectors were grown overnight in LB containing 150 µg/ml ampicillin (pGEX) or 35 µg/ml kanamycin (pET28a and pET19b). After

16-18 hours, the overnight cultures were used to subculture fresh LB containing the appropriate antibiotic and grown to an OD_{600} of ~0.8 at 37 °C with shaking, followed by protein induction with 0.5 mM IPTG at 16 °C for ~18 h. Protein purification for the GST fusion proteins was done identically, as outlined in section 2.2.3 for the TYMV PRO and plant deubiquitinases. Purification of AT3G in pET28a and pET19b was done as mentioned in section 2.2.4.

4.2.3 DUB Assays

Ub-AMC assays were carried out as detailed in section 3.2.7 using a SpectraMax iD5 microplate reader (Molecular Dimensions). K48- and K63- di-Ub chain cleavage assay was performed using K48- and K63- di Ub (UbiQ, UbiQ-L04) as deubiquitination substrates. The assay was performed using assay buffer (50 mM Tris-HCl, pH 8.0, 100 mM NaCl, 1 mM DTT) containing 1 µg substrate and 2 µM AtAT3G. After incubation at 25°C for 18 hours, reactions were stopped by adding 2X SDS-PAGE sample buffer. Reactions were visualized by carrying out TRIS-Tricine PAGE (10%) and subsequent detection using a Pierce Silver Stain Kit (Thermo Fisher Scientific).

4.2.4 Structural Prediction

AlphaFold-based predictions of the three-dimensional structures of AtAT3G, and AtAT2G were made with ColabFold (AlphaFold2.ipynb)(269,270). The Local Distance Difference test (IDDT) results are presented in the Appendix, Figure A16.

The NMR solution structure of human Ataxin-3 (PDB:1YZB) was used to predict the structural resemblance of AtAT2G and AtAT3G with the predicted structures from ColabFold Protein structure database.

4.2.5 Crystallization screening

A single peak corresponding to the His_6-AtAT3G was pooled from the size exclusion chromatography. It was concentrated to 10 mg/mL for crystallization trials. Initial crystals were observed from preliminary screens under the conditions of 0.2M Magnesium chloride, 0.1M HEPES pH 7.5, 15% (w/v) PEG 400. Then, these crystals were identified as salt crystals because they were not illuminated with ultraviolet (UV) light.

4.3 Results

4.3.1 Construction of MJD family DUBs of *A. thaliana*

The AtAT1G, AtAT2G and AtAT3G were designed based on the predicted plant deubiquitinases from NCBI and TAIR databases. The predicted Josephin domain of AtAT2G spans between residues 13-168, and AT3G spans between residues 15-170. A sequence alignment with HsAtaxin-3 (Figure. 4.1A-B, alignment) revealed relatively low sequence similarity with AtAT2G (~23 %) and AT3G (~41 %) but did reveal that the catalytic Cys and His residues are conserved (orange triangles). After test inductions for protein expression, only AtAT3G was found to be soluble, AtAT2G was insoluble, and AtAT1G was not expressed (Figure 4.1C-E). The pET AtAT3G plasmids were constructed for X-ray crystallization screening because the yield from pGEX6PI was not sufficient.

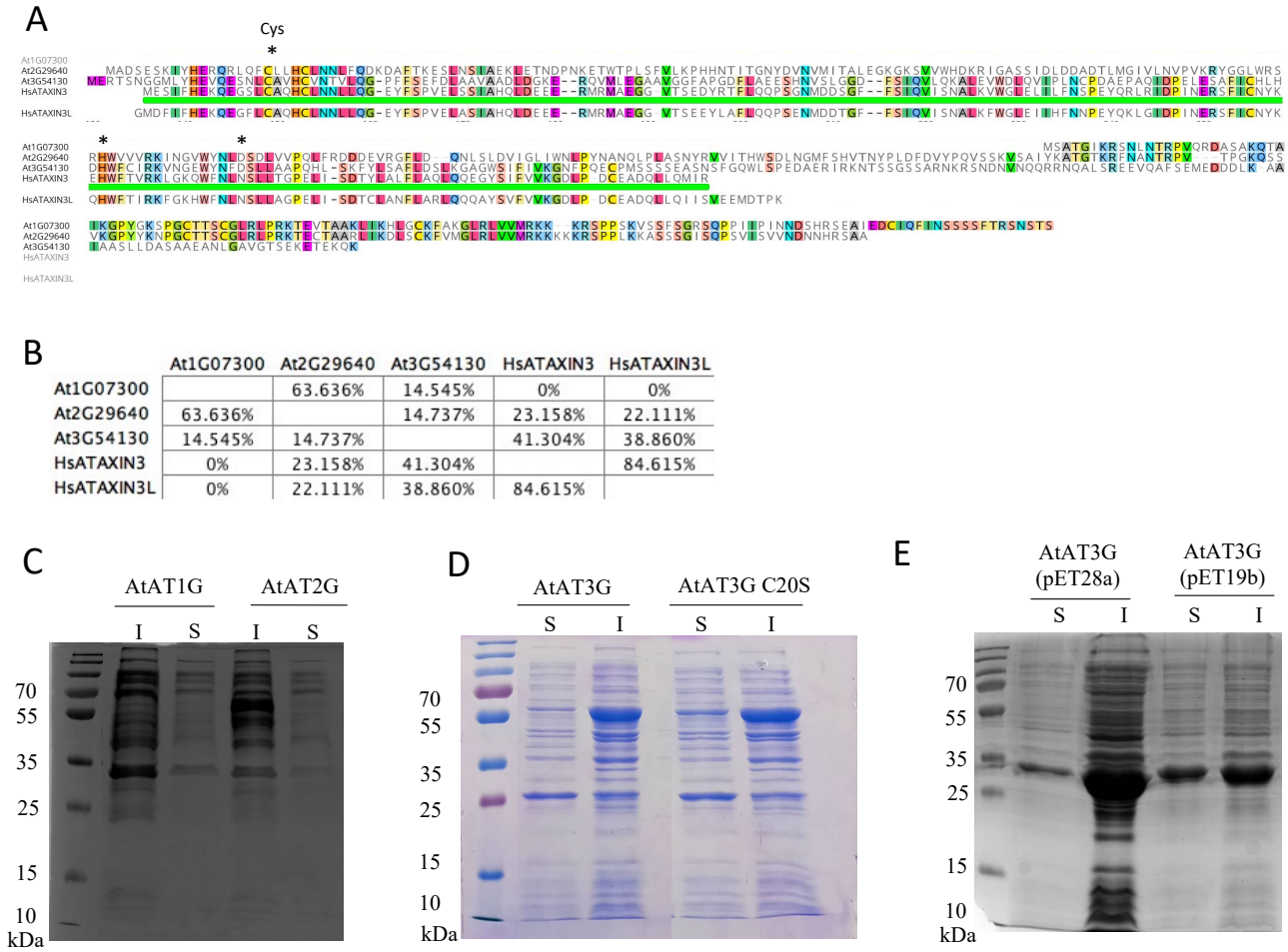

Figure 4. 1 Construction of MJD family DUBs of *A. thaliana*

(A) Sequence alignment of the full-length sequence of MJD family DUBs of *A. thaliana* (At1g54130, At2g29640 and At3g54130) and human MJD family DUBs (HsATAXIN3 and HsATAXIN2L). The catalytic residues are noted by black asterisk, including catalytic Cys. B) The percentage of sequence identity matric. C) SDS-PAGE gel of test induction of AtAT1G, AT2G and (D) AtAT3G with pGEX vector. (E) AT3G with pET28a and pET19b. The sequence alignment of MJD family DUBs shows that the AtAT1G sequence does not contain catalytic Cys, and the predicted protein of AtAT1G was only a peptide sequence according to SWISS-MODEL prediction.

4.3.2 Structure Prediction of AtAT2G and AtAT3G

Using the ColabFold online software, Alphafold predicted proteins were created and the superposition structures were visualized using PyMoL software (Figure 4.3A-B). The superposition model resembled the DUB domain of human MJD family deubiquitinases (PDB: 1YZB).

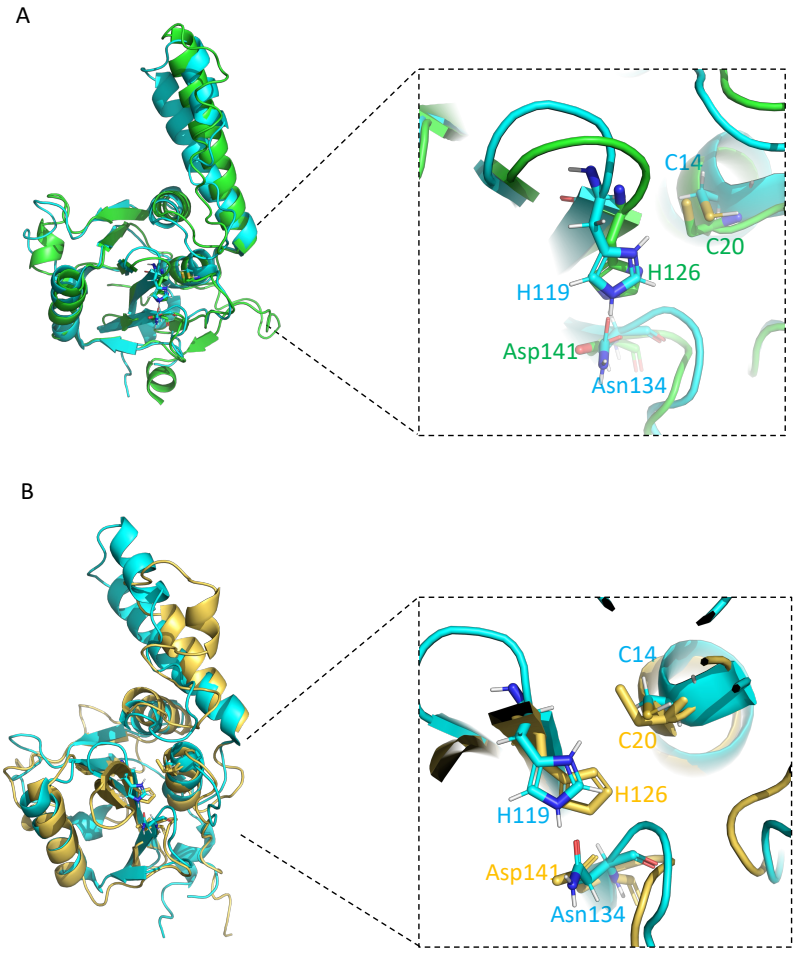

Figure 4. 2 Superposition of X-ray structure of HsATAXIN and predicted MJD DUBs of *A. thaliana*

(A) The superposition predicted AtAT3G (green) and (B) AtAT2G (yellow) with of 1YZB (cyan) The close-up view shows the catalytic residues. Based on the superposition structures, C20 was identified as a catalytic Cys residue of the AtAT3G enzyme.

4.3.3 Exploring the DUB activity of AtAT3G

As mentioned earlier, the Ub-AMC assay was performed to identify the DUB activity of mutated AtAT3G C20S and AtAT3G. Activity assays were performed at significantly higher molecular concentrations of the enzyme to demonstrate the activity (10-20 µM) [25°C for 3,600s in 50mM Tris HCl pH 8.0, 100mM NaCl and 5mM DTT]. Relative to the wild-type AtAT3G, the DUB activity of AtAT3G C20S was less (Figure 4.2A-B).

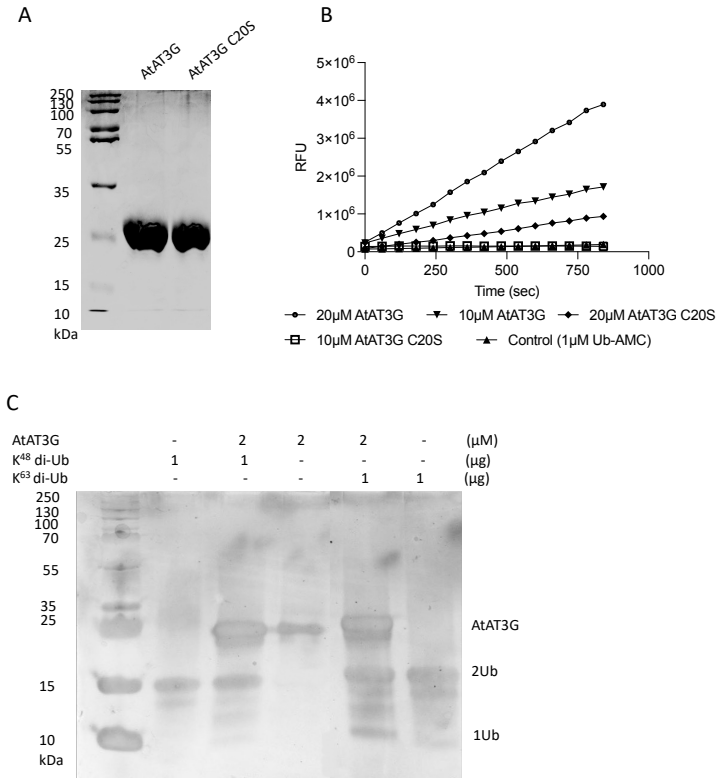

Figure 4. 3 DUB activity of AtAT3G and AtAT3G C20S

(A) SDS-PAGE gel of purified AtAT3G and AtAT3G C20S. (B) Ub-AMC hydrolysis with different concentrations of AtAT3G and AtAT3G C20S. (C) K48- and K63- di-Ub chain cleavage of AtAT3G after 20 hours of incubation at room temperature.

4.4 Discussion

In plants, the MJD subfamily of deubiquitinases is under study. There are three predicted MJD proteases have been found in Arabidopsis genome such as NM_100604.3, NM_128518.2 and NM_115273.4. The sequence alignment of HsAtaxin3, HsAtaxin3L, At1g07300, At2g29640 and At3g54130 showed the shared MJD domain with the amino acid sequence. The predicted catalytic triad residues of At2g29640 and At3g54130 are aligned with catalytic triad residues of HsAtaxin3 (Figure 4.2). In humans, the MJD family DUB consists of four members, Ataxin-3, Ataxin-3L, JOSD1, and JOSD and Ataxin-3L demonstrated higher deubiquitinase activity than other members (70). Also, Ataxin-3 and Ataxin-3L have different binding modes for ubiquitin-binding (71). This might be the reason that At3g54130 showed less DUB activity *in vitro* because the protein resembles more with Ataxin-3.

The catalytic sites for AtAT3G (Cys20, His126 and Asp141) and for AtAT2G (C18, H129 and Asp 144) were predicted using Expassy Scanprosite and Alphafold structure prediction (Figure 4.2) . Based on the superposition model and active sites of the DUB domain, AtAT2G may also be a DUB. Unfortunately however, none of the AtAT2G constructs expressed as soluble proteins in *E.coli*. The construction of AtAT2G would need to be optimized for future analysis. Nevertheless, human Ataxin3 and Ataxin3L recognize the K48- and K63-linked Ub chains (68), and AtAT3G exhibited slight cleavage of di-Ub of K48 and K63 (Figure 4.3). Further study is needed to optimize the ubiquitin-binding in AtAT3G.

Crystallization AtAT3G for structural studies by X-ray crystallography was not successful even after several attempts, which could be due to the presence of disordered regions within the protein. Only salt crystals were observed (Appendix, Figure A16). Phyre2 and PSIPRED prediction were performed to identify disordered regions and regions for protein binding. These predictions suggest that disordered regions exist within the expressed domain of AtAT3G that should be removed before attempting further crystallization trials for X-ray

crystallography studies. Alternatively, NMR spectroscopy could be used to elucidate the structure of AtAT3G, as was done for human Ataxin3 and Ataxin3L (265). Future structural studies would further verify AtAT3G as a member of the MJD family and set the stage for mutational studies aimed an elucidating its role in plant physiology

CHAPTER 5: BIOCHEMICAL ANALYSIS OF PORCINE REPRODUCTIVE RESPIRATORY SYNDROME VIRUS (PRRSV) PAPAIN-LIKE PROTEASE 2

CONTRIBUTION STATEMENT

The research work presented here was done by myself following discussions with Dr. Mark and Dr. Khajehpour. The figures in the Appendix were prepared by Dr. Ben Bailey (Dr. Mark Lab, Department of Microbiology) and Dr. Robert C. M. Knaap (Dr. Kikkert Lab, Leiden University Center of Infectious Diseases)

5.1 Introduction

The pork industry faces significant financial losses due to PRRSV outbreaks. Scientists and veterinarians have invested considerable resources in creating vaccines to prevent and control the spread of this virus . PRRSV is a positive-sense, single-stranded RNA virus and a member of the family *Arteriviridae* . Two strains of PRRSV, PRRSV-1 and PRRSV-2, are distinct viral species that infect livestock (271). While MLV (modified live virus) vaccines are used to manage outbreaks, they often have limitations (272). These include inadequate protection against different PRRSV strains and the potential for vaccine strains (MLV) to regain their ability to cause disease (273)(273,274).

PRRSV replicates with the help of four viral proteases, one of which is papain-like protease 2 (PLP2). Early studies suggested PLP2 belonged to a family of cysteine proteases. Further research revealed that PLP2 in PRRSV functions as a deubiquitinase enzyme (OTU family cysteine protease), helping the virus evade the host immune response. The PLP2 protein within PRRSV nsp2 has a complex structure. It includes an N-terminal PLP2 domain with deubiquitinase activity, a hypervariable region, a transmembrane domain, and a cysteine-rich domain. Interestingly, a slippery sequence allows the production of two alternative protein products – nsp2TF and nsp2N – through programmed ribosomal frameshifting. These products differ in their transmembrane domains and likely serve distinct roles during infection (120,275).

A key challenge in studying PLP2 is that its deubiquitinase activity and its role in viral polyprotein processing rely on the same active site residues. For this project, crystallographic data defining the Ub binding interface of these viral enzymes was used to guide the introduction of site-directed mutations (191). In addition to my research on blocking deubiquitinase activity

in plant viruses TYMV, I had the opportunity to contribute to this project investigating the structure and function of a deubiquitinase of PRRSV.

To better understand the specific mechanisms used by PRRSV to suppress host immune responses during infection, we investigated the structure of a critical multifunctional PRRSV protease, PLP2, which processes the viral polyprotein during replication and is capable of suppressing host antiviral immune responses. Using a crystal structure of PLP2 bound to its cellular substrate ubiquitin (Ub), we characterized the residues forming the substrate binding surface. This was used as a platform to guide the design of PLP2 mutants with reduced capacity to bind ubiquitin and provided a clear link between PLP2 deubiquitinating activity and host innate immune evasion. Using structure-guided mutagenesis and reverse genetics methods for PRRSV, we demonstrate that specific PLP2 residues that are critically involved in substrate recognition are under selective pressure to revert to wild-type during infection. These findings are in contrast to what has been observed with the equine arteritis virus (EAV) PLP2 domain, and uniquely highlight the specific importance of PRRSV PLP2 deubiquitinating activity with respect to viral replication. Here, I present the detailed kinetic characterization of PRSSV PLpro wt enzyme (PRRSV PLP2) and its major mutants *in vitro*.

5.2 Materials and Methodology

5.2.1 Site-directed mutagenesis of PRRSV DV385-578 for in vitro activity assays

Site-directed mutants of PRRSV DV $PLP2_{(385-578)}$ were previously constructed by Dr. Ben Bailey-Elkin in the Mark laboratory using the Q5 site-directed mutagenesis kit E0554S from New England Biolabs. *E.coli* C2523 was co-transformed with mutants or wild-type PLP2 and plasmid pCGI expressing Ubp1, as previously described (276).

5.2.2 Expression and purification

The cultures were grown overnight at 37 °C and then then used to inoculate 1 L of fresh LB supplemented with appropriate antibiotics and grown at 37 °C with shaking to an OD_{600} of 0.7 to 0.8. Expression of recombinant PRRSV $DV_{385-578}$ was induced by adding 200 ng/ml anhydrotetracycline followed by incubation with shaking at 16 °C for 18 h. Cells were then pelleted by centrifugation.

Cell pellets were resuspended in ice-cold lysis buffer (50 mM Tris HCl [pH 7.2], 250 mM NaCl, 2 mM DTT) and lysed using an Avestin Emulsiflex C3 high-pressure cell homogenizer. Cell lysates were purified by centrifugation (13,500 rpm at 4°C for 40 minutes), and supernatants containing proteins were mixed end-over-end for 1 h at 4°C with nickel-nitrilotriacetic acid resin (Qiagen), pre-equilibrated in the lysis buffer. The lysate/resin slurry was then poured into a gravity column and washed with 20 column volumes of the lysis buffer, followed by ten column volumes of the lysis buffer supplemented with 15 mM imidazole, followed by ten column volumes of the lysis buffer supplemented with 30 mM imidazole and finally eluted with the lysis buffer supplemented with 500 mM imidazole. Eluted proteins were then further purified using a Superdex 75 gel filtration column.

5.2.3 Kinetic characterization of wild-type and mutant PRRSV DV PLP $_{385\text{-}578}$

Enzyme kinetics assays were performed at 25 °C in black-round bottom 384-well microtiter plates (Corning Inc.) using Ub-AMC (R&D Systems) as substrate. Reaction progress was monitored by fluorescence using SpectraMax iD5 Multi-Mode Microplate Reader (Molecular Devices), and data were collected using SoftMax Pro Software. Data were analyzed using Sigmaplot and GraphPad. The standard curve of fluorogenic substrate AMC alone in assay buffer (20mM Tris/pH 7.2, 150mM NaCl, 1mM DTT) and data measured with SpectraMax iD5 plate reader under the same instrument conditions as the enzyme assays.

The deubiquitinase activity assay buffer contained 50mM Tris HCl pH 7.2, 100mM NaCl and 5mM DTT. Assays were run at the following enzyme concentrations: wild-type PLP2 (0.005μM), PLP2$_{V518S}$ (0.5μM), PLP2$_{V520A}$ (1.0μM), PLP2$_{V518S/V520A}$ (1.0μM) and PLP2$_{C429S/H498A}$ (1.0μM), and Ub-AMC concentrations ranging from 0-60 μM, 0-15μM and 0-10μM respectively for 3,600 s. Fluorescence was monitored at $\lambda_{Ex}/\lambda_{Em}$=340/360nm. Initial rates were calculated from the fluorescence traces using the equation $\frac{d[AMC]}{dt} = \left(\frac{dF}{dt}\right) \Big/ \left(\frac{dF}{d[AMC]}\right)$ in which $\frac{dF}{dt}$ is the initial rate of fluorescence change (V_0) and $\frac{dF}{d[AMC]}$ is the slope of the AMC standard curve. The initial rates for wild-type PLP2 were fit to the Michaelis-Menten equation $\left(\frac{d[AMC]}{dt}\right)_0 = \frac{k_{cat}\,[enzyme][Ub-AMC]}{K_m+[Ub-AMC]}$ to obtain k_{cat} and K_m values; whereas, due to reduced activity, mutant forms of the enzyme could only be reliably fit to the linear portion of the Michaelis-Menten equation $\left(\frac{d[AMC]}{dt}\right)_0 = \frac{k_{cat}\,[enzyme][Ub-AMC]}{K_m}$ (when [S] is much smaller than K_m) to yield only specificity constants $\frac{k_{cat}}{K_m}$.

5.3 Results

To understand the link between deubiquitinase activity of PRRSV PLP2 and its role in evading the immune system, Dr. Ben Bailey characterized a crystal structure of PLP2 bound to its cellular target, ubiquitin (Ub). This structure allows the identification of the key amino acid residues forming the binding surface between PLP2 and Ub.

Using this information as a guide, Dr. Ben Bailey (Dr. Mark Lab) and Dr. Robert C. M. Knaap (Dr. Kikkert Lab) designed and generated mutated versions of PLP2 with reduced capacity to bind ubiquitin. Furthermore, they employed structure-guided mutagenesis combined with reverse genetics methods for PRRSV. This approach revealed that specific PLP2 residues crucial for substrate recognition experience strong selective pressure to revert to their wild-type form during infection. The detailed kinetic characterization of PRRSV PLpro wt and its mutants was presented in this chapter.

The mutants of PRRSV such as V518S, V520A, V518S/V520A and C429S/H498A were constructed using site-directed mutagenesis. Despite some inclusion bodies when the enzymes were expressed in *E.coli*, sufficient yield of enzymes was obtained for the enzyme assay (Figure 5.1A). According to the objective of this experiment, the DUB activity of wt PRRSV $PLP2_{(385-578)}$ and its V518S, V520A, V518S/V520A and C429S/H498A mutants were measured *in vitro* using Ub-AMC as a fluorogenic substrate to investigate the effects of these mutations on the catalytic activity. The rates of Ub-AMC hydrolysis of wt PRRSV demonstrate hyperbolic concentration dependence (Figure 5.1), permitting the determination of Michaelis-menten parameters such as V_{max} (maximum velocity), K_{cat} (Catalytic rate constant) and K_m (Michaelis-Menten constant). Based on the specificity constant (K_{cat}/K_m) of each enzyme, the percentage of relative activity was determined.

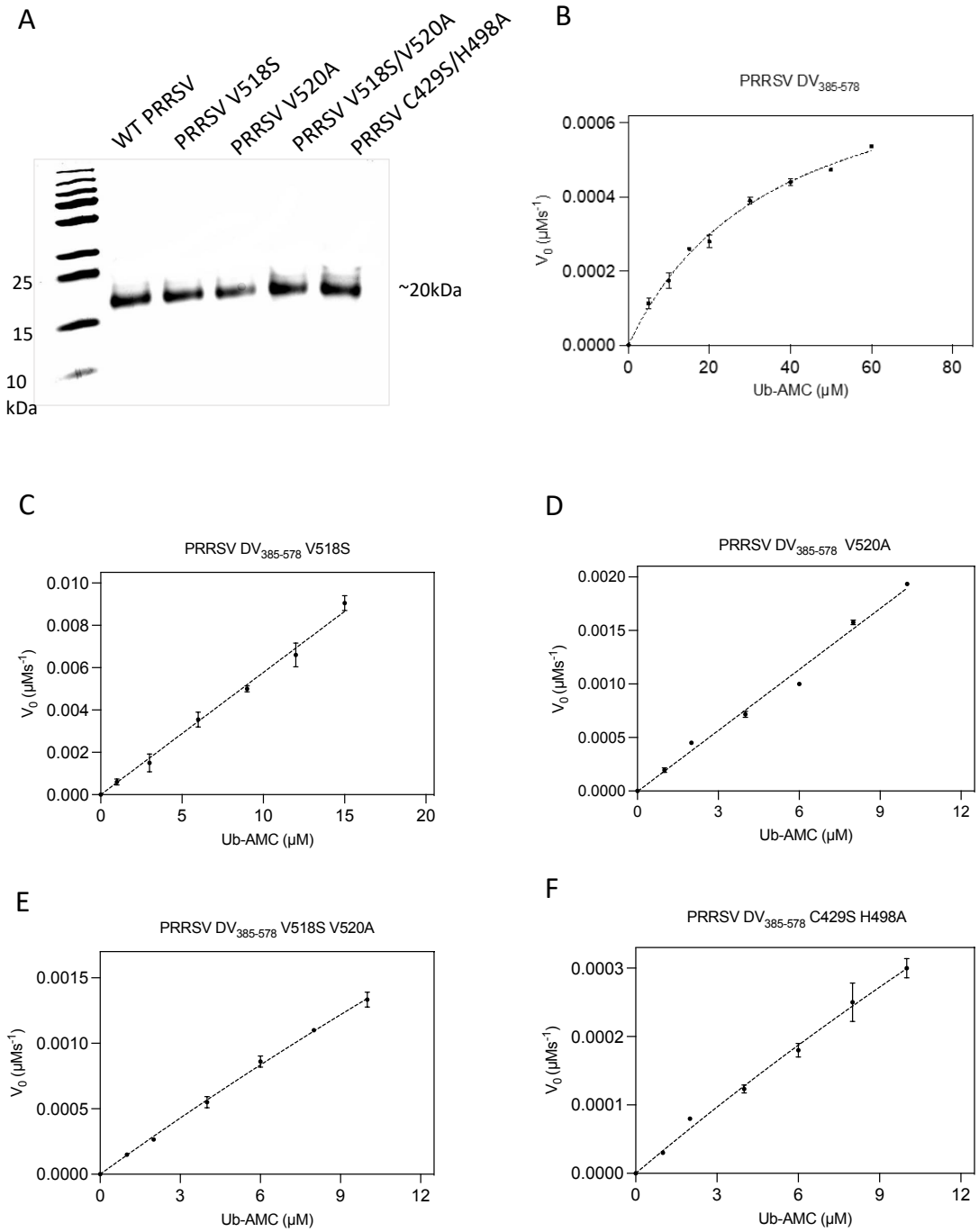

Figure 5. 1 Deubiquitinase activity of PRRSV$_{385-578}$ enzyme and Michaelis- Menton plot for PRRSV DV$_{385-578}$ mutants

(A) SDS-PAGE gel of purified PRRSV enzymes (~20kDa). Michaelis-Menten plots of PRRSV DV$_{385-578}$ mutant enzymes (B; PRRSV DV$_{385-578}$, C; PRRSV DV$_{385-578}$ V518S, D; PRRSV DV$_{385-578}$ V520A, E; PRRSV DV$_{385-578}$ V518S/V520A, F; PRRSV DV$_{385-578}$ C429S/H498A). To obtain specificity constants, data were fit to the equation $\frac{k_{cat}\,[enzyme][Ub-AMC]}{K_m}$ using linear regression. The hydrolysis was measured at 25 °C under the conditions defined in the MM section. Data points represent averages of at least two technical replicates, and error bars represent the standard deviation.

Table 5. 1 Linear regression analysis results of the fluorescence time traces of Ub-AMC hydrolysis by PRRSV $DV_{385-578}$ and mutants over time. The data was fitted to the equation: $y=y_0+(V_0)*x$, to obtain initial rates (V_0).

Ub-AMC (μM)	y_0	V_0	R^2
PRRSV $DV_{385-578}$			
5.0×10^{-6}	$(7.75\pm0.09) \times 10^{-2}$	$(1.13\pm0.15) \times 10^{-4}$	0.9899
1.0×10^{-5}	$(8.35\pm0.02) \times 10^{-2}$	$(1.75\pm0.21) \times 10^{-4}$	0.9909
1.5×10^{-5}	$(2.10\pm0.05) \times 10^{-2}$	$(2.60\pm0.00) \times 10^{-4}$	0.9893
2.0×10^{-5}	$(1.82\pm0.01) \times 10^{-2}$	$(2.80\pm0.17) \times 10^{-4}$	0.9637
3.0×10^{-5}	$(1.29\pm0.04) \times 10^{-2}$	$(3.90\pm0.10) \times 10^{-4}$	0.9835
4.0×10^{-5}	$(1.17\pm0.05) \times 10^{-2}$	$(4.40\pm0.10) \times 10^{-4}$	0.9850
5.0×10^{-5}	$(1.02\pm0.02) \times 10^{-2}$	$(4.73\pm0.57) \times 10^{-4}$	0.9917
6.0×10^{-5}	$(1.05\pm0.07) \times 10^{-2}$	$(5.37\pm0.05) \times 10^{-4}$	0.9944
PRRSV $DV_{385-578}$ V518S			
1.0×10^{-6}	$(6.20\pm1.20) \times 10^{-2}$	$(5.67\pm1.05) \times 10^{-4}$	0.9983
3.0×10^{-6}	$(1.85\pm0.07) \times 10^{-1}$	$(1.40\pm0.34) \times 10^{-3}$	0.9882
6.0×10^{-6}	$(3.15\pm0.12) \times 10^{-1}$	$(3.55\pm0.35) \times 10^{-3}$	0.9949
9.0×10^{-6}	$(3.95\pm0.07) \times 10^{-1}$	$(5.00\pm0.14) \times 10^{-3}$	0.9888
1.2×10^{-5}	$(3.20\pm0.56) \times 10^{-1}$	$(6.60\pm0.10) \times 10^{-3}$	0.9994
1.5×10^{-5}	$(2.50\pm1.27) \times 10^{-1}$	$(9.05\pm0.35) \times 10^{-3}$	0.9980
PRRSV $DV_{385-578}$ V520A			
1.0×10^{-6}	$(2.10\pm0.40) \times 10^{-2}$	$(1.95\pm0.21) \times 10^{-4}$	0.9862
2.0×10^{-6}	$(6.30\pm0.56) \times 10^{-2}$	$(4.50\pm0.00) \times 10^{-4}$	0.9927
4.0×10^{-6}	$(2.30\pm0.47) \times 10^{-2}$	$(7.17\pm0.28) \times 10^{-4}$	0.9876
6.0×10^{-6}	$(2.35\pm1.40) \times 10^{-2}$	$(1.00\pm0.00) \times 10^{-3}$	0.9637
8.0×10^{-6}	$(3.05\pm1.06) \times 10^{-2}$	$(1.58\pm0.21) \times 10^{-3}$	0.9835
1.0×10^{-5}	$(7.00\pm1.05) \times 10^{-2}$	$(1.94\pm0.00) \times 10^{-3}$	0.9850
PRRSV $DV_{385-578}$ V518S/V520A			
1.0×10^{-6}	$(3.23\pm0.20) \times 10^{-2}$	$(1.50\pm0.00) \times 10^{-4}$	0.9925
2.0×10^{-6}	$(3.27\pm0.17) \times 10^{-2}$	$(2.65\pm0.07) \times 10^{-4}$	0.9933
4.0×10^{-6}	$(3.63\pm0.25) \times 10^{-2}$	$(5.50\pm0.42) \times 10^{-4}$	0.9948
6.0×10^{-6}	$(2.60\pm0.16) \times 10^{-2}$	$(8.55\pm0.35) \times 10^{-4}$	0.9959
8.0×10^{-6}	$(1.30\pm0.17) \times 10^{-2}$	$(1.10\pm0.00) \times 10^{-3}$	0.9960
1.0×10^{-5}	$(6.10\pm0.55) \times 10^{-2}$	$(1.27\pm0.00) \times 10^{-3}$	0.9936
PRRSV $DV_{385-578}$ C429S H498A			
1.0×10^{-6}	$(4.17\pm1.20) \times 10^{-3}$	$(3.23\pm0.20) \times 10^{-5}$	0.9756
2.0×10^{-6}	$(2.07\pm0.68) \times 10^{-3}$	$(8.40\pm0.00) \times 10^{-5}$	0.9673
4.0×10^{-6}	$(5.97\pm1.25) \times 10^{-3}$	$(1.23\pm0.50) \times 10^{-4}$	0.9828
6.0×10^{-6}	$(3.23\pm0.16) \times 10^{-2}$	$(1.85\pm0.00) \times 10^{-4}$	0.9771
8.0×10^{-6}	$(9.87\pm2.77) \times 10^{-3}$	$(2.33\pm0.57) \times 10^{-4}$	0.9843
1.0×10^{-5}	$(1.35\pm1.22) \times 10^{-2}$	$(2.90\pm0.17) \times 10^{-4}$	0.9815

For the V518S, V520A, V518S/V520A mutants, specificity constants ($\frac{k_{cat}}{K_m}$) were determined due to an inability to achieve substrate saturation (Table 5.2).

Table 5. 2 Michaelis-Menten kinetics parameters of PRRSV DV $_{385-578}$ and mutants of PRRSV DV$_{385-578}$ for Ub-AMC substrate

Enzyme	k_{cat} (s^{-1})	K_m (μM)	K_{cat}/K_m (μM^{-1} s^{-1})	% Relative activity[a]
wt PLP2	$(1.7 \pm 0.7) \times 10^{-1}$	36 ± 6	$(5 \pm 2) \times 10^{-3}$	100
V518S	ND[b]	ND	$(1.1 \pm 0.4) \times 10^{-3}$	22 ± 9
V520A	ND	ND	$(1.9 \pm 0.2) \times 10^{-4}$	4 ± 2
V518S/V520A	ND	ND	$(1.33 \pm 0.06) \times 10^{-4}$	2.4 ± 0.9
C429S/H498A	ND	ND	$(3.0 \pm 0.2) \times 10^{-5}$	0.6 ± 0.2

[a]Percentage of catalytic efficiency (K_{cat}/K_m) of enzymes relative to PRRSV DV$_{385-578}$

[b]ND, not determined

It is clear that these mutations affect the hydrolysis of Ub-AMC. Compared to point mutations, the double mutant showed reduced activity. Based on the relative activity to wt PRRSV PLP2, affinity of Ub-AMC was changed : V518S > V520A > V518S/V520A > C429S/H498A.

5.4 Discussion

To understand how PLP2 interacts with ubiquitin (Ub), the crystal structure of the PLP2 domain from a specific PRRSV was determined bound to Ub was determined by Dr. Ben Bailey (Appendix, Figure A17). This structure revealed that residues V518 and V520 within PLP2 play a crucial role in Ub recognition by interacting with a hydrophobic patch on the Ub molecule (Appendix, Figure A17). Both the deubiquitinase activity of PLP2 and its role in processing viral polyproteins rely on the same active site residues. Since polyprotein cleavage is essential for viral replication, creating a completely inactive PLP2 would not allow us to study its deubiquitinase function in the live virus.

To overcome this hurdle, specific residues (V518 and V520) were mutated to disrupt Ub binding while preserving polyprotein cleavage activity (which is thought to rely on residues closer to the active site). The binding of Ub to enzyme was interrupted by these mutations without affecting polyprotein processing activity.

The effect of these DUB-deficient PLP2 mutants on cellular production of interferon-beta (IFN-β), a vital component of the innate immune response and the study was performed by Dr.Robert C. M. Knaap. Cells were transfected with a reporter construct containing firefly luciferase under the control of the IFN-β promoter. Activation of the innate immune response was triggered by introducing a constitutively active form of RIG-I, a protein that detects viral infection. This resulted in robust IFN-β promoter activity in the absence of PLP2. As expected, the expression of wild-type PLP2 significantly reduced RIG-I-dependent IFN-β promoter activity (Appendix, Figure A18). However, this suppression was partially restored when cells expressed the PLP2 DUB mutants. Furthermore, a double mutant combining V518S and V520A mutations displayed an even greater restoration of IFN-β reporter activity compared to viruses with single mutations (Appendix, Figure A18). These findings collectively

suggest that PLP2 directly interferes with Ub-dependent pathways involved in IFN-β induction and that this function is distinct from its polyprotein processing activity.

To confirm the effect of mutations on enzyme activity, the deubiquitinase activity of wild-type PLP2 and its V518S, V520A, V518S/V520A, and C429S/H498A mutants were measured *in vitro* using Ub-AMC substrate. The C429S/H498A mutant disrupts the catalytic site and serves as a control. Wild-type PLP2 displayed typical Michaelis-Menten behavior, while the V518S, V520A, and V518S/V520A mutants exhibited a reduced ability to reach substrate saturation (Table 5.2, Figure 5.1). All mutations significantly reduced enzyme activity, with the V518S/V520A double mutant showing the most dramatic effect, approaching the level of the catalytically inactive C429S/H498A mutant. This contribution I provided to the research verified that the mutations targeting the Ub binding cleft on the PRRSV Plp2 did indeed disrupt the DUB activity as expected. The V518S/V520A mutant reduced DUB activity the most, even approaching the catalytic mutant C429S/H498A. Yet this double mutant was still able to cleave the nsp2C|3 cleavage site, confirming that the mutation affected DUB activity only. Loss of DUB function appears to to reduced Ub affinity as represented by Km, with the V520A mutation in particular causing the greatest reduction affinity for Ub.

CHAPTER 6: CONCLUSION

6.1 Summary of Findings

In summary, this thesis not only advances our understanding of the inhibitory capabilities of UbVs against viral proteases but also contributes to the broader field of virology and deubiquitinase biology. The promising results motivate continued research to optimize the application of UbVs in diverse plant systems, ultimately enhancing our capacity to develop effective antiviral strategies in agriculture.

The study in Chapter 2 demonstrates a preliminary investigation of the inhibitory capabilities of UbVs against TYMV protease activity and deubiquitinase activity. The findings demonstrated that UbVs can inhibit TYMV protease activity, suggesting their potential utility as antiviral agents in plants. Structural analyses, including X-ray crystallization and small-angle X-ray scattering, provide further insights into the mechanism of action of UbVs and confirm their ability to bind tightly with TYMV protease. These promising results lay the groundwork for the next phase of research, which involves the transgenic expression of the most potent inhibitor in *A. thaliana*. In Chapter 3, the transgenic expression of UbV inhibitor in *A. thaliana* against TYMV presents an insightful exploration into the effectiveness of this inhibitory strategy, particularly considering the broad infectivity of TYMV across *Brassica* spp., including *A. thaliana*. However, the efficacy of the inhibitor varies, as demonstrated by protoplast infection and whole plant infection studies indicating that it may take more than 24 hours to detect inhibitory effects, with outcomes differing among plants due to their heterogeneous populations. These findings emphasize the potential of UbV inhibitors as a promising strategy for combating viral infections in plants, yet they also highlight the need for further refinement and development.

The results in Chapter 3 demonstrated that AtAT3G has DUB activity, which is quite exciting as a lot of work regarding this enzyme has only been theorized. However, the DUB activity is weak compared to other known and experimentally characterized DUBs. The activity of DUBs can be regulated by various factors, including phosphorylation, interaction with other proteins, and subcellular localization.

In addition to the ubiquitin variant study, the critical residues responsible for ubiquitin-binding sites of PRRSV PLP2 were studied. Several substitutions at V518 and V520 and catalytic knockout mutants (C429S/H498A) were also further tested, comparing Michaelis-Menten kinetics and identified C429S/H498A mutation in PRRSV PLP2 can disrupt the DUB activity of PLP2.

6.2 Future Directions

The main objective of this thesis has been to develop a rational approach to combat plant viruses using inhibitors based Ub variants (UbV), which bind with the deubiquitinase (DUB) domain of viral protease. Initially, this strategy was developed against animal viruses and only demonstrated using cell culture assays. The major obstacle of using UbVs against human viruses is the difficulty of delivering them into cells. Although human applications may not be immediately practical, creating transgenic plants expressing these UbVs could serve as proof of concept for the effectiveness of UbVs in protecting crops from viral diseases.

As a preliminary study, the ubiquitin variants were tested against the Tymoviridae plant virus, Turnip Yellow Mosaic Virus (TYMV), in model plant *A. thaliana*. Through biochemical and structural analyses of the specificity of the UbV to viral protease were made that UbV may help to combat a group of plant viruses, especially the Tymoviridae family viruses, which have the same structural similarity with TYMV protease. Interestingly, only a few plant viral proteases with this DUB activity were structurally characterized, and most of them are still

predicted (refer to Figure 1.8 in the literature review section). An additional structural and biochemical study of characterizing these important plant viral proteases can help direct future research in plant virology.

As mentioned in Chapter 3, the preliminary infection results of the transgenic study were inadequate. Further study is needed to select the most effective transgenic plants under TYMV selection pressure and continue the study once after obtaining stable homozygous transgenic lines against TYMV. Due to the affordability, efficiency and simplicity of the CRISPR-Cas system, this strategy can be used along with this protein-based ubiquitin variant system in plants which may help to protect plants with paired protection. As mentioned in Chapters 2 and 3 (refer to Figures 2.6 and 3.1), off-target binding of UbVs against a representative panel of *A. thaliana* DUBs and analysis of phenotypic parameters showed that the UbV strategy can be employed without having any detrimental effects on the plant. However, a detailed experiment is needed, such as an analysis of differentially expressed ubiquitin-related proteins in transgenic plants under the selection pressure of TYMV. Therefore, the genes that are induced or silenced can be identified to analyze how TYMV manipulates the cellular machinery in plants. However, the magnitude of these changes will be unknown until transgenic plants show any deformations and changes in phenotype. Therefore, this type of detailed analysis should be performed along with the stability test of the genotype of the transgenic plant.

Given the results of this thesis, additional studies can be conducted to develop an antiviral strategy using protein-based inhibitors against plant viruses. Several studies have demonstrated that viral protease and other viral proteins, such as RNA-dependent RNA polymerase and helicases, are synthesized by host cellular machinery and are essential for viral replication. Targeting one or several viral proteins using an inhibitor strategy would expedite the research in controlling the most important viral infections in major crops.

While constructing the panel of *A. thaliana* DUBs to determine the off-target bindings of UbVs, the predicted plant DUB of MJD (Machado Josephin Domain) family deubiquitinase (At3g54130) was confirmed to have DUB activity. Based on the results in Chapter 4, plant DUB recognized both K48 and K63 di-Ub chains slightly. Although not presented in this thesis work, the initial investigation of linkage specificity (K6, K11, K27, K29, K33, K48, K63) was performed, and none of these di-Ub was cleaved by At3g54130 except K48 and K63 linked di-Ub. This shows that this predicted plant DUB would function related to proteasomal degradation or DNA damage repair in plant cells. However, the actual role and the location of expression of At3g54130 in the plant is still unknown. Therefore, an extensive study can be carried out to understand the role of At3g54130. The quantitative reverse transcription-qPCR can be carried out to confirm and identify the expression levels of At3g54130 in wild-type *A. thaliana* Col-0. The immunofluorescence staining and subcellular fractionation can be used to detect protein localization. In addition, Mass spectrometry and Western blot detection techniques can be used to identify the subcellular localization of the protein.

To understand the actual function of At3g54130, a panel of transgenic knockdown plants and overexpressed plants for At3g54130 can be developed. These transgenic plants will be analyzed for any phenotypic changes due to knockdown or overexpression of At3g54130 and confirm the role of this protein in plants. The same study can be performed for At2g29640 because At2g29640 also share the conserved Josephin domain as At3g54130. Out of seven prominent deubiquitinase families, MJD, ZUFSP, and MINDY are still not discovered in plants (refer to literature review section), and the study of determining interactions of these proteins will help to fill the knowledge gap of these DUBs to advance in plant physiology.

Chapter 5 centered around the enzyme kinetics of the papain-like protease of the Porcine Reproductive and Respiratory Syndrome virus (PRRSV). Determination of Michaelis-Menten parameters and catalytic efficiency of the viral protease and its mutants were key

aspects. The project results mark the first study to demonstrate the enzyme kinetics of both the protease and its mutants of PRRSV. The same type of kinetic study can be employed for Tymoviridae family viral proteases because none of these enzymes are biochemically characterized. This study will show the critical catalytic sites that can be targeted when developing a CRISPR-Cas system or any other inhibition mechanism against plant viruses.

As one of the natural plant defence mechanisms, RNA silencing and resistance gene-based defences play a key role against both RNA and DNA viruses. Even though plants employ different defence mechanisms, most viruses invade plants by encoding viral proteins or cooperating host proteins to suppress these responses. Among them, plant viral proteases with deubiquitinase activity enhance the ability of a virus to escape plant defence. Altogether, these proposed studies will provide a way for plants to overcome viral infections by protein-based inhibitors along with CRISPR-Cas system. Further research in this area could help to identify new strategies for combating plant viruses and improving agricultural productivity. The work presented in this thesis provides a foundation upon which these proposed studies can be developed.

APPENDIX

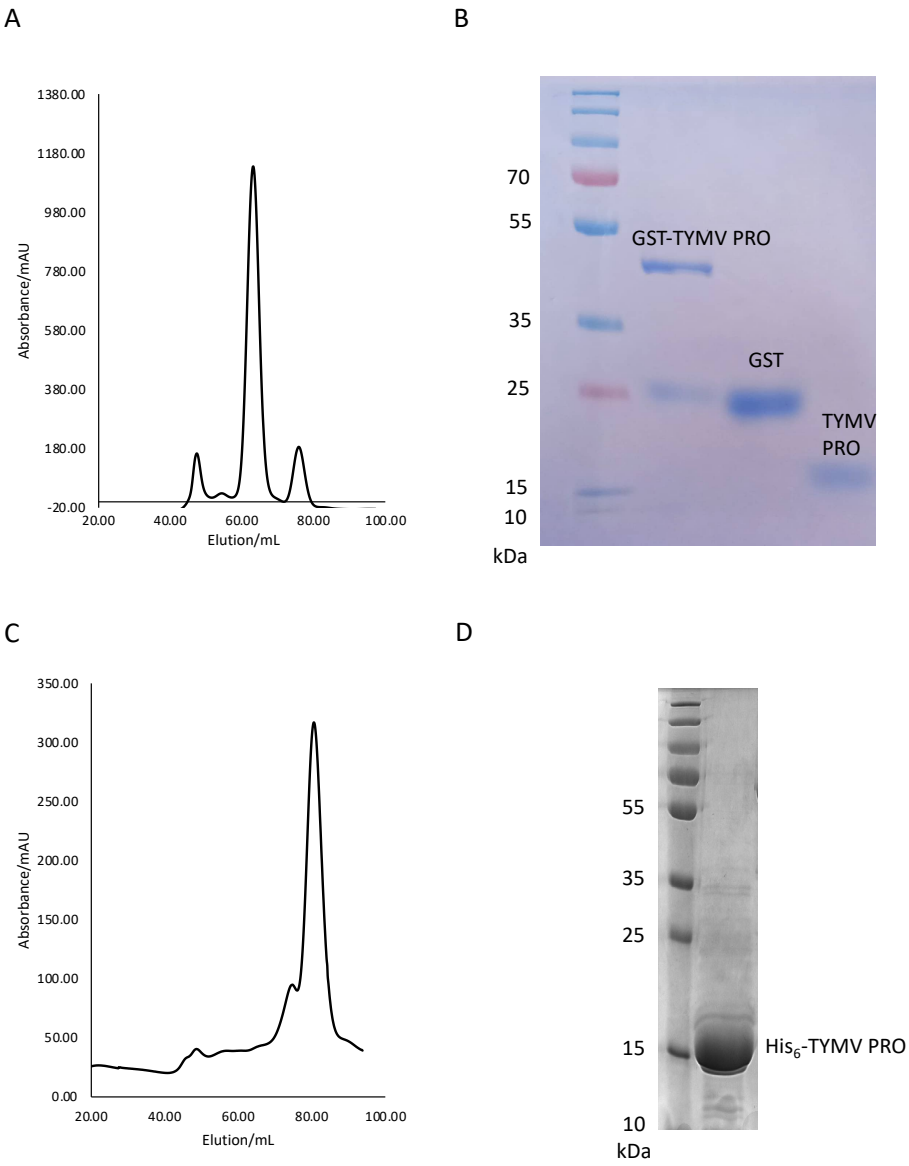

Figure A1: Purification of GST-TYMV PRO and His_6-TYMV PRO. (A) Chromatogram (FPLC) of His_6-TYMV PRO using Superdex 75 column (GE Healthcare) equilibrated with 20 mM TRIS, 150 mM NaCl, 2 mM DTT, pH 8.0. The third peak (~78 ml) is TYMV PRO. (B) 12% SDS PAGE gel of purified TYMV PRO without GST tag (cleaved by HRV3c Precision Protease) and the fractions collected from each peak as follows, 1:GST tagged TYMV PRO (~43kDa), 2:GST (25kDa) and 3: TYMV PRO (~18kDa). (C) Chromatogram of His_6-TYMV PRO. (D) 12% SDS PAGE gel of purified His_6-TYMV PRO (~18kDa).

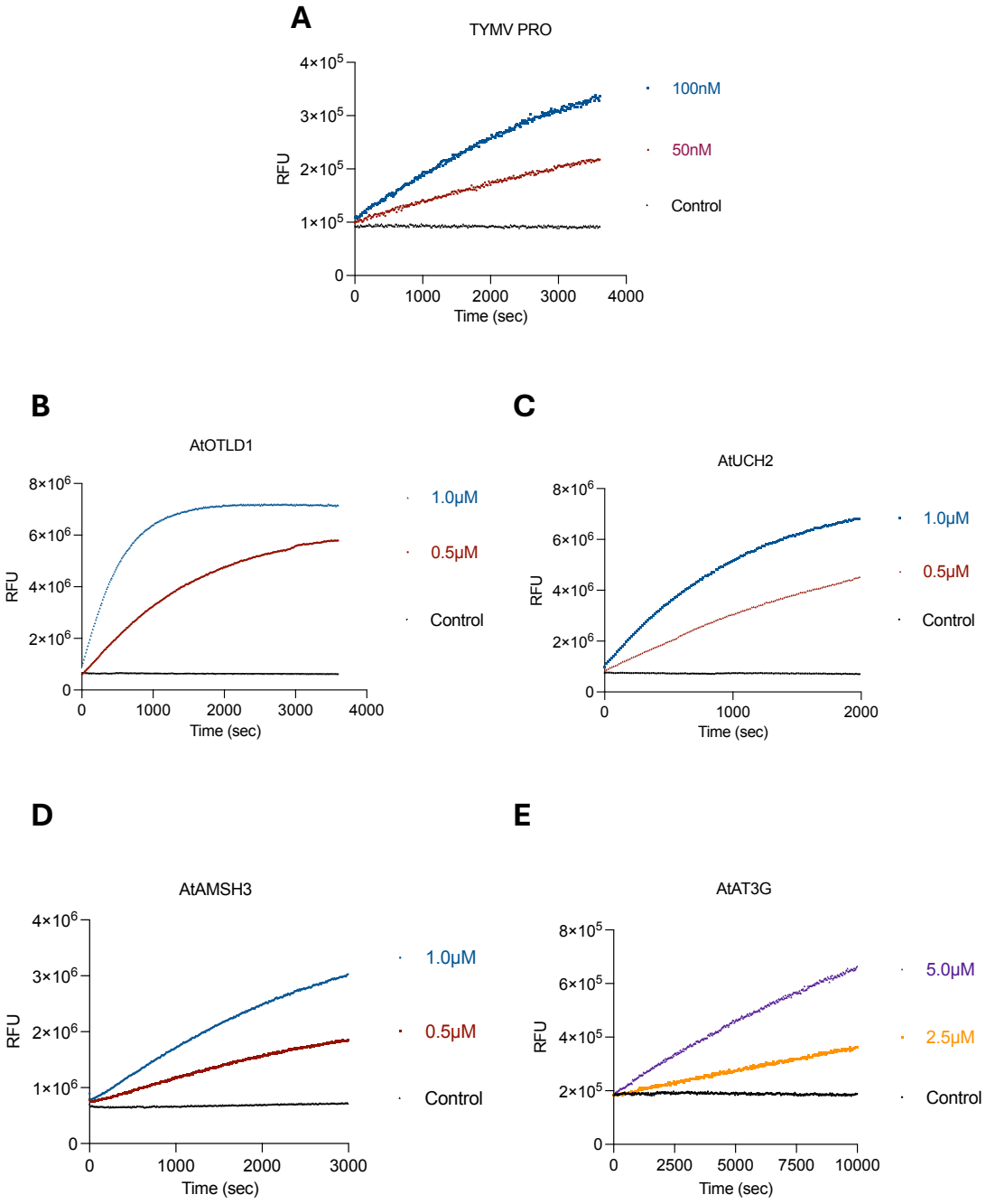

Figure A2: The deubiquitinase activity of TYMV PRO and *A. thaliana* plant DUBs. The DUB activity of TYMV PRO (A), AtOTLD1 (B), AtUCH2 (C), AtAMSH3 (D) and AtAT3G (E). The concentrations of enzymes are as follows: dark blue, 1μM; red, 0.5 μM; magenta, 5.0μM; orange, 2.5μM. The black line represents the control (Ub-AMC substrate, 1μM)

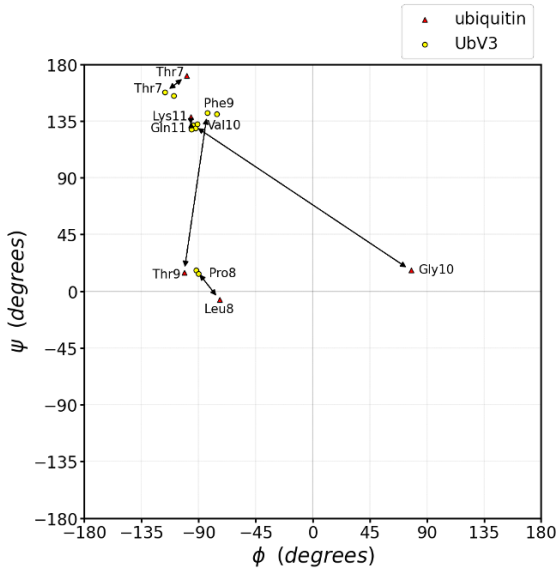

Figure A3: Ramachandran plot showing dihedral angles of amino acids on β1-β2 loop (^{7}TLTGK^{11}). Amino acids of Ub are indicated as red triangle marker (PDB ID: 1UBQ), amino acids of UbV3 were indicated as yellow dot marker.

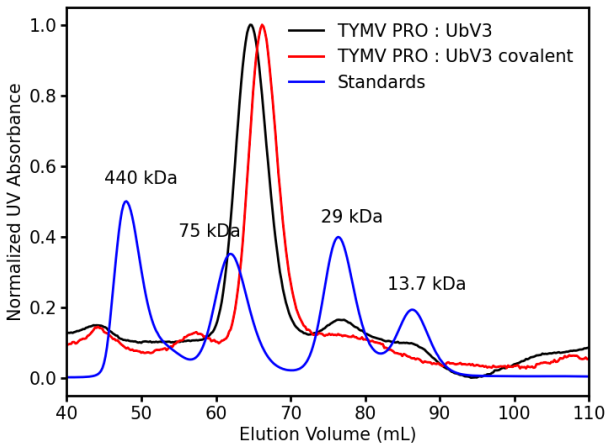

Figure A4: Size exclusion chromatography profile of TYMV PRO : UbV3 dimer complex and covalent complex of TYMV PRO : UbV3 dimer.

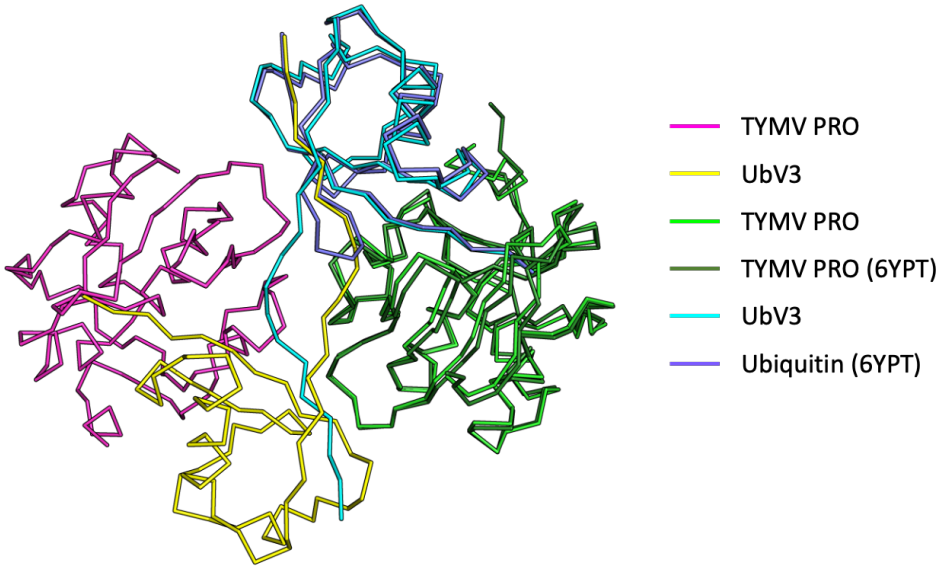

Figure A5: Alignment of TYMV PRO: ubiquitin complex structure (PDB ID: 6YPT) and TYMV PRO: UbV3. 1:1 complex of 6YPT was superimposed on the half of 2:2 complex of TYMV PRO : UbV3.

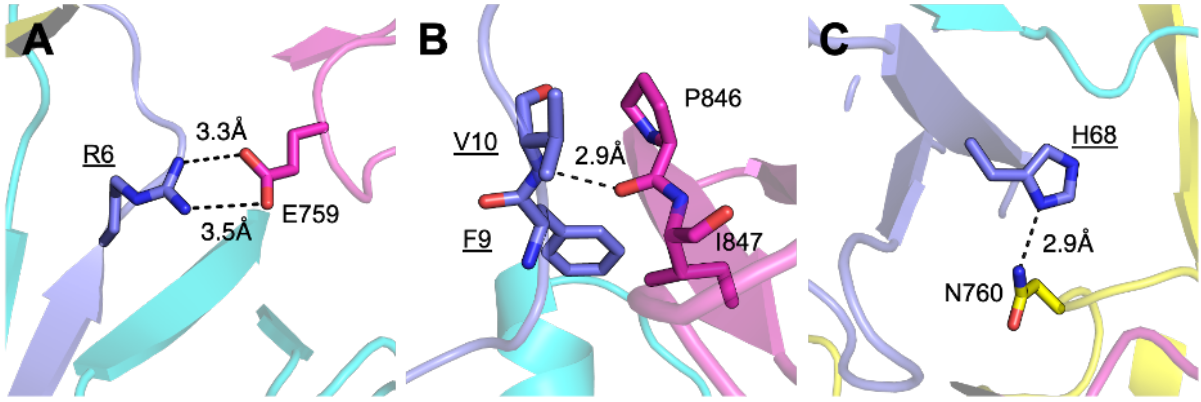

Figure A6: Polar interactions between UbV3 and TYMV PRO other than the active site of TYMV PRO. (A) Salt-bridge between UbV3 R6 and TYMV PRO E759. (B) Hydrogen bond between the backbone amide N atom of UbV3 V10 and the carbonyl O atom of TYMV PRO P846. (C) Hydrogen bond between UbV3 H68 and TYMV PRO N760. Possible interactions were are indicated by a dashed line with distance. Residues of UbV3 are labeled with underline, and the key residues of TYMV PRO/DUB active site are labelled.

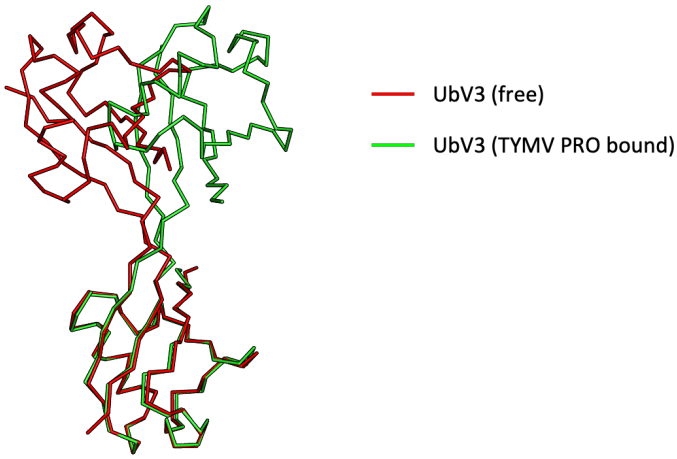

Figure A7: Alignment of UbV3 dimers from two different crystal structures. Free UbV3 dimer is colored red, TYMV PRO bound UbV3 dimer is colored green. Single chains of ubiquitin are aligned together to show the orientation of the second ubiquitin chain.

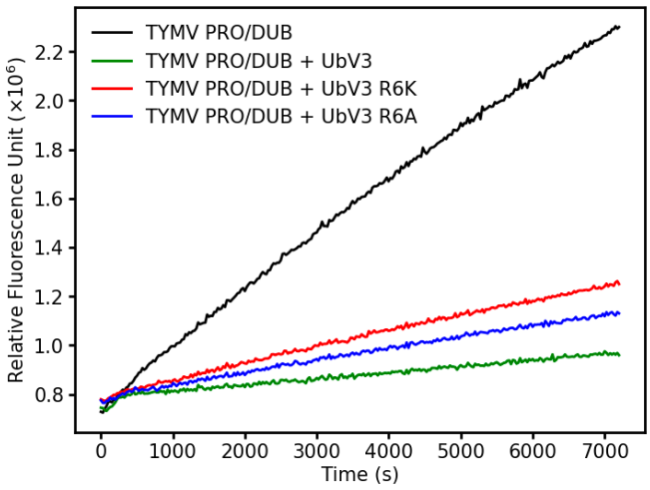

Figure A8: TYMV PRO Ub-AMC hydrolysis assay with three inhibitor constructs: UbV3, UbV3 R6K and R6A mutants.

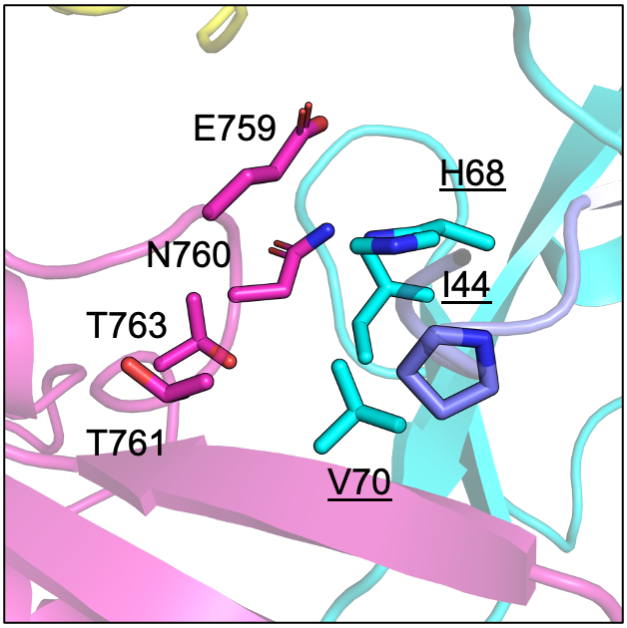

Figure A9: TYMV PRO and UbV3 dimer complex structure. TYMV PRO does not form hydrophobic interaction with the I44 patch of Ub. The two copies of TYMV PRO are coloured magenta and yellow and the monomers of the UbV3 dimer are colored cyan and blue. Some key residues are labelled with residue numbers, underlined for UbV3.

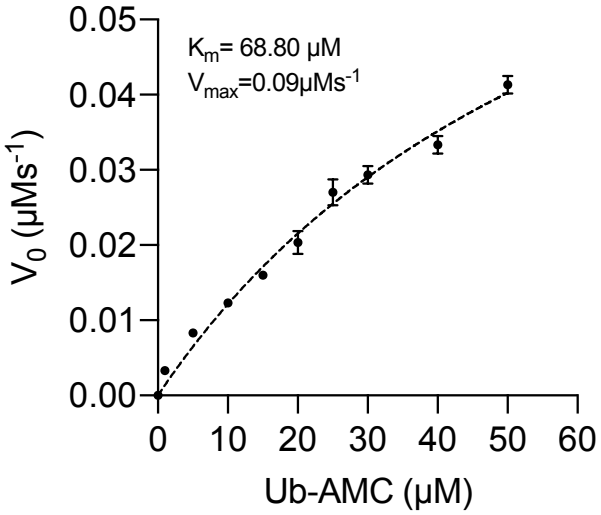

Figure A10: Michealis-Menten plot for TYMV PRO. The hydrolysis of Ub-AMC was measured at 25 ºC under the conditions defined in the MM section. Data points represent averages of at least two technical replicates, and error bars represent the standard deviation.

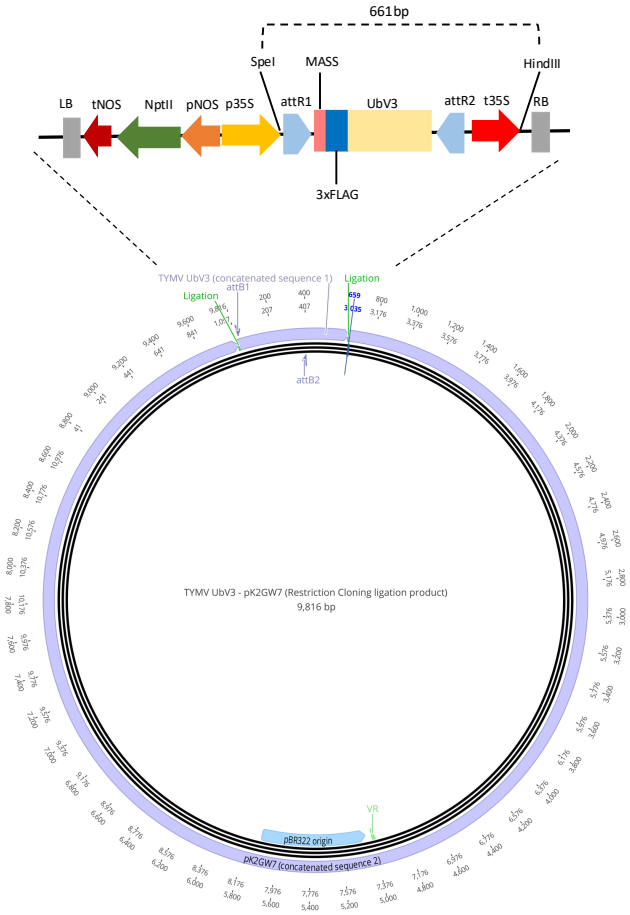

Figure A11: Physical map of recombinant binary vector pK2GW7. Expression cassette consisted with LB, left border; tNOS, terminator of NptII; NptII, neomycin phosphotransferase II gene; pNOS, promoter of NptII; p35S, CaMV 35S promoter; attR1 sequence; MASS, Met-Ala-Ser-Ser sequence; 3x FLAG tag sequence; UbV3, open reading frame; attR2 sequence; t35S, CaMV terminator sequence and RB, right border

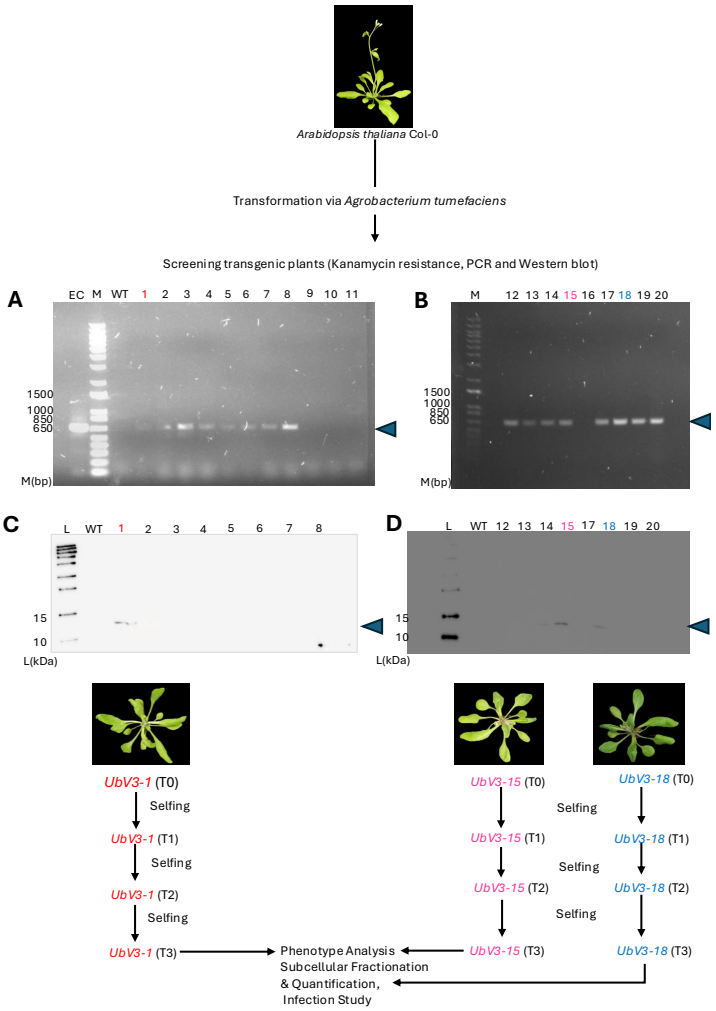

Figure A12: Selection scheme for *UbV3* transgenic plants. Transgenic plants were generated by *Agrobacterium*-mediated transformation, and plants that showed kanamycin resistance were further screened via PCR and Western blot analysis for the presence of the UbV expression cassette and protein, respectively. The size of the expression cassette (EC) is 661bp. During the initial screening, 20 plants (A: 1-11 plants and B: 12-20) were screened by PCR, and the resulting amplicons were highlighted by blue arrows (M: DNA molecular weight marker). PCR amplicons were sequenced to confirm the transgene. Selected transgenic lines were screened by Western blot analysis to confirm the presence of FLAG-tagged- UbV3 protein (~12kDa) [L: Molecular weight marker]. Three transgenic lines (*UbV3-1*, *UbV3-15* and *UbV3-18*) expressed FLAG-tagged UbV3 (C and D). These lines were allowed to self-pollinate. The *UbV3-1, UbV3-15* and *UbV3-18* plants were selected for phenotypic analysis, subcellular fractionation, and the preliminary infection studies. The *UbV3-1* line was then selected for the further *in vivo* infection study (After two successive selfings, the only *UbV3-1* transgenic plant lines yielded a stable phenotype (third-generation plants, T3), and all T3 plants expressed UbV3 inhibitor).

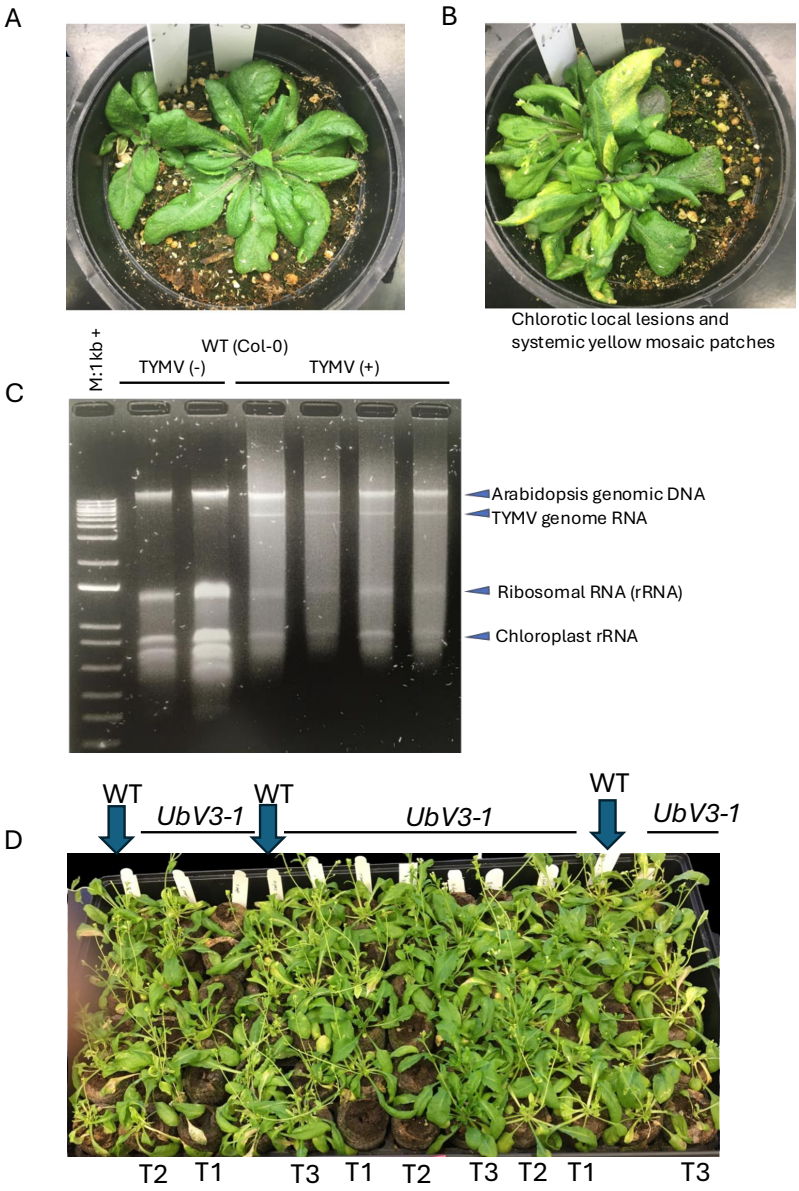

Figure A13: Phenotypic changes after TYMV infection and symptom variability. Wild-type *A. thaliana* Col-0 (A: H_2O treatment and B: TYMV infection). (C) Gel electrophoresis of total nucleic acid extracts from wild-type *A. thaliana* with and without TYMV infection. The rRNA and chloroplast rRNA are reduced after TYMV infection. (D) TYMV infection experiment setup and symptom variability. The WT (*A. thaliana* Col-0) and Transgenic *A. thaliana* (UbV3-1) with different generations (T1, T2 and T3) were sprayed with TYMV before flowering and at a late stage (foliar spray). This figure shows the late-stage infection symptoms in plants. Plants were kept under fluorescent lights at ~24°C and 12 h day length. The third transgenic generation plants (T3) were used for the coat protein determination experiment.

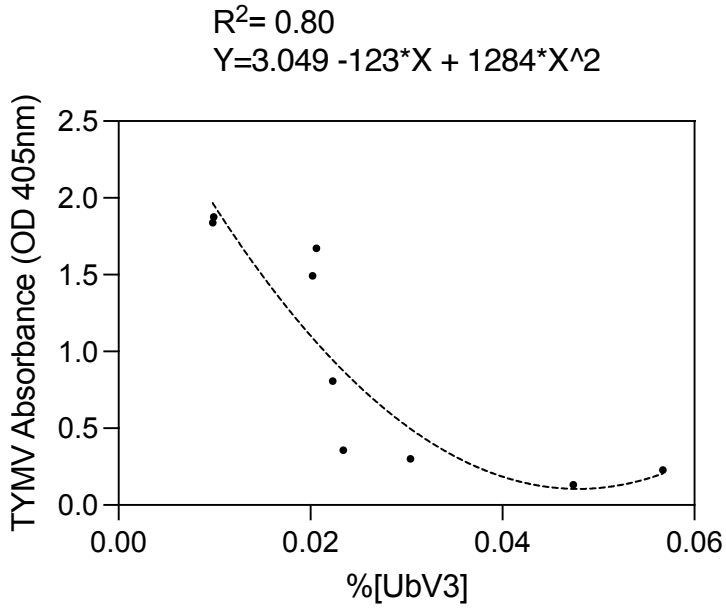

Figure A14: Quadratic regression analysis between TYMV detection and the amount of UbV3 expression in transgenic plants (*UbV3-1*). The data were statistically analyzed using Quadratic regression analysis and strong negative correlation was observed in the transgenic line *UbV3-1* (R^2= 0.80).

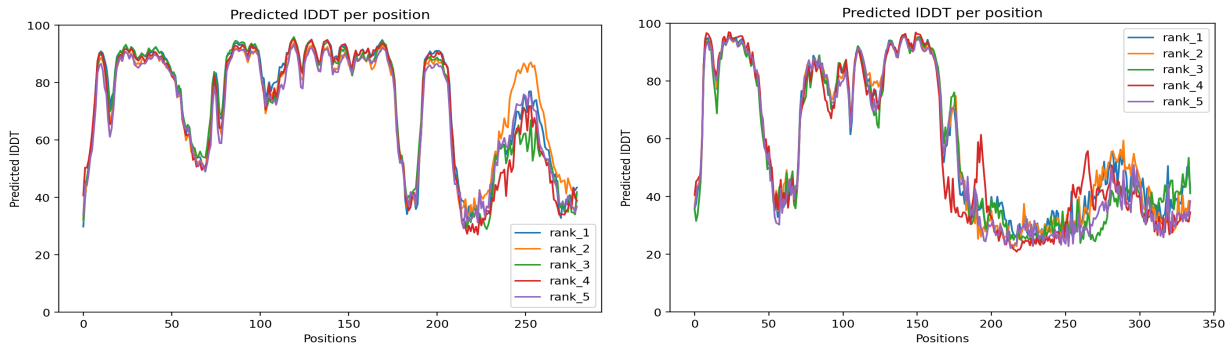

Figure A15: IDDT prediction (local superposition-free score to compare protein structures or models using distance difference tests) for AtAT3G (left) and AtAT2G (right)

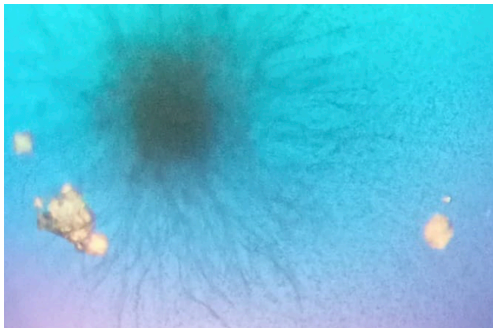

Figure A16: Salt crystals observed after crystallization initial screening of AtAT3G

These crystals were observed under conditions of 0.2M Magnesium chloride, 0.1M HEPES pH 7.5, 15% (w/v) PEG 400. Precipitation was observed in the middle of the crystallization drop.

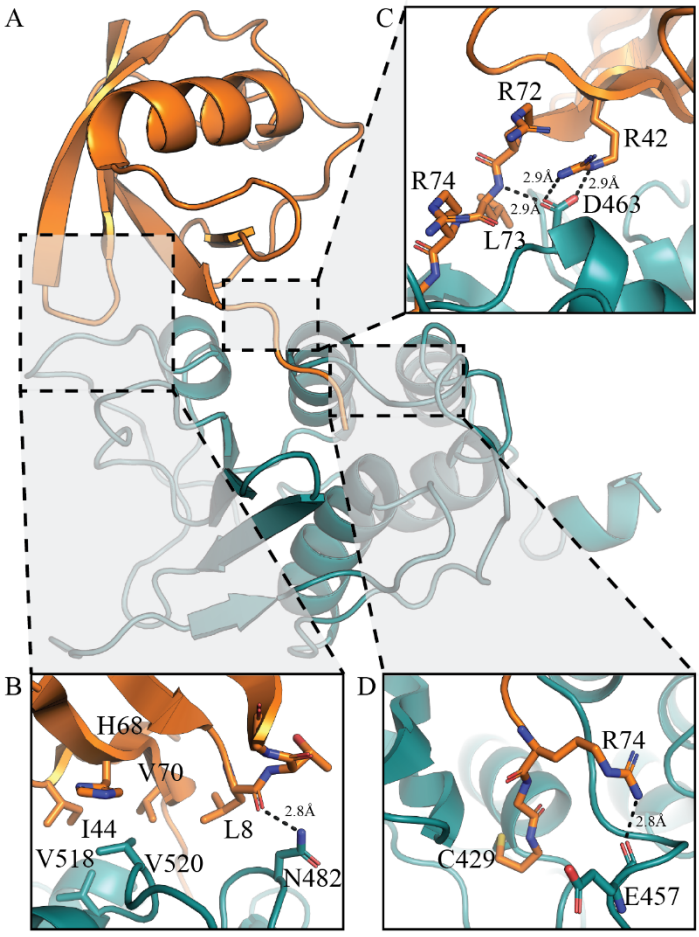

Figure A17. Crystal structure of the PLP2-Ub complex. (A) The PLP2 domain is shown in teal, with the bound Ub domain shown in orange. Interactions relevant with respect to Ub binding are shown in dashed boxes, with detailed interactions highlighted in panels B-D.

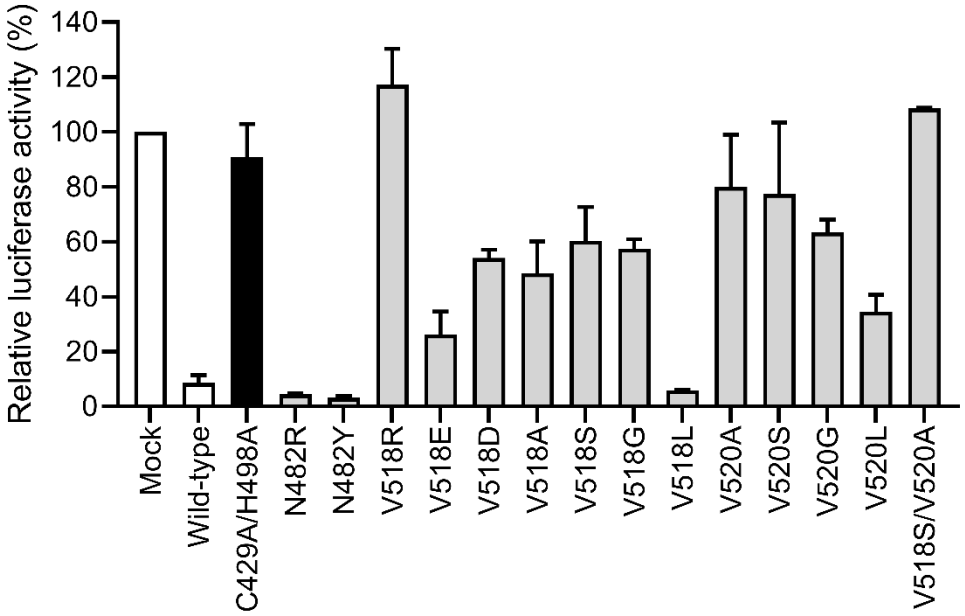

Figure A18. Inhibition of IFN-β promoter activity by rationally designed PLP2 mutants. HEK293T cells were co-transfected with plasmids expressing various PLP2 mutants, firefly luciferase under the control of the IFN-β promoter, renilla luciferase as endogenous control and RIG-I(2card) to induce the innate immune response. Wild-type PLP2 significantly inhibited IFN-β promoter activity, while the inactivated C429A restored this activity. Expression of DUB-specific V518 and V520 mutants all significantly increased IFN-β promoter activity with the exception of V518L, while both N482 mutants did not have an effect. All experiments were performed in triplicate and independently repeated at least twice. Bars correspond to the mean with error bars showing the standard deviation.

Table A19: The data for binding potency of UbVs

	TYMV PRO	AtAMSH3	AtUCH2	AtOTLD1	AtAT3G	BSA	GST
UbV1	0.0093	0.0396	0.0819	0.0179	0.0033	0.0097	0.0031
UbV2	0.3842	0.1430	0.0855	0.0193	0.0593	0.0005	0.0700
UbV3	0.8160	0.0808	0.0646	0.0032	0.0798	0.0012	0.0003

*The data was normalized to plot the heatmap

Table A20: TYMV coat protein detection by DAS-ELISA (TYMV Detection kit, Creative Diagnostics)

	<>	1	2	3	4	5	6	7	8	9	10	11	12		
	A	None	None	None	None	None	None	None	None	None	None	None	None		
	B	None	col-o 1	col-o 2	col-o 3	col-o 4	col-o 5	col-o 6	col-o 7	GMO 1, 1	GMO 1, 2	+C	None		
	C	None											None		
	D	None	GMO 1-3	GMO 1-4	GMO 1-5	GMO 1-6	GMO 1-7	GMO 1-8	GMO 2-1	GMO 2-2	GMO 2-3	-C	None		
	E	None											None		
	F	None	GMO 2-4	GMO 2-5	GMO 2-6	GMO 2-7	GMO 2-8	GMO 2-9	GMO 3-1	GMO 3-2	GMO 3-3	GMO 3-4	None		
	G	None											None		
	H	None	None	None	None	None	None	None	None	None	None	None	None		
Plate 1	Mode	Absorbance													
	Name	ELISA													
	Measurement wavelength [nm]				405										
	Number of flashes				3										
	Settle time [ms]				50										
	Part of Plate				A1-H12										
	Start Time				2022-11-30 13:24:26										
	Temperature [°C]				19.4										
	<>	1	2	3	4	5	6	7	8	9	10	11	12		
	A	0.0676	0.065	0.0629	0.0617	0.0635	0.0594	0.063	0.0641	0.0694	0.0629	0.0648	0.0629		
	B	0.0634	1.4494	0.2541	2.0184	0.1308	0.5663	1.917	1.993	1.9737	0.3791	1.7107	0.0519		
	C	0.0636	1.3865	0.2237	1.8769	0.1147	0.5171	1.8288	1.8612	1.9035	0.3697	1.6138	0.0594		
	D	0.0603	1.7983	1.1415	0.5496	1.9124	0.2268	1.7	0.678	1.3889	0.108	0.1234	0.065		0.34315
	E	0.0587	1.7852	1.0911	0.5435	1.8755	0.2268	1.6883	0.661	1.3822	0.1117	0.1069	0.0633		
	F	0.0641	1.5678	0.2771	1.3428	0.8746	0.3128	0.1055	1.8255	0.1511	1.0343	1.8591	0.0629		
	G	0.0647	1.668	0.275	1.3738	0.913	0.3228	0.105	1.8598	0.1779	1.2008	1.9367	0.0626		
	H	0.064	0.0632	0.0632	0.0689	0.0665	0.0648	0.0736	0.0671	0.0656	0.0627	0.063	0.0627		
	<>	1	2	3	4	5	6	7	8	9	10	11	12		
	A	None	None	None	None	None	None	None	None	None	None	None	None		
	B	None	GMO 3-5	GMO 3-6	GMO 3-7	GMO 3-8	GMO 3-9	GMO 3-10	GMO 4-1	GMO 4-2	GMO 4-3	+C	None		
	C	None											None		
	D	None	GMO 4-4	GMO 4-5	GMO 4-6	GMO 4-7	GMO 4-8	GMO 5-1	GMO 5-2	GMO 5-3	GMO 5-4	-C	None		
	E	None											None		
	F	None	GMO 5-5	GMO 5-6	GMO 5-7	GMO 5-8	GMO 5-9	GMO 5-10	Joi Choi 1	Joi Choi 2	Joi Choi 3	Joi Choi 4	None		
	G	None											None		
	H	None	None	None	None	None	None	None	None	None	None	None	None		
	Mode	Absorbance													
	Name	ELISA													
Plate 2	Measurement wavelength [nm]				405										
	Number of flashes				3										
	Settle time [ms]				50										
	Part of Plate				A1-H12										
	Start Time				2022-11-30 13:25:37										
	Temperature [°C]				19.5										
	<>	1	2	3	4	5	6	7	8	9	10	11	12		
	A	0.068	0.0647	0.0645	0.0644	0.0637	0.0649	0.0649	0.0647	0.0656	0.0641	0.0631	0.0644		
	B	0.0671	0.4305	1.244	0.1107	0.6834	0.5524	2.038	1.7748	0.357	1.6441	1.9556	0.0626		
	C	0.0701	0.4187	1.044	0.1173	0.6399	0.5019	1.8939	1.6847	0.2629	1.4802	1.7519	0.0633		
	D	0.068	0.8549	0.1144	1.6098	0.3837	0.1159	1.4999	0.3473	0.2137	1.8486	0.0994	0.0637		0.346575
	E	0.064	0.8525	0.1082	1.6438	0.3597	0.1148	1.4853	0.3685	0.2414	1.9016	0.1016	0.0635		
	F	0.065	0.121	0.3076	0.7934	0.1315	1.6349	1.8232	1.9001	1.7297	0.0977	0.1076	0.0627		
	G	0.0635	0.1415	0.2963	0.8214	0.1383	1.7092	1.8546	1.8976	1.8337	0.113	0.1351	0.0622		
	H	0.0646	0.0694	0.0686	0.0725	0.07	0.0646	0.0541	0.0552	0.0649	0.0664	0.0635	0.0627		

Table A21*:* FLAG-tagged UbV3 detection [FLAG-tag detection ELISA kit (Cayman Chemical 501560)]

	Sample	Average Absorbance at 405nm	Average Absorbance-Non Specific Binding Absorbance	SD	Concentration; mg/mL;200uL	Concentration after 3 days/(mg/mL)150uL	%FLAG/Total Protein
1	ColO-1	1.41795	1.35795	0.04447702	3.228	2.156	#NUM!
2	ColO-2	0.2389	0.1789	0.02149605	1.732	1.288	#NUM!
3	ColO-3	1.94765	1.88765	0.10005561	2.531	2.164	#NUM!
4	ColO-4	0.12275	0.06275	0.01138442	1.163		
5	ColO-5	0.5417	0.4817	0.03478965	1.71		
6	ColO-6	1.8729	1.8129	0.06236682	3.857		
7	ColO-7	1.9271	1.8671	0.09319667	2.895		
8	GMO1-1	1.9386	1.8786	0.0496389	3.509	2.329	0.02552478
9	GMO1-2	0.3744	0.3144	0.0066468	1.477	1.387	0.02269863
10	GMO1-3	1.79175	1.73175	0.0092631	3.229	2.952	0.01296838
11	GMO1-4	1.1163	1.0563	0.03563818	2.738	2.342	0.02234217
12	GMO1-5	0.54655	0.48655	0.00431335	0.768		
13	GMO1-6	1.89395	1.83395	0.02609224	2.988	2.51	#NUM!
14	GMO1-7	0.2268	0.1668	0	0.551		
15	GMO1-8	1.69415	1.63415	0.00827315	2.807	2.238	0.01195618
16	GMO2-1	0.6695	0.6095	0.01202082	0.729		
17	GMO2-2	1.38555	1.32555	0.00473762	1.205	1.166	0.01431265
18	GMO2-3	0.10985	0.04985	0.0026163	0.58		
19	GMO2-4	1.6179	1.5579	0.0708521	1.85	1.492	0.02688799
20	GMO2-5	0.27605	0.21605	0.00148492	1.012	0.924	0.0360012
21	GMO2-6	1.3583	1.2983	0.02192031	0.58		
22	GMO2-7	0.8938	0.8338	0.0271529	0.805		
23	GMO2-8	0.3178	0.2578	0.00707107	0.354		
24	GMO2-9	0.10525	0.04525	0.00035355	0.893	0.875	0.04878601
25	GMO3-1	1.84265	1.78265	0.02425376	2.126	1.452	0.03191649
26	GMO3-2	0.1645	0.1045	0.01895046	1.707	1.146	0.07313777
27	GMO3-3	1.11755	1.05755	0.11773328	1.027	0.902	0.08637386
28	GMO3-4	1.89785	1.83785	0.0549422	1.379	1.654	0.02956168
29	GMO3-5	0.4246	0.3646	0.00834386	1.958	1.482	0.08108185
30	GMO3-6	1.144	1.084	0.14142136	1.936	1.726	0.01815985
31	GMO3-7	0.114	0.054	0.0046669	0.256		
32	GMO3-8	0.66165	0.60165	0.03075914	2.78	1.723	0.04796489
33	GMO3-9	0.52715	0.46715	0.03570889	7.236	4.521	0.01539218
34	GMO3-10	1.96595	1.90595	0.10189409	1.328	1.053	0.02014444
35	GMO4-1	1.73475	1.67475	0.05663925	1.673	1.459	0.01117544
36	GMO4-2	0.30995	0.24995	0.06653875	0.764		
37	GMO4-3	1.56215	1.50215	0.1158948	1.262	1.307	#NUM!
38	GMO4-4	0.8537	0.7937	0.00169706	1.803	1.587	0.01290438
39	GMO4-5	0.1113	0.0513	0.00438406	0.744		
40	GMO4-6	1.6268	1.5668	0.02404163	2.496	2.135	0.01003335
41	GMO4-7	0.3717	0.3117	0.01697056	1.559	1.325	0.02479617
42	GMO4-8	0.11535	0.05535	0.00077782	0.952		
43	GMO5-1	1.4926	1.4326	0.01032376	1.978	1.529	0.02022188
44	GMO5-2	0.3579	0.2979	0.01490066	1.134	1.048	0.02349473
45	GMO5-3	0.22755	0.16755	0.01958686	2.21	2.177	0.05671421
46	GMO5-4	1.8751	1.8151	0.03747666	2.774	2.414	0.00999739
47	GMO5-5	0.13125	0.07125	0.01449569	1.087	1.077	0.04743361
48	GMO5-6	0.30195	0.24195	0.00799031	1.074	0.969	0.03044725
49	GMO5-7	0.8074	0.7474	0.01979899	1.089	1.041	0.02234427
50	GMO5-8	0.1349	0.0749	0.00480833	0.412		
51	GMO5-9	1.67205	1.61205	0.05253803	2.363	2.029	0.02068529
52	GMO5-10	1.8389	1.7789	0.02220315	2.915	2.268	0.00983176

*GMO1-5 are different generations of transgenic line *UbV3-1*, +C; positive control and -C; negative control

REFERENCES

1. van Vliet VJE, De Silva A, Mark BL, Kikkert M. Viral deubiquitinating proteases and the promising strategies of their inhibition. Virus Res. 2024 Jun;344:199368.

2. Kerscher O, Felberbaum R, Hochstrasser M. Modification of proteins by ubiquitin and ubiquitin-like proteins. Annu Rev Cell Dev Biol. 2006;22:159–80.

3. VerPlank JJS, Goldberg AL. Regulating protein breakdown through proteasome phosphorylation. Biochem J. 2017 Sep 24;474(19):3355–71.

4. Ciechanover A. Intracellular protein degradation: from a vague idea, through the lysosome and the ubiquitin-proteasome system, and onto human diseases and drug targeting (Nobel lecture). Angew Chem Int Ed Engl. 2005 Sep 19;44(37):5944–67.

5. Isaacson MK, Ploegh HL. Ubiquitination, ubiquitin-like modifiers, and deubiquitination in viral infection. Cell Host & Microbe. 2009 Jun;5(6):559–70.

6. Pickart CM. Mechanisms underlying ubiquitination. Annu Rev Biochem. 2001;70:503–33.

7. Ciechanover A, Heller H, Katz-Etzion R, Hershko A. Activation of the heat-stable polypeptide of the ATP-dependent proteolytic system. Proc Natl Acad Sci U S A. 1981 Feb;78(2):761–5.

8. Hu H, Sun SC. Ubiquitin signaling in immune responses. Cell Res. 2016 Apr;26(4):457–83.

9. Zhang Q, Jia Q, Gao W, Zhang W. The role of deubiquitinases in virus replication and host innate immune response. Front Microbiol. 2022 Feb 24;13:839624.

10. Schnell JD, Hicke L. Non-traditional functions of ubiquitin and ubiquitin-binding proteins. J Biol Chem. 2003 Sep 19;278(38):35857–60.

11. Wilkinson KD. Regulation of ubiquitin-dependent processes by deubiquitinating enzymes. FASEB J. 1997 Dec;11(14):1245–56.

12. Reyes-Turcu FE, Ventii KH, Wilkinson KD. Regulation and cellular roles of ubiquitin-specific deubiquitinating enzymes. Annu Rev Biochem. 2009;78:363–97.

13. Glickman MH, Ciechanover A. The ubiquitin-proteasome proteolytic pathway: destruction for the sake of construction. Physiol Rev. 2002 Apr;82(2):373–428.

14. Mukhopadhyay D, Riezman H. Proteasome-independent functions of ubiquitin in endocytosis and signaling. Science. 2007 Jan 12;315(5809):201–5.

15. Kwasna D, Abdul Rehman SA, Natarajan J, Matthews S, Madden R, De Cesare V, et al. Discovery and characterization of ZUFSP/ZUP1, a distinct deubiquitinase class important for genome stability. Mol Cell. 2018 Apr 5;70(1):150-164.e6.

16. Nijman SMB, Luna-Vargas MPA, Velds A, Brummelkamp TR, Dirac AMG, Sixma TK, et al. A genomic and functional inventory of deubiquitinating enzymes. Cell. 2005 Dec 2;123(5):773–86.

17. Amerik AY, Hochstrasser M. Mechanism and function of deubiquitinating enzymes. Biochim Biophys Acta. 2004 Nov 29;1695(1–3):189–207.

18. Abdul Rehman SA, Kristariyanto YA, Choi SY, Nkosi PJ, Weidlich S, Labib K, et al. MINDY-1 Is a member of an evolutionarily conserved and structurally distinct new family of deubiquitinating enzymes. Mol Cell. 2016 Jul 7;63(1):146–55.

19. Maurer T, Wertz IE. Length Matters: MINDY is a new deubiquitinase family that preferentially cleaves long polyubiquitin chains. Mol Cell. 2016 Jul 7;63(1):4–6.

20. Bailey-Elkin BA, Knaap RCM, Kikkert M, Mark BL. Structure and function of viral deubiquitinating enzymes. J Mol Biol. 2017 Nov;429(22):3441–70.

21. Luo R, Yang K, Xiao W. Plant deubiquitinases: from structure and activity to biological functions. Plant Cell Rep [Internet]. 2022 Dec 26 [cited 2023 Feb 13]; Available from: https://link.springer.com/10.1007/s00299-022-02962-y

22. Yan N, Doelling JH, Falbel TG, Durski AM, Vierstra RD. The ubiquitin-specific protease family from Arabidopsis. *At* UBP1 and 2 are required for the resistance to the amino acid analog canavanine. Plant Physiol. 2000 Dec 1;124(4):1828–43.

23. Komander D, Clague MJ, Urbé S. Breaking the chains: structure and function of the deubiquitinases. Nat Rev Mol Cell Biol. 2009 Aug;10(8):550–63.

24. Liu Y, Wang F, Zhang H, He H, Ma L, Deng XW. Functional characterization of the Arabidopsis ubiquitin-specific protease gene family reveals specific role and redundancy of individual members in development. Plant J. 2008 Sep;55(5):844–56.

25. Zhou H, Zhao J, Cai J, Patil SB. UBIQUITIN-SPECIFIC PROTEASES function in plant development and stress responses. Plant Mol Biol. 2017 Aug;94(6):565–76.

26. de Jong RN, Ab E, Diercks T, Truffault V, Daniëls M, Kaptein R, et al. Solution structure of the human ubiquitin-specific protease 15 DUSP domain. J Biol Chem. 2006 Feb 24;281(8):5026–31.

27. Gross CT, McGinnis W. DEAF-1, a novel protein that binds an essential region in a Deformed response element. EMBO J. 1996 Apr 15;15(8):1961–70.

28. Sunnerhagen M, Pursglove S, Fladvad M. The new MATH: homology suggests shared binding surfaces in meprin tetramers and TRAF trimers. FEBS Lett. 2002 Oct 23;530(1–3):1–3.

29. Ye H, Park YC, Kreishman M, Kieff E, Wu H. The structural basis for the recognition of diverse receptor sequences by TRAF2. Mol Cell. 1999 Sep;4(3):321–30.

30. Larsen CN, Krantz BA, Wilkinson KD. Substrate specificity of deubiquitinating enzymes: ubiquitin C-terminal hydrolases. Biochemistry. 1998 Mar 10;37(10):3358–68.

31. Chandler JS, McArdle B, Callis J. AtUBP3 and AtUBP4 are two closely related Arabidopsis thaliana ubiquitin-specific proteases present in the nucleus. Mol Gen Genet. 1997 Jul;255(3):302–10.

32. Doelling JH, Phillips AR, Soyler-Ogretim G, Wise J, Chandler J, Callis J, et al. The ubiquitin-specific protease subfamily UBP3/UBP4 is essential for pollen development and transmission in Arabidopsis. Plant Physiol. 2007 Nov;145(3):801–13.

33. Moon BC, Choi MS, Kang YH, Kim MC, Cheong MS, Park CY, et al. Arabidopsis ubiquitin-specific protease 6 (AtUBP6) interacts with calmodulin. FEBS Lett. 2005 Jul 18;579(18):3885–90.

34. Ewan R, Pangestuti R, Thornber S, Craig A, Carr C, O'Donnell L, et al. Deubiquitinating enzymes AtUBP12 and AtUBP13 and their tobacco homologue NtUBP12 are negative regulators of plant immunity. New Phytol. 2011 Jul;191(1):92–106.

35. Brazma A, Parkinson H, Sarkans U, Shojatalab M, Vilo J, Abeygunawardena N, et al. ArrayExpress--a public repository for microarray gene expression data at the EBI. Nucleic Acids Res. 2003 Jan 1;31(1):68–71.

36. Jeong JS, Jung C, Seo JS, Kim JK, Chua NH. The Deubiquitinating enzymes UBP12 and UBP13 positively regulate MYC2 levels in jasmonate responses. Plant Cell. 2017 Jun;29(6):1406–24.

37. Cui X, Lu F, Li Y, Xue Y, Kang Y, Zhang S, et al. Ubiquitin-specific proteases UBP12 and UBP13 act in circadian clock and photoperiodic flowering regulation in Arabidopsis. Plant Physiol. 2013 Jun;162(2):897–906.

38. Derkacheva M, Liu S, Figueiredo DD, Gentry M, Mozgova I, Nanni P, et al. H2A deubiquitinases UBP12/13 are part of the Arabidopsis polycomb group protein system. Nat Plants. 2016 Aug 15;2:16126.

39. Doelling JH, Yan N, Kurepa J, Walker J, Vierstra RD. The ubiquitin-specific protease UBP14 is essential for early embryo development in Arabidopsis thaliana: AtUBP14 is essential for embryogenesis. Plant J. 2001 Dec 23;27(5):393–405.

40. Xu Y, Jin W, Li N, Zhang W, Liu C, Li C, et al. Ubiquitin-specific protease14 interacts with ULTRAVIOLET-B INSENSITIVE4 to regulate endoreduplication and cell and organ growth in Arabidopsis. Plant Cell. 2016 May;28(5):1200–14.

41. Li WF, Perry PJ, Prafulla NN, Schmidt W. Ubiquitin-specific protease 14 (UBP14) is involved in root responses to phosphate deficiency in Arabidopsis. Mol Plant. 2010 Jan;3(1):212–23.

42. Du L, Li N, Chen L, Xu Y, Li Y, Zhang Y, et al. The ubiquitin receptor DA1 regulates seed and organ size by modulating the stability of the ubiquitin-specific protease UBP15/SOD2 in Arabidopsis. Plant Cell. 2014 Feb;26(2):665–77.

43. Zhou H, Zhao J, Yang Y, Chen C, Liu Y, Jin X, et al. Ubiquitin-specific protease16 modulates salt tolerance in Arabidopsis by regulating Na(+)/H(+) antiport activity and serine hydroxymethyltransferase stability. Plant Cell. 2012 Dec;24(12):5106–22.

44. Zhao J, Zhou H, Zhang M, Gao Y, Li L, Gao Y, et al. Ubiquitin-specific protease 24 negatively regulates abscisic acid signalling in Arabidopsis thaliana. Plant Cell Environ. 2016 Feb;39(2):427–40.

45. Sridhar VV, Kapoor A, Zhang K, Zhu J, Zhou T, Hasegawa PM, et al. Control of DNA methylation and heterochromatic silencing by histone H2B deubiquitination. Nature. 2007 Jun 7;447(7145):735–8.

46. Schmitz RJ, Tamada Y, Doyle MR, Zhang X, Amasino RM. Histone H2B deubiquitination is required for transcriptional activation of FLOWERING LOCUS C and for proper control of flowering in Arabidopsis. Plant Physiol. 2009 Feb;149(2):1196–204.

47. Pan R, Kaur N, Hu J. The Arabidopsis mitochondrial membrane-bound ubiquitin protease UBP27 contributes to mitochondrial morphogenesis. Plant J. 2014 Jun;78(6):1047–59.

48. Yang P, Smalle J, Lee S, Yan N, Emborg TJ, Vierstra RD. Ubiquitin C-terminal hydrolases 1 and 2 affect shoot architecture in Arabidopsis: De-ubiquitination modifies shoot architecture. Plant J. 2007 Jun 8;51(3):441–57.

49. Popp MW, Artavanis-Tsakonas K, Ploegh HL. Substrate filtering by the active site crossover loop in UCHL3 revealed by sortagging and gain-of-function mutations. J Biol Chem. 2009 Feb 6;284(6):3593–602.

50. Hayama R, Yang P, Valverde F, Mizoguchi T, Furutani-Hayama I, Vierstra RD, et al. Ubiquitin carboxyl-terminal hydrolases are required for period maintenance of the circadian clock at high temperature in Arabidopsis. Sci Rep. 2019 Nov 19;9(1):17030.

51. Bard JAM, Goodall EA, Greene ER, Jonsson E, Dong KC, Martin A. Structure and Function of the 26S Proteasome. Annu Rev Biochem. 2018 Jun 20;87:697–724.

52. Grethe C, Schmidt M, Kipka GM, O'Dea R, Gallant K, Janning P, et al. Structural basis for specific inhibition of the deubiquitinase UCHL1. Nat Commun. 2022 Oct 10;13(1):5950.

53. Osaka H. Ubiquitin carboxy-terminal hydrolase L1 binds to and stabilizes monoubiquitin in neuron. Hum Mol Genet. 2003 Jul 1;12(16):1945–58.

54. Scheuermann JC, de Ayala Alonso AG, Oktaba K, Ly-Hartig N, McGinty RK, Fraterman S, et al. Histone H2A deubiquitinase activity of the Polycomb repressive complex PR-DUB. Nature. 2010 May 13;465(7295):243–7.

55. Gaytán de Ayala Alonso A, Gutiérrez L, Fritsch C, Papp B, Beuchle D, Müller J. A genetic screen identifies novel polycomb group genes in Drosophila. Genetics. 2007 Aug;176(4):2099–108.

56. Sahtoe DD, van Dijk WJ, Ekkebus R, Ovaa H, Sixma TK. BAP1/ASXL1 recruitment and activation for H2A deubiquitination. Nat Commun. 2016 Jan 7;7:10292.

57. Steinhauer WR, Walsh RC, Kalfayan LJ. Sequence and structure of the Drosophila melanogaster ovarian tumor gene and generation of an antibody specific for the ovarian tumor protein. Mol Cell Biol. 1989 Dec;9(12):5726–32.

58. Makarova KS, Aravind L, Koonin EV. A novel superfamily of predicted cysteine proteases from eukaryotes, viruses and Chlamydia pneumoniae. Trends in Biochemical Sciences. 2000 Feb;25(2):50–2.

59. Radjacommare R, Usharani R, Kuo CH, Fu H. Distinct phylogenetic relationships and biochemical properties of Arabidopsis ovarian tumor-related deubiquitinases support their functional differentiation. Front Plant Sci. 2014;5:84.

60. Keren I, Citovsky V. The histone deubiquitinase OTLD1 targets euchromatin to regulate plant growth. Sci Signal. 2016 Dec 20;9(459):ra125.

61. Krichevsky A, Zaltsman A, Lacroix B, Citovsky V. Involvement of KDM1C histone demethylase–OTLD1 otubain-like histone deubiquitinase complexes in plant gene repression. Proc Natl Acad Sci USA. 2011 Jul 5;108(27):11157–62.

62. Balakirev MY, Tcherniuk SO, Jaquinod M, Chroboczek J. Otubains: a new family of cysteine proteases in the ubiquitin pathway. EMBO Rep. 2003 May;4(5):517–22.

63. Liu S, Luo J, Zhen X, Qiu J, Ouyang S, Luo ZQ. Interplay between bacterial deubiquitinase and ubiquitin E3 ligase regulates ubiquitin dynamics on Legionella phagosomes. eLife. 2020 Nov 2;9:e58114.

64. Mevissen TET, Hospenthal MK, Geurink PP, Elliott PR, Akutsu M, Arnaudo N, et al. OTU deubiquitinases reveal mechanisms of linkage specificity and enable ubiquitin chain restriction analysis. Cell. 2013 Jul;154(1):169–84.

65. Edelmann MJ, Iphöfer A, Akutsu M, Altun M, di Gleria K, Kramer HB, et al. Structural basis and specificity of human otubain 1-mediated deubiquitination. Biochem J. 2009 Mar 1;418(2):379–90.

66. Komander D, Barford D. Structure of the A20 OTU domain and mechanistic insights into deubiquitination. Biochem J. 2008 Jan 1;409(1):77–85.

67. Nanao MH, Tcherniuk SO, Chroboczek J, Dideberg O, Dessen A, Balakirev MY. Crystal structure of human otubain 2. EMBO Rep. 2004 Aug;5(8):783–8.

68. Burnett B. The polyglutamine neurodegenerative protein ataxin-3 binds polyubiquitylated proteins and has ubiquitin protease activity. Hum Mol Genet. 2003 Sep 30;12(23):3195–205.

69. Burnett BG, Pittman RN. The polyglutamine neurodegenerative protein ataxin 3 regulates aggresome formation. Proc Natl Acad Sci USA. 2005 Mar 22;102(12):4330–5.

70. Grasty KC, Weeks SD, Loll PJ. Structural insights into the activity and regulation of human Josephin-2. J Struct Biol: X. 2019 Jul;3:100011.

71. Zeng C, Zhao C, Ge F, Li Y, Cao J, Ying M, et al. Machado-Joseph deubiquitinases: from cellular functions to potential therapy targets. Front Pharmacol. 2020 Aug 26;11:1311.

72. Bichelmeier U, Schmidt T, Hübener J, Boy J, Rüttiger L, Häbig K, et al. Nuclear localization of Ataxin-3 is required for the manifestation of symptoms in SCA3: in vivo evidence. J Neurosci. 2007 Jul 11;27(28):7418–28.

73. Haahr P, Borgermann N, Guo X, Typas D, Achuthankutty D, Hoffmann S, et al. ZUFSP deubiquitylates K63-linked polyubiquitin chains to promote genome stability. Mol Cell. 2018 Apr 5;70(1):165-174.e6.

74. Hewings DS, Heideker J, Ma TP, AhYoung AP, El Oualid F, Amore A, et al. Reactive-site-centric chemoproteomics identifies a distinct class of deubiquitinase enzymes. Nat Commun. 2018 Mar 21;9(1):1162.

75. Hermanns T, Pichlo C, Woiwode I, Klopffleisch K, Witting KF, Ovaa H, et al. A family of unconventional deubiquitinases with modular chain specificity determinants. Nat Commun. 2018 Feb 23;9(1):799.

76. Liu P, Liu S, Zhu C, Li Y, Li Y, Fei X, et al. The deubiquitinating enzyme MINDY2 promotes pancreatic cancer proliferation and metastasis by stabilizing ACTN4 expression and activating the PI3K/AKT/mTOR signaling pathway. Front Oncol. 2023 May 3;13:1169833.

77. Abdul Rehman SA, Armstrong LA, Lange SM, Kristariyanto YA, Gräwert TW, Knebel A, et al. Mechanism of activation and regulation of deubiquitinase activity in MINDY1 and MINDY2. Mol Cell. 2021 Oct 21;81(20):4176-4190.e6.

78. Sato Y, Yoshikawa A, Yamagata A, Mimura H, Yamashita M, Ookata K, et al. Structural basis for specific cleavage of Lys 63-linked polyubiquitin chains. Nature. 2008 Sep 18;455(7211):358–62.

79. Maytal-Kivity V, Reis N, Hofmann K, Glickman MH. MPN+, a putative catalytic motif found in a subset of MPN domain proteins from eukaryotes and prokaryotes, is critical for Rpn11 function. BMC Biochem. 2002 Sep 20;3:28.

80. Cao S, Engilberge S, Girard E, Gabel F, Franzetti B, Maupin-Furlow JA. Structural insight into ubiquitin-like protein recognition and oligomeric states of JAMM/MPN+ proteases. Structure. 2017 Jun 6;25(6):823-833.e6.

81. Worden EJ, Padovani C, Martin A. Structure of the Rpn11-Rpn8 dimer reveals mechanisms of substrate deubiquitination during proteasomal degradation. Nat Struct Mol Biol. 2014 Mar;21(3):220–7.

82. Book AJ, Gladman NP, Lee SS, Scalf M, Smith LM, Vierstra RD. Affinity purification of the Arabidopsis 26 S proteasome reveals a diverse array of plant proteolytic complexes. J Biol Chem. 2010 Aug 13;285(33):25554–69.

83. Wang F, Muto A, Van de Velde J, Neyt P, Himanen K, Vandepoele K, et al. Functional analysis of Arabidopsis TETRASPANIN gene family in plant growth and development. Plant Physiol. 2015 Sep 28;pp.01310.2015.

84. Kwok SF, Solano R, Tsuge T, Chamovitz DA, Ecker JR, Matsui M, et al. Arabidopsis homologs of a c-Jun coactivator are present both in monomeric form and in the COP9 complex, and their abundance is differentially affected by the pleiotropic cop/det/fus mutations. Plant Cell. 1998 Nov;10(11):1779–90.

85. Jin D, Wu M, Li B, Bücker B, Keil P, Zhang S, et al. The COP9 Signalosome regulates seed germination by facilitating protein degradation of RGL2 and ABI5. PLoS Genet. 2018 Feb;14(2):e1007237.

86. Dohmann EMN, Kuhnle C, Schwechheimer C. Loss of the CONSTITUTIVE PHOTOMORPHOGENIC9 signalosome subunit 5 is sufficient to cause the cop/det/fus mutant phenotype in Arabidopsis. Plant Cell. 2005 Jul;17(7):1967–78.

87. Singh AK, Chamovitz DA. Role of Cop9 signalosome subunits in the environmental and hormonal balance of plant. Biomol. 2019 Jun 9;9(6):224.

88. Singh AK, Dhanapal S, Finkelshtein A, Chamovitz DA. CSN5A subunit of COP9 signalosome is required for resetting transcriptional stress memory after recurrent heat stress in Arabidopsis. Biomol. 2021 Apr 30;11(5):668.

89. Singer R, Atar S, Atias O, Oron E, Segal D, Hirsch JA, et al. Drosophila COP9 signalosome subunit 7 interacts with multiple genomic loci to regulate development. Nucleic Acids Res. 2014 Sep;42(15):9761–70.

90. Singh AK, Yadav BS, Dhanapal S, Berliner M, Finkelshtein A, Chamovitz DA. CSN5A subunit of COP9 signalosome temporally buffers response to heat in Arabidopsis. Biomol. 2019 Nov 29;9(12):805.

91. Chamovitz DA. Revisiting the COP9 signalosome as a transcriptional regulator. EMBO Rep. 2009 Apr;10(4):352–8.

92. Isono E, Katsiarimpa A, Müller IK, Anzenberger F, Stierhof YD, Geldner N, et al. The deubiquitinating enzyme AMSH3 is required for intracellular trafficking and vacuole biogenesis in Arabidopsis thaliana. The Plant Cell. 2010 Jul 28;22(6):1826–37.

93. Katsiarimpa A, Muñoz A, Kalinowska K, Uemura T, Rojo E, Isono E. The ESCRT-III-interacting deubiquitinating enzyme AMSH3 is essential for degradation of ubiquitinated membrane proteins in Arabidopsis thaliana. Plant Cell Physiol. 2014 Apr;55(4):727–36.

94. Katsiarimpa A, Kalinowska K, Anzenberger F, Weis C, Ostertag M, Tsutsumi C, et al. The deubiquitinating enzyme AMSH1 and the ESCRT-III subunit VPS2.1 are required for autophagic degradation in Arabidopsis. Plant Cell. 2013 Jun;25(6):2236–52.

95. Katsiarimpa A, Anzenberger F, Schlager N, Neubert S, Hauser MT, Schwechheimer C, et al. The Arabidopsis deubiquitinating enzyme AMSH3 interacts with ESCRT-III subunits and regulates their localization. Plant Cell. 2011 Aug;23(8):3026–40.

96. Block-Schmidt AS, Dukowic-Schulze S, Wanieck K, Reidt W, Puchta H. BRCC36A is epistatic to BRCA1 in DNA crosslink repair and homologous recombination in Arabidopsis thaliana. Nucleic Acids Res. 2011 Jan;39(1):146–54.

97. Forterre P. The origin of viruses and their possible roles in major evolutionary transitions. Virus Res. 2006 Apr;117(1):5–16.

98. Banks L, Pim D, Thomas M. Viruses and the 26S proteasome: hacking into destruction. Trends Biochem Sci. 2003 Aug;28(8):452–9.

99. Bailey-Elkin BA, van Kasteren PB, Snijder EJ, Kikkert M, Mark BL. Viral OTU deubiquitinases: A structural and functional comparison. Rall GF, editor. PLoS Pathog. 2014 Mar 27;10(3):e1003894.

100. Kumari P, Kumar H. Viral deubiquitinases: role in evasion of anti-viral innate immunity. Crit Rev Microbiol. 2018 May 4;44(3):304–17.

101. Kumar R, Mehta D, Mishra N, Nayak D, Sunil S. Role of host-mediated post-translational modifications (PTMs) in RNA virus pathogenesis. Int J Mol Sci. 2020 Dec 30;22(1):323.

102. Proulx J, Borgmann K, Park IW. Role of virally-encoded deubiquitinating enzymes in regulation of the virus life cycle. IJMS. 2021 Apr 23;22(9):4438.

103. Luo H. Interplay between the virus and the ubiquitin-proteasome system: molecular mechanism of viral pathogenesis. Curr Opin Virol. 2016 Apr;17:1–10.

104. Saridakis V, Sheng Y, Sarkari F, Holowaty MN, Shire K, Nguyen T, et al. Structure of the p53 binding domain of HAUSP/USP7 bound to Epstein-Barr nuclear antigen 1. Mol Cell. 2005 Apr;18(1):25–36.

105. Lata S, Mishra R, Banerjea AC. Proteasomal degradation machinery: Favorite target of HIV-1 proteins. Front Microbiol. 2018 Nov 21;9:2738.

106. Dubiella U, Serrano I. The ubiquitin proteasome system as a double agent in plant-virus interactions. Plants. 2021 May 6;10(5):928.

107. Clementz MA, Chen Z, Banach BS, Wang Y, Sun L, Ratia K, et al. Deubiquitinating and interferon antagonism activities of coronavirus papain-like proteases. J Virol. 2010 May;84(9):4619–29.

108. Balakirev MY, Jaquinod M, Haas AL, Chroboczek J. Deubiquitinating function of adenovirus proteinase. J Virol. 2002 Jun;76(12):6323–31.

109. Honig JE, Osborne JC, Nichol ST. Crimean-Congo hemorrhagic fever virus genome L RNA segment and encoded protein. Virol. 2004 Mar 30;321(1):29–35.

110. Sulea T, Lindner HA, Purisima EO, Ménard R. Deubiquitination, a new function of the severe acute respiratory syndrome coronavirus papain-like protease. J Virol. 2005 Apr;79(7):4550–1.

111. Lindner HA, Fotouhi-Ardakani N, Lytvyn V, Lachance P, Sulea T, Ménard R. The papain-like protease from the severe acute respiratory syndrome coronavirus is a deubiquitinating enzyme. J Virol. 2005 Dec;79(24):15199–208.

112. Barretto N, Jukneliene D, Ratia K, Chen Z, Mesecar AD, Baker SC. The papain-like protease of severe acute respiratory syndrome coronavirus has deubiquitinating activity. J Virol. 2005 Dec;79(24):15189–98.

113. Ratia K, Kilianski A, Baez-Santos YM, Baker SC, Mesecar A. structural basis for the ubiquitin-linkage specificity and deISGylating activity of SARS-CoV Papain-like protease. Rey FA, editor. PLoS Pathog. 2014 May 22;10(5):e1004113.

114. Frias-Staheli N, Giannakopoulos NV, Kikkert M, Taylor SL, Bridgen A, Paragas J, et al. Ovarian tumor domain-containing viral proteases evade ubiquitin- and ISG15-dependent innate immune responses. Cell Host Microbe. 2007 Dec 13;2(6):404–16.

115. James TW, Frias-Staheli N, Bacik JP, Levingston Macleod JM, Khajehpour M, García-Sastre A, et al. Structural basis for the removal of ubiquitin and interferon-stimulated gene 15 by a viral ovarian tumor domain-containing protease. Proc Natl Acad Sci U S A. 2011 Feb 8;108(6):2222–7.

116. Akutsu M, Ye Y, Virdee S, Chin JW, Komander D. Molecular basis for ubiquitin and ISG15 cross-reactivity in viral ovarian tumor domains. Proc Natl Acad Sci U S A. 2011 Feb 8;108(6):2228–33.

117. Bergeron E, Albariño CG, Khristova ML, Nichol ST. Crimean-Congo hemorrhagic fever virus-encoded ovarian tumor protease activity is dispensable for virus RNA polymerase function. J Virol. 2010 Jan;84(1):216–26.

118. Tchesnokov EP, Bailey-Elkin BA, Mark BL, Götte M. Independent inhibition of the polymerase and deubiquitinase activities of the Crimean-Congo Hemorrhagic Fever Virus full-length L-protein. PLoS Negl Trop Dis. 2020 Jun;14(6):e0008283.

119. Xing Y, Chen J, Tu J, Zhang B, Chen X, Shi H, et al. The papain-like protease of porcine epidemic diarrhea virus negatively regulates type I interferon pathway by acting as a viral deubiquitinase. J Gen Virol. 2013 Jul;94(Pt 7):1554–67.

120. Sun Z, Chen Z, Lawson SR, Fang Y. The cysteine protease domain of porcine reproductive and respiratory syndrome virus nonstructural protein 2 possesses deubiquitinating and interferon antagonism functions. J Virol. 2010 Aug;84(15):7832–46.

121. Xiong Y, Huang B, Yang Y, Fu X, Fu Z, Xu H, et al. The substrate selectivity of papain-like proteases from human-infecting coronaviruses correlates with innate immune suppression. Sci Signal. 2023 May 2;16(783):eade1985.

122. Chen X, Yang X, Zheng Y, Yang Y, Xing Y, Chen Z. SARS coronavirus papain-like protease inhibits the type I interferon signaling pathway through interaction with the STING-TRAF3-TBK1 complex. Protein Cell. 2014 May;5(5):369–81.

123. Cao D, Duan L, Huang B, Xiong Y, Zhang G, Huang H. The SARS-CoV-2 papain-like protease suppresses type I interferon responses by deubiquitinating STING. Sci Signal. 2023 May 2;16(783):eadd0082.

124. Mielech AM, Chen Y, Mesecar AD, Baker SC. Nidovirus papain-like proteases: Multifunctional enzymes with protease, deubiquitinating and deISGylating activities. Virus Res. 2014 Dec;194:184–90.

125. Shin D, Mukherjee R, Grewe D, Bojkova D, Baek K, Bhattacharya A, et al. Papain-like protease regulates SARS-CoV-2 viral spread and innate immunity. Nature. 2020 Nov;587(7835):657–62.

126. Liu G, Lee JH, Parker ZM, Acharya D, Chiang JJ, van Gent M, et al. ISG15-dependent activation of the sensor MDA5 is antagonized by the SARS-CoV-2 papain-like protease to evade host innate immunity. Nat Microbiol. 2021 Apr;6(4):467–78.

127. Rut W, Lv Z, Zmudzinski M, Patchett S, Nayak D, Snipas SJ, et al. Activity profiling and crystal structures of inhibitor-bound SARS-CoV-2 papain-like protease: A framework for anti-COVID-19 drug design. Sci Adv. 2020 Oct;6(42):eabd4596.

128. Rodamilans B, Shan H, Pasin F, García JA. Plant Viral Proteases: Beyond the Role of Peptide Cutters. Front Plant Sci. 2018 May 17;9:666.

129. Wu X, Valli A, García J, Zhou X, Cheng X. The Tug-of-War between plants and viruses: Great progress and many remaining questions. Viruses. 2019 Feb 28;11(3):203.

130. Hua Z, Doroodian P, Vu W. Contrasting duplication patterns reflect functional diversities of ubiquitin and ubiquitin-like protein modifiers in plants. Plant J. 2018 Jul;95(2):296–311.

131. Lombardi C, Ayach M, Beaurepaire L, Chenon M, Andreani J, Guerois R, et al. A compact viral processing proteinase/ubiquitin hydrolase from the OTU family. Kuhn RJ, editor. PLoS Pathog. 2013 Aug 15;9(8):e1003560.

132. Chenon M, Camborde L, Cheminant S, Jupin I. A viral deubiquitylating enzyme targets viral RNA-dependent RNA polymerase and affects viral infectivity: TYMV DUB targets viral RdRp. EMBO J. 2012 Feb 1;31(3):741–53.

133. Martelli GP, Sabanadzovic S, Abou-Ghanem Sabanadzovic N, Edwards MC, Dreher T. The family Tymoviridae. Arch Virol. 2002 Sep;147(9):1837–46.

134. Fieulaine S, Witte MD, Theile CS, Ayach M, Ploegh HL, Jupin I, et al. Turnip yellow mosaic virus protease binds ubiquitin suboptimally to fine-tune its deubiquitinase activity. J Biol Chem. 2020 Oct;295(40):13769–83.

135. Jakubiec A, Drugeon G, Camborde L, Jupin I. Proteolytic Processing of *Turnip Yellow Mosaic Virus* Replication Proteins and Functional Impact on Infectivity. J Virol. 2007 Oct 15;81(20):11402–12.

136. Jupin I, Ayach M, Jomat L, Fieulaine S, Bressanelli S. A mobile loop near the active site acts as a switch between the dual activities of a viral protease/deubiquitinase. PLoS Pathog. 2017 Nov 8;13(11):e1006714.

137. Camborde L, Planchais S, Tournier V, Jakubiec A, Drugeon G, Lacassagne E, et al. The ubiquitin-proteasome system regulates the accumulation of Turnip yellow mosaic virus

RNA-Dependent RNA polymerase during viral infection. The Plant Cell. 2010 Oct 27;22(9):3142–52.

138. Liebe S, Maiss E, Varrelmann M. The arms race between beet necrotic yellow vein virus and host resistance in sugar beet. Front Plant Sci. 2023;14:1098786.

139. Hehn A, Fritsch C, Richards KE, Guilley H, Jonard G. Evidence for in vitro and in vivo autocatalytic processingof the primary translation product of beet necrotic yellowvein virus RNA 1 by a papain-like proteinase. Arch Virol. 1997 May;142(5):1051–8.

140. Pakdel A, Mounier C, Klein E, Hleibieh K, Monsion B, Mutterer J, et al. On the interaction and localization of the beet necrotic yellow vein virus replicase. Virus Res. 2015 Jan 22;196:94–104.

141. Koonin EV, Gorbalenya AE, Purdy MA, Rozanov MN, Reyes GR, Bradley DW. Computer-assisted assignment of functional domains in the nonstructural polyprotein of hepatitis E virus: delineation of an additional group of positive-strand RNA plant and animal viruses. Proc Natl Acad Sci U S A. 1992 Sep 1;89(17):8259–63.

142. Patel A. Biochemically investigating the roles of papain-like proteases from +ssRNA viruses in replication and innate immune suppression [Internet]. University of Manitoba; 2021. Available from: https://mspace.lib.umanitoba.ca/items/96ef1dd3-82b5-41bd-8a99-198ad6d00fa3

143. Cho WK, Lian S, Kim SM, Park SH, Kim KH. Current insights into research on Rice stripe virus. Plant Pathol J. 2013 Sep;29(3):223–33.

144. Ishikawa K, Omura T, Hibino H. Morphological Characteristics of Rice Stripe Virus. J Gen Virol. 1989 Dec 1;70(12):3465–8.

145. Zhao S, Gu X, Li J, Liang C. The N-terminal cysteine protease domain of rice stripe tenuivirus Pc1 possesses deubiquitinating enzyme activity. Virus Genes. 2021 Feb;57(1):117–20.

146. Morch MD, Boyer JC, Haenni AL. Overlapping open reading frames revealed by complete nucleotide sequencing of turnip yellow mosaic virus genomic RNA. Nucleic Acids Res. 1988 Jul 11;16(13):6157–73.

147. Hammond RW, Ramirez P. Molecular characterization of the genome of Maize rayado fino virus, the type member of the genus Marafivirus. Virol. 2001 Apr 10;282(2):338–47.

148. Prod'homme D, Jakubiec A, Tournier V, Drugeon G, Jupin I. Targeting of the Turnip Yellow Mosaic Virus 66K Replication Protein to the Chloroplast Envelope Is Mediated by the 140K Protein. J Virol. 2003 Sep;77(17):9124–35.

149. Lefkowitz EJ, Dempsey DM, Hendrickson RC, Orton RJ, Siddell SG, Smith DB. Virus taxonomy: the database of the International Committee on Taxonomy of Viruses (ICTV). Nucleic Acids Res. 2018 Jan 4;46(D1):D708–17.

150. Edwards MC, Weiland JJ, Todd J, Stewart LR, Lu S. ORF43 of maize rayado fino virus is dispensable for systemic infection of maize and transmission by leafhoppers. Virus Genes. 2016 Apr;52(2):303–7.

151. Izadpanah K, Zhang YP, Daubert S, Masumi M, Rowhani A. Sequence of the coat protein gene of Bermuda grass etched-line virus, and of the adjacent "marafibox" motif. Virus Genes. 2002 Mar;24(2):131–4.

152. Edwards MC, Weiland JJ. Coat protein expression strategy of oat blue dwarf virus. Virol. 2014 Feb;450–451:290–6.

153. Schirawski J, Voyatzakis A, Zaccomer B, Bernardi F, Haenni AL. Identification and functional analysis of the turnip yellow mosaic tymovirus subgenomic promoter. J Virol. 2000 Dec;74(23):11073–80.

154. Giegé R, Florentz C, Dreher TW. The TYMV tRNA-like structure. Biochimie. 1993;75(7):569–82.

155. Wu S, Li X, Wang G. tRNA-like structures and their functions. FEBS J. 2022 Sep;289(17):5089–99.

156. Colussi TM, Costantino DA, Hammond JA, Ruehle GM, Nix JC, Kieft JS. The structural basis of transfer RNA mimicry and conformational plasticity by a viral RNA. Nature. 2014 Jul 17;511(7509):366–9.

157. Patel A, McBride JAM, Mark BL. The endopeptidase of the maize-affecting Marafivirus type member maize rayado fino virus doubles as a deubiquitinase. J Biol Chem. 2021 Aug;297(2):100957.

158. Ratia K, Pegan S, Takayama J, Sleeman K, Coughlin M, Baliji S, et al. A noncovalent class of papain-like protease/deubiquitinase inhibitors blocks SARS virus replication. Proc Natl Acad Sci U S A. 2008 Oct 21;105(42):16119–24.

159. Freitas BT, Durie IA, Murray J, Longo JE, Miller HC, Crich D, et al. Characterization and noncovalent inhibition of the deubiquitinase and deISGylase activity of SARS-CoV-2 Papain-Like Protease. ACS Infect Dis. 2020 Aug 14;6(8):2099–109.

160. Shen Z, Ratia K, Cooper L, Kong D, Lee H, Kwon Y, et al. Design of SARS-CoV-2 PLpro inhibitors for COVID-19 antiviral therapy leveraging binding cooperativity. J Med Chem. 2022 Feb 24;65(4):2940–55.

161. Sanders BC, Pokhrel S, Labbe AD, Mathews II, Cooper CJ, Davidson RB, et al. Potent and selective covalent inhibition of the papain-like protease from SARS-CoV-2. Nat Commun. 2023 Mar 28;14(1):1733.

162. Ma C, Sacco MD, Xia Z, Lambrinidis G, Townsend JA, Hu Y, et al. Discovery of SARS-CoV-2 papain-like protease inhibitors through a combination of high-throughput screening and a FlipGFP-based reporter assay. ACS Cent Sci. 2021 Jul 28;7(7):1245–60.

163. Jadhav P, Huang B, Osipiuk J, Zhang X, Tan H, Tesar C, et al. Structure-based design of SARS-CoV-2 papain-like protease inhibitors. Eur J Med Chem. 2024 Jan 15;264:116011.

164. Ratia K, Saikatendu KS, Santarsiero BD, Barretto N, Baker SC, Stevens RC, et al. Severe acute respiratory syndrome coronavirus papain-like protease: Structure of a viral deubiquitinating enzyme. Proc Natl Acad Sci USA. 2006 Apr 11;103(15):5717–22.

165. Shan H, Liu J, Shen J, Dai J, Xu G, Lu K, et al. Development of potent and selective inhibitors targeting the papain-like protease of SARS-CoV-2. Cell Chem Biol. 2021 Jun 17;28(6):855-865.e9.

166. Báez-Santos YM, Barraza SJ, Wilson MW, Agius MP, Mielech AM, Davis NM, et al. X-ray structural and biological evaluation of a series of potent and highly selective inhibitors of human coronavirus papain-like proteases. J Med Chem. 2014 Mar 27;57(6):2393–412.

167. Klemm T, Ebert G, Calleja DJ, Allison CC, Richardson LW, Bernardini JP, et al. Mechanism and inhibition of the papain-like protease, PLpro, of SARS-CoV-2. EMBO J. 2020 Sep 15;39(18):e106275.

168. Calleja DJ, Kuchel N, Lu BGC, Birkinshaw RW, Klemm T, Doerflinger M, et al. Insights into drug repurposing, as well as specificity and compound properties of piperidine-based SARS-CoV-2 PLpro inhibitors. Front Chem. 2022;10:861209.

169. Ernst A, Sidhu SS. Engineering ubiquitin to modulate the ubiquitin proteosome system. Cell Cycle. 2013 Jun 1;12(11):1651–2.

170. van Vliet VJE, Huynh N, Palà J, Patel A, Singer A, Slater C, et al. Ubiquitin variants potently inhibit SARS-CoV-2 PLpro and viral replication via a novel site distal to the protease active site. Perlman S, editor. PLoS Pathog. 2022 Dec 22;18(12):e1011065.

171. Zhang W, Bailey-Elkin BA, Knaap RCM, Khare B, Dalebout TJ, Johnson GG, et al. Potent and selective inhibition of pathogenic viruses by engineered ubiquitin variants. Whelan SPJ, editor. PLoS Pathog. 2017 May 18;13(5):e1006372.

172. Li G, Hilgenfeld R, Whitley R, De Clercq E. Therapeutic strategies for COVID-19: progress and lessons learned. Nat Rev Drug Discov. 2023 Jun;22(6):449–75.

173. Damgaard RB. The ubiquitin system: from cell signalling to disease biology and new therapeutic opportunities. Cell Death Differ. 2021 Feb;28(2):423–6.

174. Swatek KN, Komander D. Ubiquitin modifications. Cell Res. 2016 Apr;26(4):399–422.

175. Yau R, Rape M. The increasing complexity of the ubiquitin code. Nat Cell Biol. 2016 Jun;18(6):579–86.

176. Moriceau L, Jomat L, Bressanelli S, Alcaide-Loridan C, Jupin I. Identification and molecular characterization of the chloroplast targeting domain of Turnip yellow mosaic virus replication proteins. Front Plant Sci. 2017 Dec 19;8:2138.

177. Wimmer P, Schreiner S. Viral mimicry to usurp ubiquitin and SUMO host pathways. Viruses. 2015 Aug 28;7(9):4854–72.

178. Gustin JK, Moses AV, Früh K, Douglas JL. Viral takeover of the host ubiquitin system. Front Microbio [Internet]. 2011 [cited 2024 Jan 30];2. Available from: http://journal.frontiersin.org/article/10.3389/fmicb.2011.00161/abstract

179. Bailey-Elkin BA, Knaap RCM, Johnson GG, Dalebout TJ, Ninaber DK, Van Kasteren PB, et al. Crystal structure of the Middle East Respiratory Syndrome Coronavirus (MERS-CoV) Papain-like protease bound to ubiquitin facilitates targeted disruption of deubiquitinating activity to demonstrate its role in innate immune suppression. J Biol Chem. 2014 Dec;289(50):34667–82.

180. Ernst A, Avvakumov G, Tong J, Fan Y, Zhao Y, Alberts P, et al. A Strategy for modulation of enzymes in the ubiquitin system. Science. 2013 Feb;339(6119):590–5.

181. Edwards MC, Weiland JJ, Todd J, Stewart LR. Infectious Maize rayado fino virus from Cloned cDNA. Phytopathology. 2015 Jun;105(6):833–9.

182. Mcgrann GRD, Grimmer MK, Mutasa-Göttgens ES, Stevens M. Progress towards the understanding and control of sugar beet rhizomania disease. Mol Plant Pathol. 2009 Jan;10(1):129–41.

183. He M, Guan SY, He CQ. Evolution of rice stripe virus. Mol Phylogenet Evol. 2017 Apr;109:343–50.

184. Reeder RH, Edgington S, Baucas NS, Joshi RC, Bas-ilan MAG, Skelton A, et al. First report of Turnip yellow mosaic virus in Chinese cabbage and rocket in the Philippines. New Disease Reports. 2017 Jul;36(1):8–8.

185. Kirino N, Inoue K, Tanina K, Yamazaki Y, Ohki ST. Turnip yellow mosaic virus isolated from Chinese cabbage in Japan. J Gen Plant Pathol. 2008 Aug;74(4):331–4.

186. Alfaro-Fernández A, Serrano A, Tornos T, Del Carmen Cebrián M, Del Carmen Córdoba-Sellés M, Jordá C, et al. Turnip yellow mosaic virus in Chinese cabbage in Spain: commercial seed transmission and molecular characterisation. Eur J Plant Pathol. 2016 Oct;146(2):433–42.

187. Kim S, Lee S, Chi HY, Kim MK, Kim JS, Lee SH, et al. Feasibility Study for Detection of Turnip yellow mosaic virus (TYMV) infection of Chinese Cabbage plants using Raman Spectroscopy. Plant Pathol J. 2013 Mar 1;29(1):105–9.

188. Drugeon G, Jupin I. Stability in vitro of the 69K movement protein of Turnip yellow mosaic virus is regulated by the ubiquitin-mediated proteasome pathway. J Gen Virol. 2002 Dec 1;83(12):3187–97.

189. Zhang W, Wu KP, Sartori MA, Kamadurai HB, Ordureau A, Jiang C, et al. System-wide modulation of HECT E3 ligases with selective ubiquitin variant probes. Mol Cell. 2016 Apr;62(1):121–36.

190. Tonikian R, Zhang Y, Boone C, Sidhu SS. Identifying specificity profiles for peptide recognition modules from phage-displayed peptide libraries. Nat Protoc. 2007 Jun;2(6):1368–86.

191. Bailey-Elkin BA, Knaap RCM, De Silva A, Boekhoud IM, Mous S, Van Vught N, et al. Demonstrating the importance of porcine reproductive and respiratory syndrome virus papain-like protease 2 deubiquitinating activity in viral replication by structure-guided mutagenesis. Letko M, editor. PLoS Pathog. 2023 Dec 14;19(12):e1011872.

192. Gubler H, Clare N, Galafassi L, Geissler U, Girod M, Herr G. Helios: History and Anatomy of a successful in-house enterprise high-throughput screening and profiling data analysis system. SLAS Discovery. 2018 Jun;23(5):474–88.

193. Varca AC, Casalena D, Chan WC, Hu B, Magin RS, Roberts RM, et al. Identification and validation of selective deubiquitinase inhibitors. Cell Chem Biol. 2021 Dec;28(12):1758-1771.e13.

194. Vadlamani G, Stubbs KA, Désiré J, Blériot Y, Vocadlo DJ, Mark BL. Conformational flexibility of the glycosidase NagZ allows it to bind structurally diverse inhibitors to suppress β-lactam antibiotic resistance. Protein Science. 2017 Jun;26(6):1161–70.

195. Bodilis J, Denet E, Brothier E, Graindorge A, Favre-Bonté S, Nazaret S. Comparative genomics of environmental and clinical Burkholderia cenocepacia strains closely related to the highly transmissible epidemic ET12 lineage. Front Microbiol. 2018 Mar 6;9:383.

196. Harper S, Speicher DW. Purification of proteins fused to glutathione S-transferase. In: Walls D, Loughran ST, editors. Protein Chromatography [Internet]. Totowa, NJ: Humana Press; 2011 [cited 2024 Mar 7]. p. 259–80. (Methods in Molecular Biology; vol. 681). Available from: https://link.springer.com/10.1007/978-1-60761-913-0_14

197. James TW, Frias-Staheli N, Bacik JP, Levingston Macleod JM, Khajehpour M, García-Sastre A, et al. Structural basis for the removal of ubiquitin and interferon-stimulated gene 15 by a viral ovarian tumor domain-containing protease. Proc Natl Acad Sci USA. 2011 Feb 8;108(6):2222–7.

198. Kabsch W. *XDS*. Acta Crystallogr D Biol Crystallogr. 2010 Feb 1;66(2):125–32.

199. Evans PR, Murshudov GN. How good are my data and what is the resolution. Acta Crystallogr D Biol Crystallogr. 2013 Jul 1;69(7):1204–14.

200. McCoy AJ, Grosse-Kunstleve RW, Adams PD, Winn MD, Storoni LC, Read RJ. *Phaser* crystallographic software. J Appl Crystallogr. 2007 Aug 1;40(4):658–74.

201. Afonine PV, Grosse-Kunstleve RW, Echols N, Headd JJ, Moriarty NW, Mustyakimov M, et al. Towards automated crystallographic structure refinement with *phenix.refine*. Acta Crystallogr D Biol Crystallogr. 2012 Apr 1;68(4):352–67.

202. Manalastas-Cantos K, Konarev PV, Hajizadeh NR, Kikhney AG, Petoukhov MV, Molodenskiy DS, et al. ATSAS 3.0: expanded functionality and new tools for small-angle scattering data analysis. J Appl Crystallogr. 2021 Feb 1;54(Pt 1):343–55.

203. Panjkovich A, Svergun DI. CHROMIXS: automatic and interactive analysis of chromatography-coupled small-angle X-ray scattering data. Bioinformatics. 2018 Jun 1;34(11):1944–6.

204. Putnam CD. Guinier peak analysis for visual and automated inspection of small-angle X-ray scattering data. J Appl Crystallogr. 2016 Oct 1;49(Pt 5):1412–9.

205. Burke JE, Butcher SE. Nucleic acid structure characterization by small angle X-ray scattering (SAXS). Curr Protoc Nucleic Acid Chem. 2012 Dec;Chapter 7:Unit7.18.

206. Svergun DI. Restoring low resolution structure of biological macromolecules from solution scattering using simulated annealing. Biophys J. 1999 Jun;76(6):2879–86.

207. Franke D, Svergun DI. DAMMIF, a program for rapid ab-initio shape determination in small-angle scattering. J Appl Crystallogr. 2009 Apr 1;42(Pt 2):342–6.

208. He F. Evidence for phosphorylation and ubiquitinylation of the Turnip yellow mosaic virus RNA-dependent RNA polymerase domain expressed in a baculovirus–insect cell system. 2000; Biochem J. 2000 Jul 15;349(2):417-25.

209. Rozanov MN, Drugeon G, Haenni AL. Papain-like proteinase of Turnip yellow mosaic virus: a prototype of a new viral proteinase group. Arch Virol. 1995 Feb;140(2):273–88.

210. Bransom KL, Wallace SE, Dreher TW. Identification of the cleavage site recognized by the Turnip yellow mosaic virus protease. Virol. 1996 Mar;217(1):404–6.

211. Yang P, Smalle J, Lee S, Yan N, Emborg TJ, Vierstra RD. Ubiquitin C-terminal hydrolases 1 and 2 affect shoot architecture in Arabidopsis: De-ubiquitination modifies shoot architecture. Plant J. 2007 Jun 8;51(3):441–57.

212. Manczyk N, Veggiani G, Gish GD, Yates BP, Ernst A, Sidhu SS, et al. Dimerization of a ubiquitin variant leads to high affinity interactions with a ubiquitin interacting motif. Protein Sci. 2019 May;28(5):848–56.

213. Gabrielsen M, Buetow L, Nakasone MA, Ahmed SF, Sibbet GJ, Smith BO, et al. A general strategy for discovery of inhibitors and activators of RING and U-box E3 ligases with ubiquitin variants. Mol Cell. 2017 Oct;68(2):456-470.e10.

214. Winget JM, Mayor T. The diversity of ubiquitin recognition: hot spots and varied specificity. Mol Cell. 2010 Jun 11;38(5):627–35.

215. Borodovsky A, Ovaa H, Kolli N, Gan-Erdene T, Wilkinson KD, Ploegh HL, et al. Chemistry-Based Functional Proteomics Reveals Novel Members of the Deubiquitinating Enzyme Family. Chem Biol. 2002 Oct;9(10):1149–59.

216. Krissinel E, Henrick K. Inference of macromolecular assemblies from crystalline state. J Mol Biol. 2007 Sep 21;372(3):774–97.

217. Marchetti M, Faggiano S, Mozzarelli A. Enzyme replacement therapy for genetic disorders associated with enzyme deficiency. Curr Med Chem. 2022;29(3):489–525.

218. Graceffa V. Intracellular protein delivery: New insights into the therapeutic applications and emerging technologies. Biochimie. 2023 Oct;213:82–99.

219. Mazzucotelli E, Belloni S, Marone D, De Leonardis A, Guerra D, Di Fonzo N, et al. The E3 ubiquitin ligase gene family in plants: Regulation by degradation. Curr Genom. 2006 Dec 1;7(8):509–22.

220. Jakubiec A, Notaise J, Tournier V, Héricourt F, Block MA, Drugeon G, et al. Assembly of Turnip Yellow mosaic virus replication complexes: Interaction between the proteinase and polymerase domains of the replication proteins. J Virol. 2004 Aug;78(15):7945–57.

221. Linden KJ, Callis J. The ubiquitin system affects agronomic plant traits. J Biol Chem. 2020 Oct 2;295(40):13940–55.

222. Fieulaine S, Witte MD, Theile CS, Ayach M, Ploegh HL, Jupin I, et al. Turnip yellow mosaic virus protease binds ubiquitin suboptimally to fine-tune its deubiquitinase activity. J Biol Chem. 2020;295(40):13769–83.

223. Forterre P. The origin of viruses and their possible roles in major evolutionary transitions. Virus Res. 2006.

224. Nguyen L, Lucas WJ, Ding B, Zaitlin M. Viral RNA trafficking is inhibited in replicase-mediated resistant transgenic tobacco plants. Proceedings of the National Academy of Sciences of the United States of America. 1996;93(22):12643–7.

225. Hwang JN, Oh CS, Kang BC. Translation elongation factor 1B (eEF1B) is an essential host factor for Tobacco mosaic virus infection in plants. Virology. 2013;439(2):105–14.

226. Souza PFN. Masters of manipulation: how do positive-sense RNA viruses employ plant proteins to replicate, move from cell to cell, and overcome antiviral immunity. J Plant Dis Prot. 2020;127(4):425–40.

227. Calil IP, Fontes EPB. Plant immunity against viruses: Antiviral immune receptors in focus. Annals of Botany. 2017;119(5):711–23.

228. Jones JDG, Dangl JL. The plant immune system. Nature. 2006.

229. Harpster M. RNA silencing in plants. Scientist. 2003;17(10):20.

230. Postel S, Kemmerling B. Plant systems for recognition of pathogen-associated molecular patterns. Semin Cell Biol 2009;20(9):1025–31.

231. Krzymowska M, Talarczyk A, Hennig J. Is tobacco response to TMV infection modulated by catalase activity. Acta Physiologiae Plantarum. 1997;19(4):577–9.

232. Mathioudakis MM, Veiga RSL, Canto T, Medina V, Mossialos D, Makris AM, et al. Pepino mosaic virus triple gene block protein 1 (TGBp1) interacts with and increases tomato catalase 1 activity to enhance virus accumulation. Mol Plant Pathol. 2013;14(6):589–601.

233. Endres MW, Gregory BD, Gao Z, Foreman AW, Mlotshwa S, Ge X, et al. Two plant viral suppressors of silencing require the ethylene-inducible host transcription factor RAV2 to block RNA silencing. PLoS Pathogens. 2010;6(1).

234. Pogany J, Nagy PD. Activation of Tomato bushy stunt virus RNA-Dependent RNA polymerase by cellular Heat Shock Protein 70 is enhanced by phospholipids in vitro . J Virol. 2015;89(10):5714–23.

235. Hsu NY, Ilnytska O, Belov G, Santiana M, Chen YH, Takvorian PM, et al. Viral reorganization of the secretory pathway generates distinct organelles for RNA replication. Cell. 2010;141(5):799–811.

236. Jones RAC, Naidu RA. Global Dimensions of Plant Virus Diseases: Current Status and Future Perspectives. Annu Rev Virol. 2019 Sep 29;6(1):387–409.

237. Niraula PM, Fondong VN. Development and adoption of genetically engineered plants for virus resistance: Advances, opportunities and challenges. Plants (Basel). 2021 Oct 29;10(11):2339.

238. Ratcliff FG, MacFarlane SA, Baulcombe DC. Gene silencing without DNA: RNA-mediated cross-protection between viruses. Plant Cell. 1999;11(7):1207–15.

239. Beachy RN. Coat-protein-mediated resistance to tobacco mosaic virus: Discovery mechanisms and exploitation. Philosophical Transactions of the Royal Society B: Biological Sciences. 1999;354(1383):659–64.

240. Tripathi S, Suzuki JY, Ferreira SA, Gonsalves D. Papaya ringspot virus-P: characteristics, pathogenicity, sequence variability and control. Mol Plant Pathol. 2008;9(3):269–80.

241. Fitch MMM, Manshardt RM, Gonsalves D, Slightom JL, Sanford JC. Virus resistant papaya plants derived from tissues bombarded with the coat protein gene of papaya ringspot virus. Bio/Technology. 1992;10(11):1466–72.

242. Scorza R, Ravelonandro M, Callahan A, Zagrai L, Polak J, Malinowski T, et al. Honeysweet (C5), the first genetically engineered plum pox vi'rus-resistant plum (Prunus domestica L.) cultivar. Hort Sci. 2016;51(5):601–3.

243. Golemboski DB, Lomonossoff GP, Zaitlin M. Plants transformed with a tobacco mosaic virus nonstructural gene sequence are resistant to the virus. Proc Natl Acad Sci USA. 1990;87(16):6311–5.

244. Wintermantel WM, Zaitlin M. Transgene translatability increases effectiveness of replicase-mediated resistance to Cucumber mosaic virus. J GenVirol. 2000;81(3):587–95.

245. Audy P, Palukaitis P, Slack SA, Zaitlin M. Replicase-mediated resistance to potato virus Y in transgenic tobacco plants. Vol. 7, Mol Plant Microbe Interact. 1994. p. 15–22.

246. Brunetti A, Tavazza M, Noris E, Tavazza R, Caciagli P, Ancora G, et al. High expression of truncated viral rep protein confers resistance to tomato yellow leaf curl virus in transgenic tomato plants. Mol Plant Microbe Interact. 1997;10(5):571–9.

247. Carr JP, Gal-On A, Palukaitis P, Zaitlin M. Replicase-mediated resistance to cucumber mosaic virus in transgenic plants involves suppression of both virus replication in the inoculated leaves and long-distance movement. Vol. 199, Virol. 1994. p. 439–47.

248. Sharma M, Sasvari Z, Nagy PD. Inhibition of phospholipid biosynthesis decreases the activity of the tombusvirus replicase and alters the subcellular localization of replication proteins. Virol. 2011;415(2):141–52.

249. Singh K, Callahan AM, Smith BJ, Malinowski T, Scorza R, Jarošová J, et al. Long-Term Efficacy and Safety of RNAi-Mediated Virus Resistance in "HoneySweet" Plum. Front Plant Sci. 2021;12:726881.

250. Sawant SV, Kiran K, Singh PK, Tuli R. Sequence Architecture Downstream of the Initiator Codon Enhances Gene Expression and Protein Stability in Plants. Plant Physiol. 2001 Aug 1;126(4):1630–6.

251. Clough SJ, Bent AF. Floral dip: a simplified method forAgrobacterium-mediated transformation ofArabidopsis thaliana: Floral dip transformation of Arabidopsis. Plant J. 1998 Dec;16(6):735–43.

252. Estavillo GM, Verhertbruggen Y, Scheller HV, Pogson BJ, Heazlewood JL, Ito J. Isolation of the plant cytosolic fraction for proteomic analysis. In: Jorrin-Novo JV, Komatsu S, Weckwerth W, Wienkoop S, editors. Plant Proteomics [Internet]. Totowa, NJ: Humana Press; 2014 [cited 2023 Feb 12]. p. 453–67. (Methods in Molecular Biology; vol. 1072). Available from: http://link.springer.com/10.1007/978-1-62703-631-3_31

253. Pasternak T, Tietz O, Rapp K, Begheldo M, Nitschke R, Ruperti B, et al. Protocol: an improved and universal procedure for whole-mount immunolocalization in plants. Plant Methods. 2015 Dec;11(1):50.

254. Weiland JJ, Dreher TW. Infectious TYMV RNA from cloned cDNA: effects in vitro and in vivo of point substitutions in the initiation codons of two extensively overlapping ORFs. Nucleic Acids Res. 1989 Jun 26;17(12):4675–87.

255. Amack SC, Antunes MS. CaMV35S promoter – A plant biology and biotechnology workhorse in the era of synthetic biology. Curr Plant Biol. 2020 Dec;24:100179.

256. Karimi M, Inzé D, Depicker A. GATEWAY vectors for Agrobacterium-mediated plant transformation. Trends Plant Sci. 2002 May;7(5):193–5.

257. Zhang X, Henriques R, Lin SS, Niu QW, Chua NH. Agrobacterium-mediated transformation of Arabidopsis thaliana using the floral dip method. Nat Protoc. 2006 Aug;1(2):641–6.

258. Monroy-Borrego AG, Steinmetz NF. Three methods for inoculation of viral vectors into plants. Front Plant Sci. 2022;13:963756.

259. Zhao J, Zhang X, Hong Y, Liu Y. Chloroplast in plant-virus interaction. Front Microbiol [Internet]. 2016 Oct 4 [cited 2023 May 12];7. Available from: http://journal.frontiersin.org/article/10.3389/fmicb.2016.01565

260. Bandopadhyay R, Haque I, Singh D, Mukhopadhyay K. Levels and stability of expression of transgenes. In: Kole C, Michler CH, Abbott AG, Hall TC, editors. Transgenic Crop Plants [Internet]. Berlin, Heidelberg: Springer Berlin Heidelberg; 2010 [cited 2024 Mar 14]. p. 145–86. Available from: http://link.springer.com/10.1007/978-3-642-04809-8_5

261. Kim HB, Kim DY, Cho TJ. Replication and packaging of Turnip yellow mosaic virus RNA containing Flock house virus RNA1 sequence. BMB Reports. 2014 Jun 30;47(6):330–5.

262. Sowa AS, Haas E, Hübener-Schmid J, Lorentz A. Ataxin-3, The Spinocerebellar Ataxia Type 3 neurodegenerative disorder protein, affects Mast cell functions. Front Immunol. 2022 Apr 26;13:870966.

263. Akutsu M, Dikic I, Bremm A. Ubiquitin chain diversity at a glance. J Cell Sci. 2016 Jan 1;jcs.183954.

264. Scaglione KM, Zavodszky E, Todi SV, Patury S, Xu P, Rodríguez-Lebrón E, et al. Ube2w and Ataxin-3 coordinately regulate the ubiquitin ligase CHIP. Mol Cell. 2011 Aug;43(4):599–612.

265. Nicastro G, Menon RP, Masino L, Knowles PP, McDonald NQ, Pastore A. The solution structure of the Josephin domain of ataxin-3: Structural determinants for molecular recognition. Proc Natl Acad Sci USA. 2005 Jul 26;102(30):10493–8.

266. Winborn BJ, Travis SM, Todi SV, Scaglione KM, Xu P, Williams AJ, et al. The deubiquitinating enzyme Ataxin-3, a polyglutamine disease protein, edits Lys63 linkages in mixed linkage ubiquitin chains. J Biol Chem. 2008 Sep;283(39):26436–43.

267. Li F, Macfarlan T, Pittman RN, Chakravarti D. Ataxin-3 is a histone-binding protein with two independent transcriptional corepressor activities. J Biol Chem. 2002 Nov;277(47):45004–12.

268. Isono E, Nagel MK. Deubiquitylating enzymes and their emerging role in plant biology. Front Plant Sci [Internet]. 2014 [cited 2024 Feb 11];5. Available from: http://journal.frontiersin.org/article/10.3389/fpls.2014.00056/abstract

269. Jumper J, Evans R, Pritzel A, Green T, Figurnov M, Ronneberger O, et al. Highly accurate protein structure prediction with AlphaFold. Nature. 2021 Aug 26;596(7873):583–9.

270. Mirdita M, Schütze K, Moriwaki Y, Heo L, Ovchinnikov S, Steinegger M. ColabFold: making protein folding accessible to all. Nat Methods. 2022 Jun;19(6):679–82.

271. Nelsen CJ, Murtaugh MP, Faaberg KS. Porcine reproductive and respiratory syndrome virus comparison: divergent evolution on two continents. J Virol. 1999 Jan;73(1):270–80.

272. Chae C. Commercial PRRS modified-live virus vaccines. Vaccines (Basel). 2021 Feb 22;9(2):185.

273. Kimman TG, Cornelissen LA, Moormann RJ, Rebel JMJ, Stockhofe-Zurwieden N. Challenges for porcine reproductive and respiratory syndrome virus (PRRSV) vaccinology. Vaccine. 2009 Jun 8;27(28):3704–18.

274. Zhou L, Ge X, Yang H. Porcine Reproductive and Respiratory Syndrome modified live virus vaccine: A "Leaky" vaccine with debatable efficacy and safety. Vaccines (Basel). 2021 Apr 9;9(4):362.

275. Fang Y, Treffers EE, Li Y, Tas A, Sun Z, van der Meer Y, et al. Efficient -2 frameshifting by mammalian ribosomes to synthesize an additional arterivirus protein. Proc Natl Acad Sci U S A. 2012 Oct 23;109(43):E2920-2928.

276. van Kasteren PB, Bailey-Elkin BA, James TW, Ninaber DK, Beugeling C, Khajehpour M, et al. Deubiquitinase function of arterivirus papain-like protease 2 suppresses the innate immune response in infected host cells. Proc Natl Acad Sci U S A. 2013 Feb 26;110(9):E838-847.